ABSTRACT

TAN, YING. Experimental and Nonlinear FEA Investigation of Elbows Leading to a New Definition of The B_2 Stress Index (Under the supervision of Dr. Vernon C. Matzen).

This study suggests a new margin-consistent procedure for the calculation of the B_2 stress index for any piping component, which is the ratio of the collapse moment of a corresponding straight pipe to the collapse moment of the piping component. It gives a B_2 value of 1.00 when applied to a straight pipe and a safety margin for the component that is always the same as for the straight pipe. An example of using this definition to calculate the value of B_2 is provided. To obtain the collapse moments of piping components, either finite element analysis (FEA) or experiments can be used. This work gives a brief review of nonlinear FEA modeling procedures. Then nonlinear FEA using ANSYS shell models and ABAQUS elbow models are used to simulate two tests on straight pipes and eight tests on elbows under in-plane closing, in-plane opening and out-of-plane bending. Constitutive models and welding effects are discussed. All correlations between FEA and measured experimental results for the load-displacement curves are excellent. It is concluded that nonlinear FEA using ANSYS SHELL181 and ABAQUS ELBOW31 can give quite accurate predictions of the global behavior of elbows and straight pipes under monotonic loading. A very preliminary study for B_2' stress index for cyclic loading is also performed, in which two elbow tests subjected to quasi static in-plane cyclic loading were simulated.

EXPERIMENTAL AND NONLINEAR FEA INVESTIGATION OF ELBOW LEADING TO A NEW DEFINITION OF THE B_2 STRESS INDEX

by

YING TAN

A dissertation submitted to the Graduate Faculty of
North Carolina State University
In partial fulfillment of the
Requirements for the Degree of
Doctor of Philosophy

CIVIL ENGINEERING

NORTH CAROLINA STATE UNIVERSITY

Raleigh

2001

APPROVED BY:

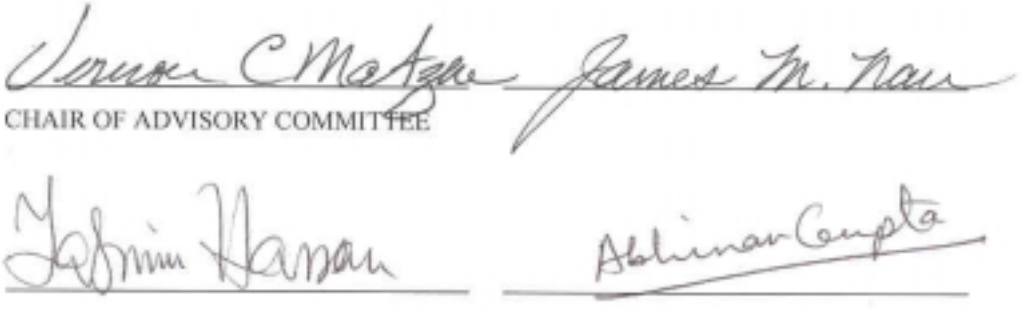

CHAIR OF ADVISORY COMMITTEE

BIOGRAPHY

Ying Tan was born in mainland China. She accomplished a 4-year BSCE program in three years at Shenzhen University, China, and received a Bachelor degree in Structural Engineering in 1994. Then she joined Tsinghua University, China, as a graduate student, focusing on experimental investigations on flexural behaviors of Steel-High-Performance-Concrete Composite Beams. In April 1998, she received a Master degree in Structural Engineering.

In the fall 1998, Ying enrolled in the doctoral program in Civil Engineering under the direction of Dr. Vernon C. Matzen, working as a Research Assistant in the Center for Nuclear Power Plant Structures, Equipment and Piping, North Carolina State University.

During her stay at North Carolina State University, she also taught three classes of “Engineering Statics (CE214)” over two semesters. The author was honored in the National Dean’s List (23rd Edition).

ACKNOWLEDGEMENTS

I would like to express my sincere appreciation to Dr. Vernon C. Matzen for giving me the opportunity of working on such an interesting and challenging project. What I have learned from Dr. Matzen is far beyond academic and research skills. Every progress of this work would not be achieved without his guidance, support, encouragement, patience and great efforts. He is always there to support me in every aspect of my stay at North Carolina State University.

I would like to express my thanks to Dr. Tasnim Hassan for sharing test data that he and his students obtained and for his assistance in the finite element modeling and reconciliation of analysis with test data. In particular, I would like to recognize his insight into the importance of including the weld bead in modeling thin-walled elbows.

I would also like to thank Dr. Abhinav Gupta, Dr. Nau and Dr. Havner for their support, encouragement and suggestions during my stay at NC State University. Taking their courses was an enlightening experience for me.

Special thanks should go to Kevin Wilkins and Matthew Modlin for their generous help in designing and conducting the experiments, to Xi Yuan for his helpful ideas on finite element analysis, and to other professors, staff and students at the Center for Nuclear Power Plant Structures, Equipment and Piping and the department of Civil Engineering for helping me in numerous occasions during the course of this work.

I would like to express my gratitude to the North Carolina Supercomputing Center for providing me access to ABAQUS package and technical assistance to fulfill this investigation.

Finally, I would like to share every achievement with my parents and my husband, Yuanyuan Li.

TABLE OF CONTENTS

LIST OF TABLES

PART II

PART III

PART IV

PART V

PART VI

APPENDIX A

LIST OF FIGURES

PART I

PART II

PART III

PART IV

PART V

PART VI

APPENDIX A

PART I

INTRODUCTION

INTRODUCTION

The ASME Boiler and Pressure Vessel Code, Section III (Nuclear Power Plant Components), Division 1 [1], hereinafter called the Code, provides design guidance for Class 1 Piping. Equation (9) of Code Subsubarticle NB-3640, which governs the primary stress intensity for design loads, has the following form:

$$B_1 \frac{PD_o}{2t} + B_2 \frac{D_o}{2I} M_i \le 1.5 S_m \qquad \text{(Eq. 9)}$$

where B_1 is primary stress index for pressure;

B_2 is primary stress index for bending;

D_o is outside diameter;

I is moment of inertia;

M_i is resultant moment due to a combination of Design Mechanical Loads;

P is design pressure;

S_m is allowable design stress intensity value; and

t is nominal wall thickness.

The work in this dissertation is focused on the B_2 stress index, specifically as applied to elbows. To understand this design equation, we introduce the concepts of stress indices, stress failure criteria, stress categories, failure mechanisms and the collapse loads as defined in the Code.

Stress Indices

In piping analysis, "For straight pipe, a relatively simple and complete theory exists"[2], while for other piping components (for example, elbows and tees) such simple theories do not exist. The stress indices are used to modify nominal stress equations for straight pipe so that the behavior of piping components such as elbows can be controlled using the same basic stress limits as for straight pipe. Moore and Rodabaugh[3] state that "The B_1 and B_2 stress indices reflect the capacities of various piping products to carry load without gross plastic deformation."

Stress Failure Theory

In the Code, the maximum shear stress criterion, also known as Tresca Criterion, is utilized. The theory asserts that material failure depends only on "the difference between the algebraically largest principal stress and the algebraically smallest principal stress at a given point"[4]. It "closely approximates experimental results and is also easy to use" [5]. In addition, it is more conservative than von Mises Criterion. As will be seen later, Equation (9) is based on the Tresca Criterion.

Stress Categories

In the Code, stresses are divided into three categories: Primary, Secondary and Peak Stress.

Primary Stress is "any normal stress or a shear stress developed by an imposed loading which is necessary to satisfy the laws of equilibrium...The basic characteristic of a primary stress is that it is not self-limiting."[6]. Primary stresses "will result in failure or, at least, in gross distortion."[6] if they considerably exceed the yield strength.

Secondary stress is "a normal stress or a shear stress developed by the constraint of adjacent material or by self-constraint of the structure. The basic characteristic of a secondary stress is that it is self-limiting."[7].

Peak stress is the "increment of stress which is additive to the primary plus secondary stresses by reason of local discontinuities or local thermal stress… The basic characteristic of a peak stress is that it does not cause any noticeable distortion and is objectionable only as a possible source of a fatigue crack or a brittle fracture" [8].

Equation (9) only governs the Primary stresses.

Failure Mechanisms

The failure mechanisms of piping systems or components can be grouped into "Burst due to pressure, Corrosion, Collapse due to loads and fatigue due to thermal cycling" [9]. Equation (9) intends to resist "gross plastic deformation"[10] or to place "bounds on loading such that necessary conditions for a collapse load will not exist anywhere in the piping system"[11].

Collapse Load

The Code-defined collapse load for plastic analysis is shown schematically in Fig. 1 below. The collapse load "is the load at the intersection of the load-deflection or load-strain curve and the collapse limit line."[12] In this dissertation, all the collapse loads of piping components are calculated following this definition. To determine collapse loads in this work, we obtain the load-deflection curves experimentally or numerically using Finite Element Analysis (FEA) and then we construct the regression line and collapse limit line as shown in Fig. 1 below.

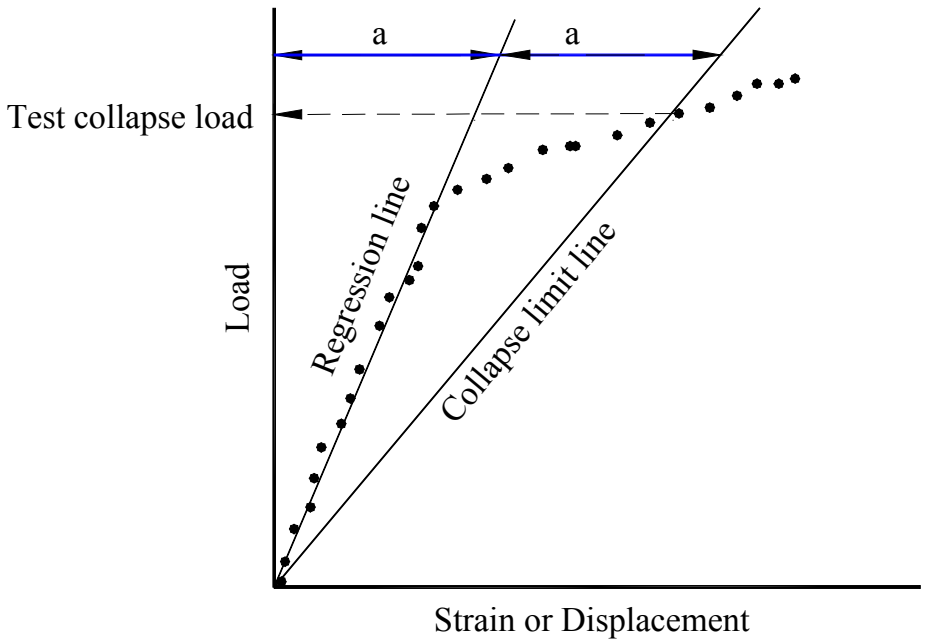

Fig. 1 Code-defined Collapse Load[13]

OBJECTIVES AND SCOPE

The objective of this work is to develop a procedure to compute the B_2 stress index and to develop guidelines for using the Finite Element Method for making this computation.

In Part II of this dissertation, the history of B_2 index is briefly reviewed and a new margin-consistent procedure for the calculation of the B_2 index is suggested.

In Parts III to V, experimental and analytical studies were conducted to demonstrate that FEA can simulate the nonlinear behavior of elbows and straight pipes under monotonic loadings within engineering accuracy. Part III focuses on the correlation between FEA and test results for straight pipes and moderately-thick-wall elbows subjected to in-plane closing and opening mode bending. In this part, the weld bead is neg-

ligible. Part IV concentrates on the FEA simulation procedures for thin-wall elbows with non-negligible welds under in-plane bending. All the elbow specimens in Parts III and IV are Stainless Steel 304L (SS304L). Part V contains an investigation of elbows (SS304L and Carbon Steel SA106-B) subjected to out-of-plane loading.

The work in Parts III to V is for monotonic loading. Conventionally, the B_2 indices are defined under monotonic loading. Even though Eq. (9) does accommodate earthquake or other dynamic loads, ASME Code committees have recently approved an equation similar to Eq. (9), but which can be applied to reversing dynamic loads, meaning severe earthquake loading. The new equation takes the form:

$$B'_1 \frac{P_D D_o}{2t} + B'_2 \frac{D_o}{2I} M_E \le 3.0 S_m$$

The B_2' stress indices of elbows and a few other components were determined from a series of high-level seismic experiments, but there is no guidance on how to calculate these B′ indices for new types of piping components. To define the B_2' index under cyclic loading, it will be necessary to redefine what is meant by collapse, and then use this definition in the calculation of a B_2 stress index. Part VI attempts to simulate two elbow tests subjected to 3/4-cycle in-plane cyclic loading, to give a preliminary indication of elbow behavior under such loading conditions.

This work covers only a few topics on B_2 stress index. There is still large amount of work to be done. For example, Equation (9) covers internal pressure, moment loadings and all possible combinations of pressure and moments. The effect of internal pressure will be an unavoidable topic (See Rodabaugh and George [14], 1957, Rodabaough[15], 1979, Prost et al. [16], 1983, Shalaby and Younan [17], 1997; [18], 1998 and Yu [19], 1998). In a

piping system, elbows are usually connected to flanges, straight pipes, valves etc. at one or both ends. The end effects or effect of flange locations will be another challenging topic (See Rodagaugh etc.[20], 1978, Natarajan and Mirza [21], 1981, Whatham and Thompson [22], 1979, Nordham and Kaldor [23], 1993; [24], 1993, Yu [19], 1998). At elevated temperatures, material properties may be significantly different from those at room temperature, which, as well as the thermal expansion, might contribute to changes of collapse behavior for piping systems or components. The effect of elevated temperature is also worth studying (See Prost et al. [16], 1983, Imazu et al. [25], 1979). This thesis does not investigate these problems. All cases are at room temperature without internal pressure and end effects.

Since this dissertation contains several papers either published or to be published, and each part is relatively independent, the literature reviews are enclosed in each individual part. Also, there is some repetition of the material to make each part a self-contained unit.

REFERENCS

1. ASME Boiler and Pressure Vessel Code. Section III, Division 1, "Nuclear Power Plant Components,", 1995 ed., ASME, New York

2. Rodabaugh, E.C. and Moore, S.E., "Evaluation of the plastic characteristics of piping products in relation to ASME code criteria", NUREG/CR-0261, ORNL/Sub-29-13/8, July, 1978, ppB-7

3 . Moore, S. E. and Rodabaugh, E. C. 1982. "Pressure Vessel and Piping Codes - Background for Changes in the 1981 Edition of the ASME Nuclear Power Plant Components Code for Controlling Primary Loads in Piping Systems," Journal of Pressure Vessel Technology, Vol. 104, p. 351.

4. ASME, 1995, Subparagraph NB-3213.1

5. Moss, D.R., "Pressure Vessel Design Mannual (2nd ed.)", Gulf Publishing Company, 1997, pp6

6. ASME, 1995, Subparagraph NB-3213.8

7. ASME, 1995, Subparagraph NB-3213.9

8. ASME, 1995, Subparagraph NB-3213.11

9. Wais, E.A. and Rodabaugh, E.C., "Background of stress intensification factors in piping design", PVP-Vol. 353, Pressure Vessel and Piping Codes and Standards, ASME 1997, pp3-12

10. Raju, P.P., WRC bulletin, Bulletin 301, Jan. 1985, ISSN 0043-2326

11. Rodabaugh, E.C. and Moore, S.E. 1978. "Evaluation of the Plastic Characteristics of Piping Products in Relation to ASME Code Criteria," NUREG/CR-0261, p. 5.

12. ASME Code, 1995, NB-3213.25

13. ASME Code, 1995, Appendix II, FIG. II-1430-1

14. Rodabaugh, E. C. and George, H. H., "Effect of Internal Pressure on Flexibility and Stress-Intensification Factors of Curved Pipe or Welding Elbows", Trans. Of ASME, May, 1957, p939-948

15. Rodabaugh, E. C., "Interpretive report on limit analysis and plastic behavior of piping products", WRC Bulletin 254, Nov., 1979, p65-82

16. Prost, J. P., Taupin Ph. and Delidais, M., "Experimental Study of Austenitic Stainless Steel Pipes and Elbows Under Pressure and moment Loadings", 7th SMiRT Conf., 1983, Chicago, G/G 5/5

17. Shalaby, M. A. and Younan, M.Y.A., "Limit loads for pipe elbows with internal pressure under in-plane closing bending moments", PVP-vol.347, ASME 1997, p203-213.

18. Shalaby, M. A. and Younan, M.Y.A., "Limit loads for pipe elbows subjected to in-plane opening moments and internal pressure", PVP-vol.368, ASME 1998, p163-170.

19. Yu, L., "Elbow stress indices using finite element analysis", NCSU Ph.D. Dissertation, Dec., 1998

20. Rodabaugh, E.C., Iskander S.K., Moore S.E., March, 1978, "End Effects on Elbows Subjected to Moment Loadings" ORNL/Sub-2915/7, Dist. Category NRC-5.

21. Natarajan, R. and Mirza, S., "Stress analysis of curved pipes with end restraints subjected to out-of-plane moments", Proceedings of SMiRT Conference, Paris, 1981, F 2/8, p1-9

22. Whatham, J. F., " The bending and pressurizing of pipe bends with flanged tangents", Nuclear Engineering and Design 54 (1979), p17-28

23. Nordham, D. J. and Kaldor, L., M., "Design prodedure for stress intensification factors of 90-deg curved pipe having various tangent lengths", J. of Pressure Vessel Technology, Aug. 1993, vol. 115, p313-324.

24. Nordham, D. J. and Kaldor, L. M., "Design procedure for flexibility factors of 90-deg curved pipe having various tangent lengths", J. of Pressure Vessel Technology, Aug. 1993, vol. 115, p319-324.

25. Imazu, A., Sakakibara, Y., Nagata, T. and Hashimoto, T., "Plastic instability test of elbows under in-plane and out-of-plane bending", Trans. of the 5th International Conf. on Structural Mechanics in Reactor Tech., 1979, Berlin, Germany, E6/5

PART II

A NEW MARGIN – CONSISTENT PROCEDURE FOR THE CALCULATION OF THE B_2 STRESS INDEX

ABSTRACT

In Section III of the ASME Boiler and Pressure Vessel Code, the design equation for primary stresses in piping contains stress equations for straight pipes that are modified by stress indices so that the equations can be applied to other piping components. In this part, a new procedure for calculating the B_2 stress index, which applies to stresses for bending, is suggested. The resulting stress index equation, which is the ratio of the collapse moment of a straight pipe to the collapse moment for any component, gives a B_2 value of 1.00 when applied to a straight pipe and a safety margin for the component that is always the same as for the straight pipe. This procedure is based on the Code-defined collapse moment, which we determine using nonlinear finite element analysis (FEA), supported by experimental data. The B_2 values for three elbow configurations subjected to in-plane closing moment will be presented. The values of B_2 obtained using this new definition are 58~86% of the values obtained using the current Code procedure when applied to stainless steel 304L 90° long radius butt-welding elbows.

1. INTRODUCTION

Most piping in nuclear power plants is designed by rules given in Section III of the ASME Boiler and Pressure Vessel Code (the Code)[1]. In the Code, stresses are di-

vided into three categories: Primary which "is any normal stress or a shear stress developed by an imposed loading which is necessary to satisfy the laws of equilibrium..."[2]; Secondary which is "a normal stress or a shear stress developed by the constraint of adjacent material or by self-constraint of the structure. The basic characteristic of a secondary stress is that it is self-limiting."[3]; and Peak stress.

In piping design, Code Equation (9), which governs the primary stress intensity for design loads, has the following form:

$$B_1 \frac{PD_o}{2t} + B_2 \frac{D_o}{2I} M_i \leq 1.5 S_m \qquad (1)$$

where B_1 and B_2 are stress indices for internal pressure and bending. The equation has been described as assuring "against catastrophic membrane failure..."[4] or placing "bounds on loading such that necessary conditions for a collapse load will not exist anywhere in the piping system"[5].

The stress indices are used to modify nominal stress equations for straight pipes so that the behavior of piping components such as elbows can be controlled using the same basic stress limits as for straight pipe. Moore and Rodabaugh[6] state that "The B_1 and B_2 stress indices reflect the capacities of various piping products to carry load without gross plastic deformation."

Paragraph NB-3682 of the Code provides the following general definition of stress indices:

$$B, C, K, \text{or } i = \frac{\sigma}{S} \qquad (2)$$

where, for the B indices, σ represents the stress magnitude corresponding to a limit load and S is a nominal stress associated with the limit load. Values for the B, C and K stress

indices are given in Table NB-3681(a)-1 for a variety of piping components. For elbows the user is referred to equations in NB-3683.7 where B_2 is defined as

$$B_2 = \frac{1.30}{h^{2/3}} \geq 1.0 \tag{3}$$

where h is the characteristic bend parameter which is defined as

$$h = \frac{tR}{r_m^2} \tag{4}$$

and where the remaining parameters are defined in the Nomenclature Section.

"For piping products not covered by NB-3680, stress indices ... shall be established by experimental analysis (Appendix II) or theoretical analysis[7]." Appendix II, however, has the following section, titled Experimental Determination of Stress Indices for Piping: "In course of preparation. Pending publication, stress indices for piping shall be determined in accordance with the rules of NB-3680[8]." The appendix does contain a procedure for obtaining experimentally a value for the collapse load[9] although there is no guidance on how to use this information to obtain the stress indices.

To fully understand Eq. (1) [Eq.(9) of the Code] and the B_2 stress index, it is necessary to understand the development of the equation and the index. In the following, the history of B_2 index is briefly reviewed and a new margin-consistent procedure for the calculation of B_2 is proposed.

2 HISTORY

As far as we know, no paper has comprehensively documented the development of Eq. (9) of the Code and the B_2 index before the current study. By reviewing the large volume of relevant literature and discussing the topic with some of the original Code

developers, we obtained a nearly complete picture of the history, which is documented in Matzen and Tan [10]. In this section, only the significant dates in the development of nuclear piping codes related to B_2 index are listed. For details, see Ref. [10].

Table 1. Significant dates in the development of nuclear piping codes

Year	Code	i or C_2	B_2
1935	B31 (first piping code)	No equations	
1955	B31.1	$i = \frac{0.9}{h^{2/3}} \geq 1$	
1969	B31.7	$C_2 = \frac{1.95}{h^{2/3}}$	$B_2 = 0.75C_2 = \frac{1.4625}{h^{2/3}} \geq 1.125$
1971	ASME Section III	$C_2 = \frac{1.95}{h^{2/3}}$	$B_2 = 0.75C_2 = \frac{1.4625}{h^{2/3}} \geq 1.125$
1981	ASME Section III	$C_2 = \frac{1.95}{h^{2/3}}$	$B_2 = \frac{2}{3}C_2 = \frac{1.30}{h^{2/3}} \geq 1.00$
1995	ASME Section III, Stress limit set to $4.5S_m$	$C_2 = \frac{1.95}{h^{2/3}}$	$B_2 = \frac{2}{3}C_2 = \frac{1.30}{h^{2/3}} \geq 1.00$
2000	ASME Section III, Stress limit set to $3.0S_m$	$C_2 = \frac{1.95}{h^{2/3}}$	$B_2 = \frac{2}{3}C_2 = \frac{1.30}{h^{2/3}} \geq 1.00$
			B_1', B_2'

3 SUGGESTED NEW PROCEDURE FOR CALCULATING A MARGIN-CONSISTENT B_2 STRESS INDEX

The work described in this dissertation is the extension work of Matzen and Yu (1998)'s research. They began by using the equation

$$B_2 = \frac{S_y Z}{M_{CL}} \tag{5}$$

where M_{CL} is obtained from either test data or finite element analysis, but then showed that, when applied to straight pipes, the equation can produce values that are less than one. This aspect of Matzen and Yu's work was discussed several times by the ASME Working Group on Piping Design from 1996 to 1999, and that group suggested that any

procedure used to calculate a B_2 stress index should produce a value of one when applied to a straight pipe. Matzen and Yu tried various modifications of Eq. (5), including replacing S_y with the equivalent von Mises stress at the point of Code-defined collapse, (this resulted in slightly lower B_2 values) and using the plastic section modulus in place of the elastic modulus Z (this resulted in a B_2 of about 1.0 for the straight pipe.)

Then, Matzen and Tan [10] suggest that a procedure that will always result in a B_2 of 1.0 for a straight pipe is to normalize Eq. (5) for any component by dividing it by the equation evaluated for a straight pipe with the same material and geometric properties as the component, i.e.

$$B_{2,\text{normalized}} = \frac{B_{2,\text{component}}}{B_{2,\text{straight pipe}}} \tag{6}$$

They observed that, when Eq. (6) was substituted into Eq. (5), the result was just the ratio of the limit moments, i.e.

$$B_{2,\text{normalized}} = \frac{\dfrac{S_y \cdot Z}{M_{CL,\text{component}}}}{\dfrac{S_y \cdot Z}{M_{CL,\text{straight pipe}}}} = \frac{M_{CL,\text{straight pipe}}}{M_{CL,\text{component}}} \tag{7}$$

Thus the question of whether Z is elastic or plastic is irrelevant. This work by Matzen and Tan is the basis for the procedure described later in this part.

Equation (7) can be derived in a more straight forward manner [11] by setting the stress limit for any component equal to the stress limit for a straight pipe, i.e.

$$\sigma_{\text{component}} = \sigma_{\text{straight pipe}} \tag{8}$$

Then, referring to Eq. (2), the definition of B_2 index, Eq. (8) can be written as follows:

$$B_{2,\text{component}} \cdot S_{\text{component}} = B_{2,\text{straight pipe}} \cdot S_{\text{straight pipe}} \qquad (9)$$

Rearranging Eq. (9), letting $B_{2,\text{straight pipe}}=1.0$, and canceling the section modulii Z, we obtain Eq. (10), i.e.:

$$\begin{aligned} B_{2,\text{component}} &= B_{2,\text{straight pipe}} \frac{S_{\text{straight pipe}}}{S_{\text{component}}} \\ &= \frac{M_{\text{CL,straight pipe}}/Z}{M_{\text{CL,component}}/Z} \\ &= \frac{M_{\text{CL,straight pipe}}}{M_{\text{CL,component}}} \end{aligned} \qquad (10)$$

This equation presumably applies to any component, although the details of its application to more complicated components such as branch connections will need to be developed. The attribute of having the B_2 stress index be 1.0 for straight pipes was acknowledged in the 1982 paper by Moore and Rodabaugh in their work on C_2 indices for different bend angles. As the subtended bend angle approaches zero, the elbow approaches a straight pipe, and the authors suggested that, in the limit, the index should approach 1.0[12].

Another advantage in using Eq. (7) as the definition for the B_2 index is that the margin for the component always turns out to be the same as the margin for the straight pipe of the same geometric and material properties. This can be seen from the following proof, where the margin is defined, as it was in the paper by Touboul et al.[13], as the ratio of the collapse moment of the component divided by the Code allowed moment of the component.

$$
\begin{aligned}
\text{Margin}_{\text{component}} &= \frac{M_{\text{CL, component}}}{M_{\text{code, component}}} \\
&= \frac{M_{\text{CL, component}}}{\left(1.5S_m \cdot Z/B_{2,\text{ normalized}}\right)_{\text{component}}} \\
&= \frac{M_{\text{CL, component}}}{1.5S_m \cdot Z} B_{2,\text{ component, normalized}} \\
&= \frac{M_{\text{CL, component}}}{1.5S_m \cdot Z} \cdot \frac{M_{\text{CL, straight pipe}}}{M_{\text{CL, component}}} \\
&= \frac{M_{\text{CL, straight pipe.}}}{1.5S_m \cdot Z} = \text{Margin}_{\text{straight pipe}}
\end{aligned}
\tag{11}
$$

4 RESULTS

We have applied our definition of B_2 to different elbow configurations, with values of h ranging from 0.072 to 0.997, subjected to in-plane-closing moment. These components are all butt-welding, seamless, 304L stainless steel, long radius, 90^o elbows without internal pressure at room temperature. Nominal geometric and Code material properties were used. Nonlinear FEA was utilized to obtain the collapse moments. The B_2 values of four schedules are tabulated in Table 2. The two rows labeled $B_{2,\text{straight pipe}}$ and $B_{2,\text{ elbow}}$ show that using Eq. (5), which would seem to be a literal reading of the Code as given in Eq. (2), can lead to values for straight pipes that are less than one. The next row, $B_{2,\text{elbow, normalized}}$, has values that are all greater than one, as expected. The last row is the ratio of the B_2 value we calculate compared to the Code value. The values for $B_{2,\text{straight pipe, normalized}}$ would, of course, all be 1.00.

Table 2. Examples of New-definition B_2 Values vs. Code B_2 Values for Elbows

Size and Schedule		8" Sch5[1]	2"Sch40[1]	2"Sch160[1]
h		0.072	0.375	0.997
Z	(in^3)	6.13 [1]	0.561 [1]	0.979 [1]
	(cm^3)	100. [1]	9.19 [1]	16.0 [1]
S_y	(ksi)	25.0 [2]	25.0 [2]	25.0 [2]
	(MPa)	172. [2]	172. [2]	172. [2]
$B_{2,straight\ pipe}$ (Eq. (5))[3]		0.92	0.89	0.83
$B_{2,elbow}$ (Eq. (5))[3]		3.95	1.46	0.94
$B_{2,elbow,\ normailized}$ (Eq.(6))[3]		4.30	1.65	1.13
$B_{2,elbow,\ code}$ (Eq. (3))		7.50	2.50	1.30
Percent Reduction [4]		43%	34%	12%

[1] Nominal geometric properties, Z is the elastic section modulus

[2] Code values

[3] Collapse moments obtained from FEA or experiments were substituted into the referenced equations. For elbows, the moments are in-plane closing.

[4] Percent Reduction $= \dfrac{\left| B_{2,elbow,\ normalized} - B_{2,elbow,\ Code} \right|}{B_{2,elbow,\ Code}}$

The results for all the cases studies are displayed graphically in Fig. 1.

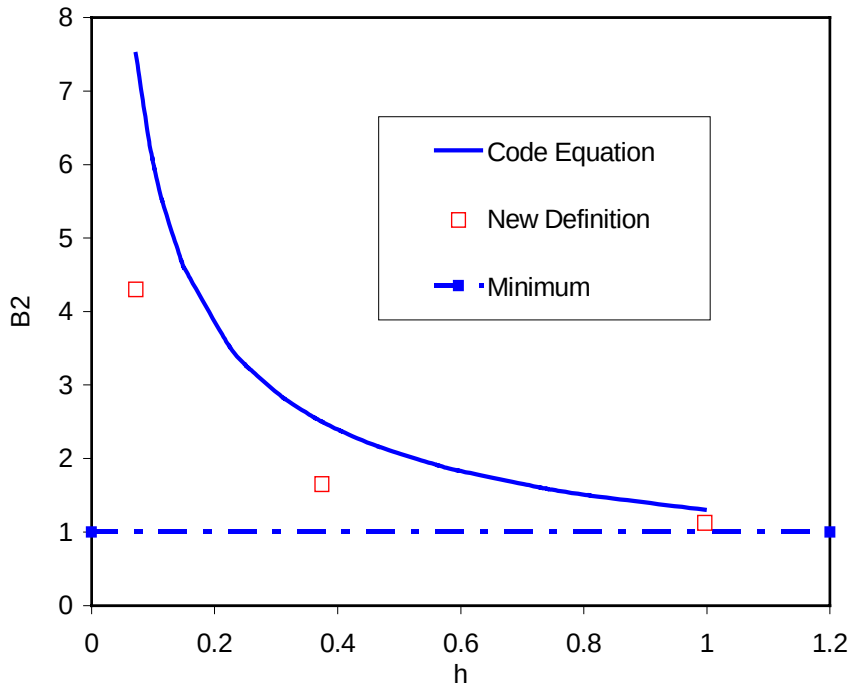

Fig. 1 B_2 Values vs. h

The FEA procedures we used above were supported by experiments, which will be demonstrated in Parts III to V. An example illustrating how to obtain the values of B_2 in Table 2 is presented in Appendix A. The FEA code using ABAQUS ELBOW31 for 8"Schedule 5 straight pipe is shown in Appendix B.

5 SUMMARY AND CONCLUSION

In our review of the history of Eq. (1) [Eq. (9) in the Code] and the B_2 index, we conclude that the developers of this equation in the Code were attempting to prevent gross plastic (and nonlinear) behavior of piping by relating the mildly plastic (and non-linear) behavior of components to straight pipes and then using appropriate allowable stresses. The term 'mildly' is used here because the Code-defined collapse load is, for most elbows, well below the instability load, that is the load for which there is an actual

physical collapse. The corollary to our conclusion is that stress index of a component should be related to the collapse behavior of a straight pipe which has the same material and geometric properties as the component. This is the basis of our suggested procedure for calculating the B_2 index as the ratio of collapse moments. Using this procedure, (a) the B_2 for a straight pipe will always be 1.00 and (b) the margin for any component will be the same as for a straight pipe with the same material and geometric properties. Also, in the examples presented, the suggested procedure results in values of B_2 which are 58~86% of the values obtained from Eq. (3). Additional work needs to be done before a more definitive statement can be made regarding the B_2 stress index values for elbows, or before it is possible to determine how the results of this procedure would relate to Code equations for other types of components.

6 NOMENCLATURES

B_1 = primary stress index for pressure
B_2 = primary stress index for bending
C_2 = secondary stress index for bending
D_o = outside diameter of pipe
h = characteristic bend parameter, tR/r_m^2
i = stress intensification factor (SIF). Also a stress index for detailed analysis in NB-3200, given in tables NB-3685.1-1&2
I = moment of inertia
K = local stress index
M_{CL} = Code defined collapse moment
M_i = resultant moment due to a combination of Design Mechanical Loads
P = design pressure
R = nominal bend radius of elbow

r_m = mean pipe radius, $(D_o-t)/2$

S = nominal stress

S_m = allowable design stress intensity value

t = nominal wall thickness

Z = section modulus

σ = stress magnitude corresponding to a limit load

7 REFERENCES

1. ASME, 1995. Boiler and Pressure Vessel Code, Section III, Division 1 – Subsections NB, NC and ND. American Society of Mechanical Engineers, New York.

2. ASME, 1995, Subparagraph NB-3213.8

3. ASME, 1995, Subparagraph NB-3213.9

4. Dodge, W.G. and Moore, S.E., " Stress Indices and Flexibility Factors for Moment Loadings on Elbows and Curved Pipe", WRC Bulletin, 179, December 1972, p. 2.

5. Rodabaugh, E.C. and Moore, S.E. 1978. "Evaluation of the Plastic Characteristics of Piping Products in Relation to ASME Code Criteria," NUREG/CR-0261, p. 5.

6 . Moore, S. E. and Rodabaugh, E. C. 1982. "Pressure Vessel and Piping Codes - Background for Changes in the 1981 Edition of the ASME Nuclear Power Plant Components Code for Controlling Primary Loads in Piping Systems," Journal of Pressure Vessel Technology, Vol. 104, p. 351.

7. ASME, 1995, Subsubparagraph NB-3681 (d)

8. ASME, 1995 Appendix II, Experimental Stress Analysis, Section II-1800, Experimental Determination of Stress Indices for Piping

9. ASME, 1995, Appendix II, Experimental Stress Analysis, Section II-1430, Criterion of Collapse Load

10. Matzen, V.C. and Tan, Y., "The History of The B_2 Stress Index and a New Margin - Consistent Procedure for its Calculation", PVP, Vol. 399, ASME 2000, pp251-258

11. Jim McCabe of the Electric Boat Division of General Dynamics, Groton, CT, suggested this form of the derivation in a private communication.

12. Moore, S. E. and Rodabaugh, E. C. 1982. "Pressure Vessel and Piping Codes - Background for Changes in the 1981 Edition of the ASME Nuclear Power Plant Components Code for Controlling Primary Loads in Piping Systems," Journal of Pressure Vessel Technology, Vol. 104, p. 351.

13. Touboul, F., Ben Djedidia M. & Acker, D., “Stress Index Method of Design: Application to In-plane Closing Collapse of Elbows,” Int. J. Pres. Vessel. & Piping, Vol. 33, 1988, pp. 153- 164.

PART III

CORRELATION OF TEST AND FEA RESULTS FOR THE NONLINEAR BEHAVIOR OF STRAIGHT PIPES AND ELBOWS

ABSTRACT

This part describes two four-point-bending tests on straight pipes, and two in-plane bending tests on elbows. Geometric and material nonlinearities were evident in both sets of tests. Nonlinear finite element analyses were carried out to simulate the tests and the correlation between test and analysis results were surprisingly good. It is concluded that nonlinear finite element analysis can simulate the complicated nonlinear behaviors of the piping components tested within acceptable limits of engineering accuracy.

1 INTRODUCTION

As computer technology advances, more and more powerful Finite Element Analysis (FEA) software becomes available with innovative finite element methodology. One area where this technology can be applied to advantage is in piping. Piping components such as elbows exhibit significant material and geometric nonlinear behavior when subjected to severe loadings. The ability to simulate this nonlinear behavior would be beneficial to the improvement of design codes because the alternative of performing experiments to carry out parametric studies for different loadings, pipe sizes, materials, etc. is costly. Although not the focus of this part, it is useful to review briefly some concepts of piping design so as to put this part in its proper context.

Section III of the ASME Boiler and Pressure Vessel Code [1](ASME, 1995) allows for design by either detailed analysis or simplified analysis. The simplified method uses stress indices, which are scalar multipliers for nominal stresses, while the detailed analysis is usually carried out using the finite element method. For many components, it is possible to select numerical values for the stress indices from tables or, for components such as elbows, obtain the values by evaluating simple equations. For those components that are not included in the table, and for which equations are not provided, the user is allowed to use experimental or analytical results. In general experimental results are reliable but may be costly, while FEA is reasonably economical. FEA can also replicate complicated loading and boundary conditions. If FEA could be shown to simulate accurately the nonlinear inelastic behavior of piping components, then it could be used to obtain values of B_2 rather than experiments. The objective of the work described in Part III, IV and V of this thesis is to demonstrate that FEA can in fact simulate this complicated behavior within acceptable limits of engineering accuracy. The two piping components considered are straight pipes and elbows.

In Part II of this thesis, the history of the B_2 stress index was presented and a new margin-consistent procedure for its calculation defined. That procedure requires a collapse load for a component and for the corresponding straight pipe segment, both of which are obtained using the FEA procedures described below.

2 BACKGROUND

In 1974, Mello and Griffin [2] carried out a series of inelastic finite element analyses on 304 stainless steel (ss), large diameter, long radius elbows using the MARC

computer program [3]. For one of these specimens, a 6" Sch40 elbow, the analytical results were compared with experimental measured data. The experimental setup is shown schematically in Fig.1-a. Their FEA studies were based on nominal piping dimensions. For the elbow portion, 3-node constant bending, pipe-bend elements were used, which admitted ovalization in the cross-section but neglected elbow-end constraints. Beam elements were used for the straight portions. Actual stress-strain data obtained from a specimen cut from the elbow were used in the analysis. The load-deflection curves predicted by FEA are compared with experimental measured data in Fig.1-b (all graphs are based on digitized data from the original papers.) Although there was general agreement in the shapes of the curves, there were substantial differences. Mello and Griffin commented that the difference was due to neglecting the elbow-end constraints.

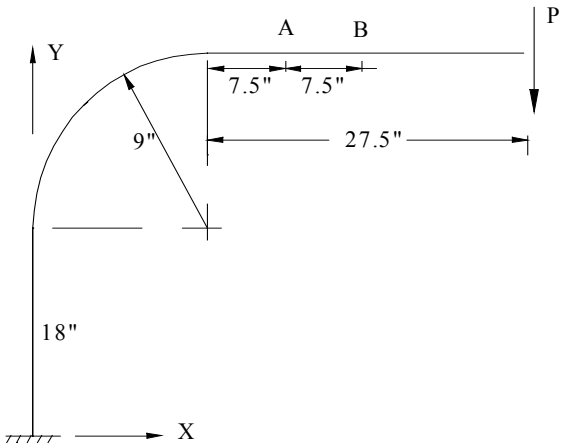

(a)

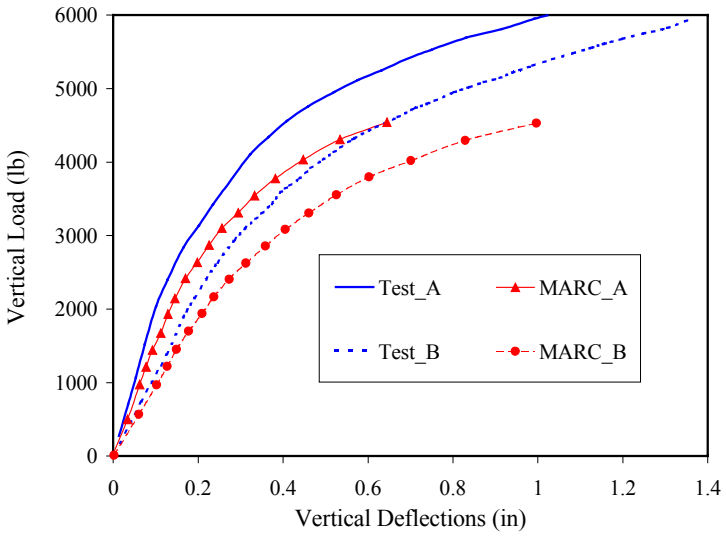

(b)

Fig. 1 Mello and Griffin Testing Arrangement and Load-Deflection Curves [2]

In 1980, Sobel and Newman [4] conducted a room temperature experiment on a 16", 90°, long radius 304ss elbow subjected to in-plane closing mode pure bending, as shown in Fig.2-(a). They carried out a simplified finite element analysis to simulate the test using MARC. In their studies average dimensions, which came from pre-test in-

spection data given in the test report, were used. For the elbow portion, the MARC pipe-bend element 17 was used, which assumed that "each elbow element deforms uniformly over its axial length, with the amount of deformation being dependent on the magnitude of the bending moment"[4]. For straight tangent portions, beam element 14 was used. Coupon specimens were cut from "a low strained region near the end of the post tested elbow"[4], and the average of two tensile coupon stress-strain curves at room temperature was used in their FEA studies. Compared with measured test data, their FEA result "underestimates the experimental buckling load by 10 percent and overestimates the deformation at a given load, particularly at the higher load levels"[4], as shown in Fig.2 (b) and (c). They concluded that the discrepancy arose from inaccuracy of the stress-strain curve for elbows. They state "Until the challenging problem of accurately determining representative stress-strain curves for complex (double curvature) components is resolved, it is going to continue to be a difficult task to make precise statements about the accuracy of various simplified and detailed methods of analysis, particularly if we are to judge this accuracy by comparing analytical and experimental results. We strongly suggest that this important material properties question be a high priority item for investigators in this area..." This was exactly the same conclusion we arrived at in our (successful) attempt to reconcile experimental and analytical results, described later in this part.

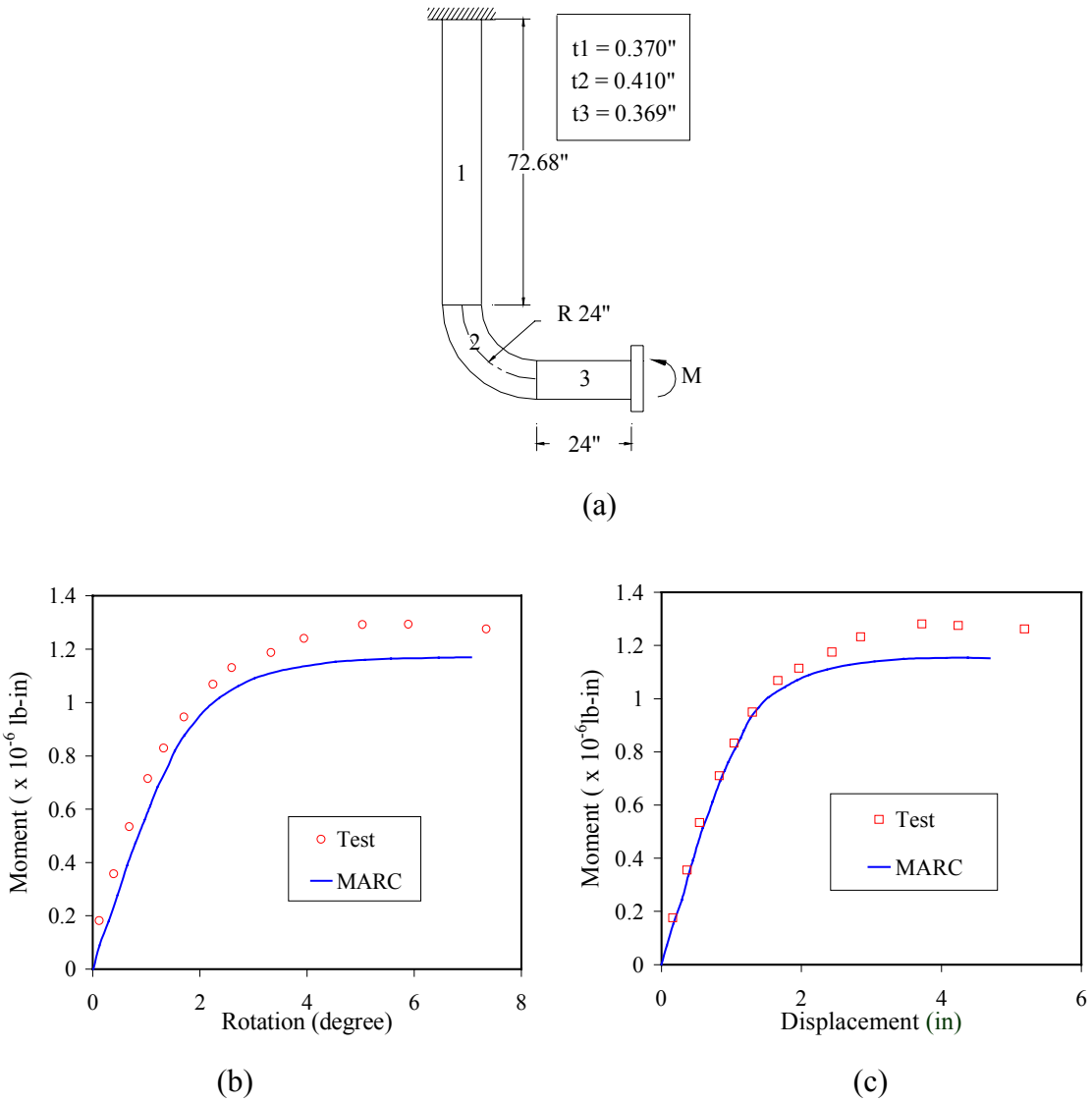

Fig. 2 Sobel and Newman 1980 Testing Arrangement and Moment-Rotation/Displacement Curves[4]

In 1986, Sobel and Newman[5] conducted two more elastic-plastic tests (plus a creep test) on specimens that had the same nominal dimensions as their 1980 test, but this time one of the tests was conducted at 1100°F. For the elevated temperature test, two coupons cut from one of the elbow specimens were tested at the elevated temperature. The authors do not address the interesting question of how the loading rate at this elevated temperature might have affected their stress-strain data. To be meaningful, the

coupon test should (and might) have been conducted at the same rate as the elbow test. Their FEA procedure was also similar to their work in 1980, except that, this time, they used both simplified and detailed MARC analyses. As before, the MARC special pipe-bend element 17 was used in elbow portions for the simplified analysis, and MARC beam element 14 was used in straight tangent portions. Consequently, the elbow "end effect" provided by the straight pipe portions was neglected. In the detailed analysis, the isoperimetric, doubly curved, quadrilateral shell element 4 was used for the entire component, which accounts for the stiffening "end effect". The correlation is shown in Fig.3 (b) for moment-rotation and Fig.3 (c) for moment-displacement. They concluded that "The simplified analysis is found to considerably overestimate the measured results (deformation)..." and the detailed analysis' predictions are in "reasonably good agreement with the measured deformation (crown strain, end rotation and displacement)"[5].

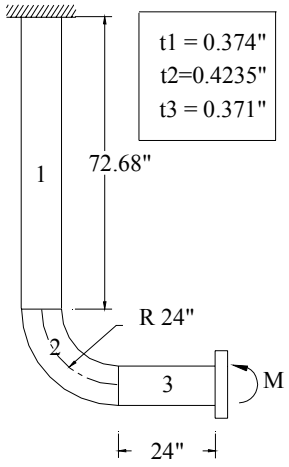

(a)

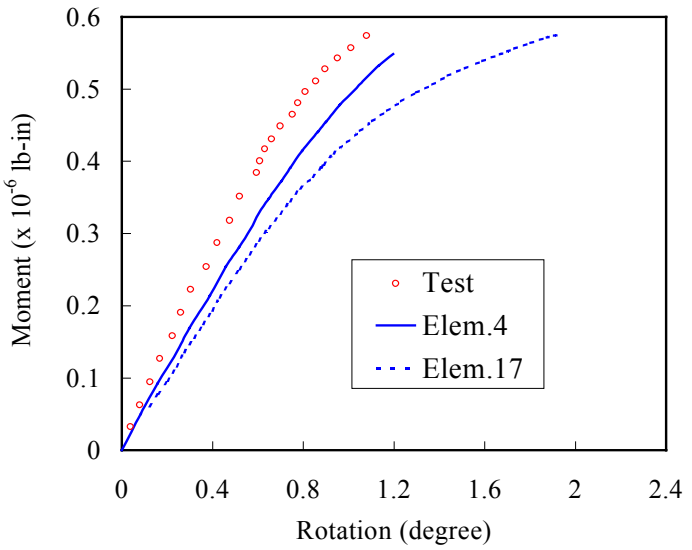

(b)

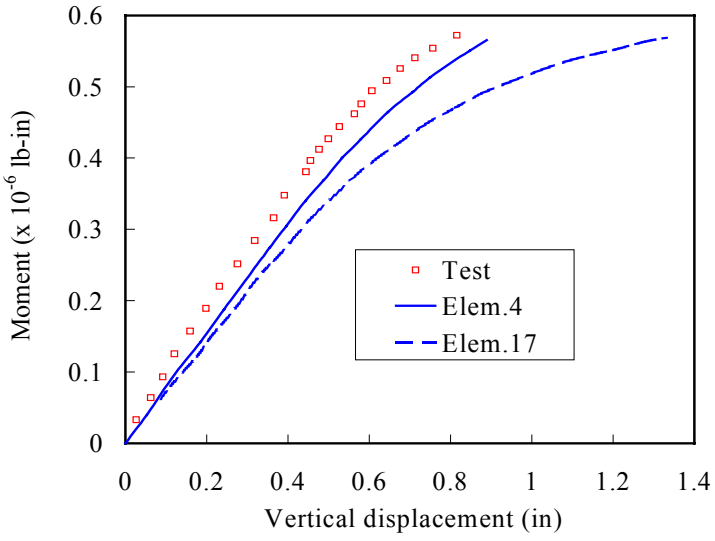

(c)

Fig. 3 Sobel and Newman 1986 Testing arrangement and Moment-Rotation/Displacement Curves [5]

In 1987, Dhalla[6] used Sobel and Newman's 1980 data (Fig.2-a) for his own attempt at reconciliation. His FEA procedure was similar to Sobel and Newman's (1986): average dimensions were used which came from pre-test inspection data given in the test report and "Time independent material properties were obtained from miniature uniaxial tension coupon specimens extracted from low strained regions near the end

of curved elbow"[6]. His study used MARC fully compatible doubly curved isoperimetric thin shell elements, taking account of both geometric and material nonlinearities. Figure 4 shows his FEA prediction compared with test data. He concluded that "shell analysis predictions were in good agreement with the measured response up to 60 percent of the measured collapse load" and "the overall correlation was not as good at higher load levels"[6]. The shell analysis prediction of collapse moment was 15 percent higher than the collapse moments measured in the test. Dhalla also commented that the discrepancy was due to inaccuracy of material properties obtained.

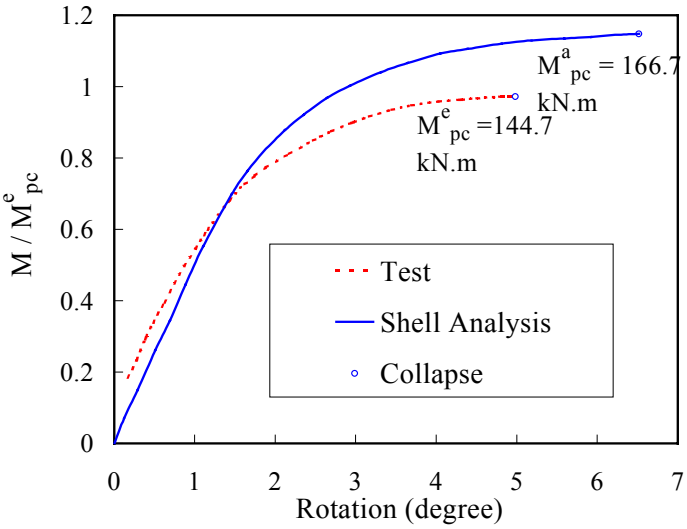

Fig. 4 Dhalla Moment-Rotation Curves[6]

In 1989, Suzuki and Nasu[7] analyzed 12" and 24" butt-welded elbows subjected to in-plane bending. The four-node shell element of ADINA/v5 was used, considering both geometric and material non-linearities. The material properties came from tensile test data of specimens and a three-linear-segment stress-strain model was used, which consists of elastic portion, perfectly plastic portion, and linear strain hardening portion. Compared with test data, good agreement for the load-displacement relationships was

obtained, with difference from “5 to 10% of the loads in the non-linear deformation range”[7], as shown in Fig.5-(b) and (c).

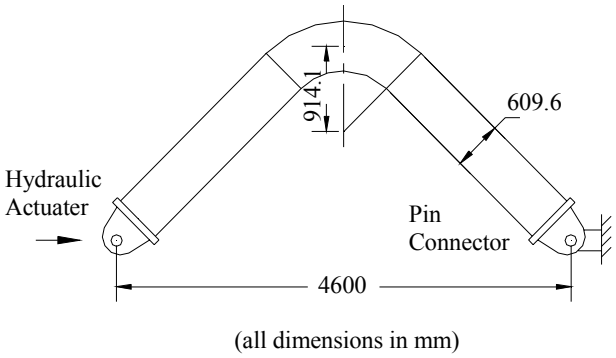

(a) 24” test

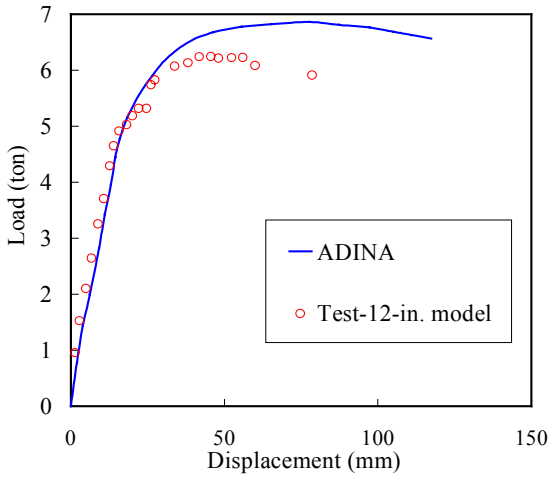

(b)

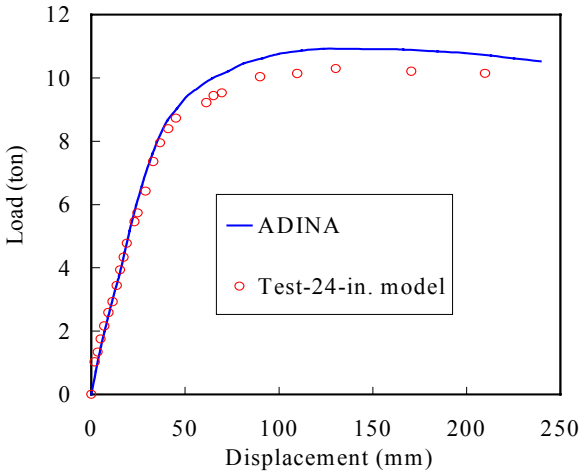

(c)

Fig.5 Suzuki and Nasu Testing Arrangement and Load-Displacement Curves[7]

In 1995, Kussmaul et al. [8] studied three 90° 400 mm pipe bends tests, in which the components were subjected to in-plane opening mode bending (IKA1), in-plane closing mode bending (IKA2), and out-of plane bending (IKA3) without internal pressure. The material was 15MnNi63, and a sample taken from a straight pipe section adjacent to the inductive manufactured pipe bend IKA1 was extracted and tested. In their study, the stress-strain relationship obtained from this material test was used, assuming that pipe and pipe bend portions have same material properties. For IKA1, special pipe and pipe bend element ELBOW31(ABAQUS[9]) was used and the numerical results were up to 15% higher in load value. For IKA2, three sets of FEA were carried out: shell elements of SAN[10], 20-node solid element of ABAQUS[9], PIPE31 and ELBOW31 of ABAQUS[9]. They concluded that those three sets of numerical results showed good agreement with measured data of the global behavior of test; and, for IKA3, FEA gave 15-20% higher load value than measured data. Graphical results were not given in their paper. In their conclusions, they also indicated that the "reasons of discrepancies were due to unknown differences in the material properties of different parts of the pipe/pipe bend assembly, which were not considered in the calculations"[8].

Considering the papers described above, it becomes clear that the problem of simulating the nonlinear inelastic behavior of elbows by FEA has not been fully solved, and one of the central issues is how to obtain an accurate representation of the material constitutive model. In this paper, an FEA procedure, including development of the monotonic constitutive model, is developed which is able to improve on the ability to simulate the nonlinear behavior of elbows. Two sets of test data are used – one from a test on straight pipes (Ju, [11]) and one from a test on elbows (Yu, [12]). In the straight

pipe tests, the loading was pure bending. For the elbow tests the loading (in-plane only) was applied through pins at each end of the specimen and was displacement controlled.

3. STRAIGHT PIPE

3.1 Experiments

As described in Part II, the calculation of the B_2 stress index for a component involves not only the behavior of piping component, but also the corresponding straight pipe (with the same geometric properties and same material properties as the component). For this reason two straight pipe experiments from Ju [11] were used (Test Numbers 6 and 11) to ensure that the FEA procedure could accurately represent the nonlinear behavior. The specimens were Aluminum 6061-T6 drawn tubes. In each test, the specimen was subjected to monotonic pure bending applied continuously until collapse. The FEA models are based on the geometric and material properties provided by Ju[11] and shown in Table 1. The fact that the material is Aluminum is inconsequential for the purposes of this study since the objective is to show that, given the material and geometric properties, the nonlinear inelastic behavior of the specimen can be simulated using FEA.

3.2 Material Model

It was assumed that the material was isotropic, though the experimental data showed that there was some anisotropy[11]. A Ramberg-Osgood model, given in Eq. (1), was used as the axial stress-strain curve in the FEA models, as recommended by Ju[11]. The values of n, σ_y, and E are given in Table 1. We used a multi-linear representation of the analytic function for the ANSYS input.

$$\varepsilon = \frac{\sigma}{E}\left[1 + \frac{3}{7}\left(\frac{\sigma}{\sigma_y}\right)^{n-1}\right] \qquad (1)$$

Table 1. Geometric and material characteristics for Ju's tests[11]

Exp. No	D_o (in)	D_o/t	L/D_o	E ($\times 10^3$ ksi)	S_y (ksi)	σ_y (ksi)	n
6	1.25	35.7	24.0	9.77	41.1	40.9	28
11	1.25	19.5	24.0	9.96	44.8	44.8	37

3.3 FEA Models

The FEA code used in this study is ANSYS v5.4 [13] and ABAQUS v6.1.

For ANSYS, Shell models were used. Taking advantage of double symmetry, quarter models of the straight pipe specimens with doubly symmetric boundaries were built using shell elements. It was assumed that the test specimens were circular cylindrical shells with uniform wall-thickness and without initial geometric imperfection, although Ju indicated that there were slight imperfections. The effective length of the test specimens was 30". Since "each end of the test specimens was fitted with a close-fitting solid extension rod, which extended more than 3 diameters into the free ends of the shell" [11], the end condition was modeled as a rigid plate. The FEA analyses were rotation controlled, where the rotation was applied at the node located at the center of the rigid plate, and the rigid body motion was prevented by constraining one of the two nodes in the double symmetry planes. In the FEA models, the ANSYS switches to include large deformation effects in a static analysis and to active stress stiffness effects in a nonlinear analysis were both turned on.

Both SHELL43 and SHELL181 were used. For Test No.11 (the thicker pipe) these elements worked very well, compared with test data, for $\kappa_1/\kappa<0.5$; and, thereafter, SHELL43 became stiffer than test results, while SHELL181 still performed surprisingly well. For Test No. 6 (very thin wall pipe), convergence difficulties using SHELL43 were encountered, while SHELL181 again worked well. The ANSYS v5.4 Help Manual indicates that "SHELL181 can be used instead of SHELL43 for many problems that have convergence difficulty with SHELL43"[14], and recommend "using SHELL181 for nonlinear structures"[15]. Thus SHELL181 was used for all subsequent analyses on the straight pipes.

By doing mesh convergence studies, it was found that using 18 elements evenly distributed around the semi-circumference for Test No.6, and 8 elements evenly distributed around the semi-circumference for Test No.11, as shown in Figs. 6 and 7, were needed to give acceptable results. Finer meshes resulted in negligible improvement.

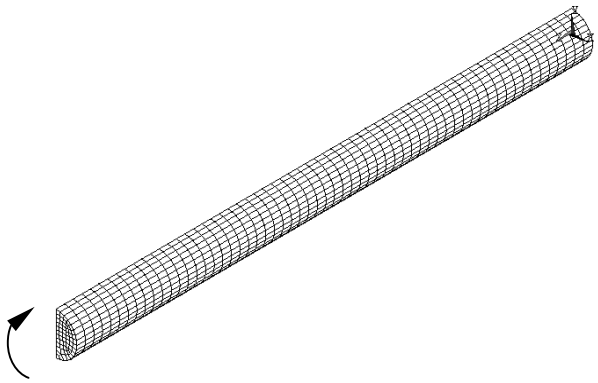

Fig. 6 Quarter FEA Shell Model for Test No.6 (D/t=35.7)

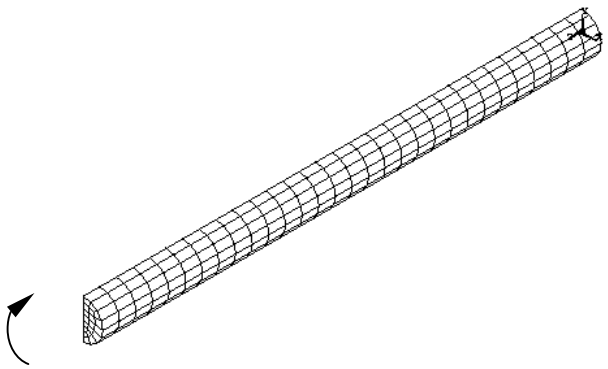

Fig. 7 Quarter FEA Shell Model for Test No.11 (D/t=19.5)

For ABAQUS, Elbow models were utilized using Element ELBOW31, which is a 2-node elbow element in space "intended to provide accurate modeling of the nonlinear response of initially circular pipes and pipebends when distortion of the cross-section by ovalization and warping dominates the behavior"[16]. In the ABAQUS Elbow models to simulate the two straight-pipe tests reported by Ju [11], it is assumed that the initial cross-sections were circular and the average measured wall thicknesses were used throughout the pipes. The boundary conditions are no warping and no distortion for both end cross-sections. For each test, twenty ELBOW31 elements were used.

3.4 Correlation of Tests and FEA results

Our FEA results along with Ju's test data are shown in Fig.8. The moments are normalized to the theoretical limit moment, as are the curvatures. The correlation is seen to be excellent for both ANSYS Shell models and ABAQUS Elbow models.

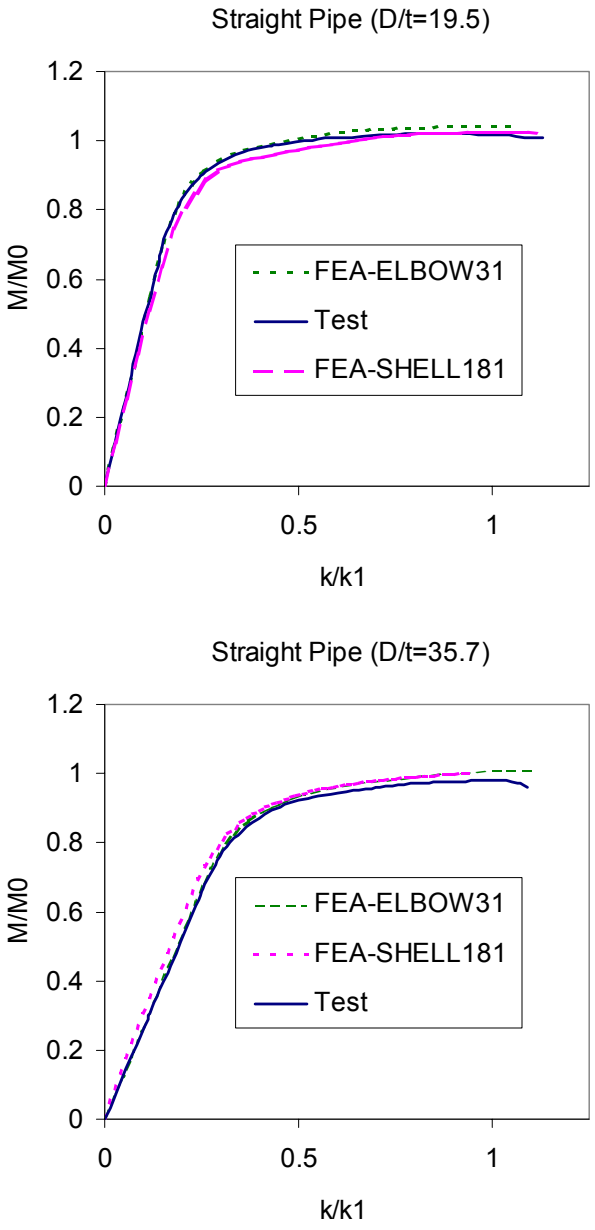

Fig. 8 Normalized moment curvature curves

4. ELBOW

4.1 Experiments

Two elbow specimens, with nearly identical configurations (see Fig.9 and Fig.10) were tested by Hassan et al [17]. One, called Pipe CM, was used for the in-plane closing mode bending test. The other, called Pipe OM, was used for the in-plane open-

ing mode bending test. “Each specimen was a 90°, 2”Sch40, long radius, stainless steel 304, seamless, butt welding elbow, with two segments of straight pipes, with lengths about 5 times the outside diameter of the elbow, welded to both ends”[12]. Actual geometrical dimensions and pipe wall thicknesses were measured (see Fig. 11 and Tables 2 and 3) before the test. The average wall thicknesses and average outside diameters are shown in Table 4.

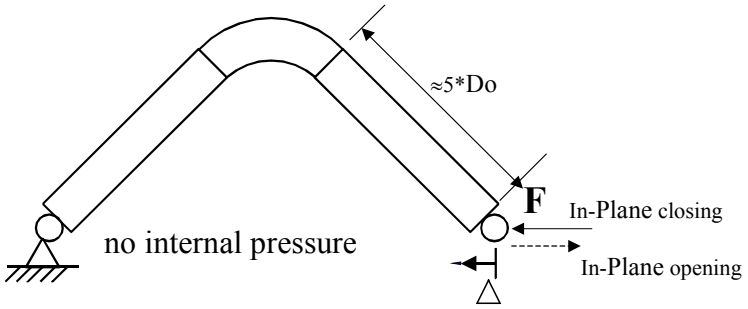

Fig. 9 In-plane closing/opening mode test

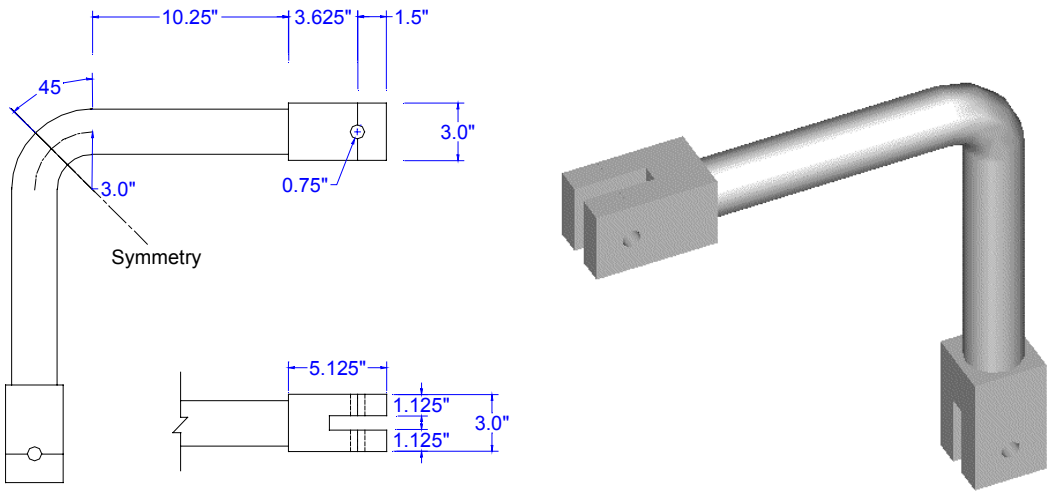

Fig. 10 Measured Dimensions of Test Specimens

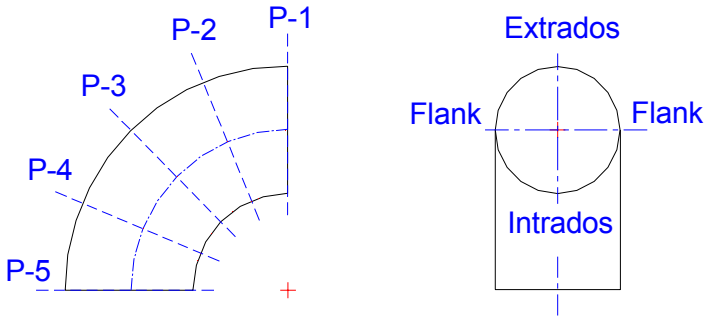

Fig. 11 Measured cross-sections

Table 2 Measured outside diameters and wall thicknesses of Pipe CM (in)

	P-1	P-2	P-3	P-4	P-5
$D_{o\ Flank\text{-}Flank}$	2.340	2.406	2.402	2.394	2.383
t - Flank	0.207	0.222	0.225	0.224	0.232
t– Flank	0.200	0.217	0.220	0.222	0.218
$D_{o\ Intra\text{-}Extra}$	2.378	2.306	2.274	2.278	2.357
t - Intrados	0.200	0.270	0.287	0.268	0.222
t - Extrados	0.212	0.213	0.205	0.209	0.213

Table 3 Measured outside diameters and wall thicknesses of Pipe OM (in)

	P-1	P-2	P-3	P-4	P-5
$D_{o\ Flank\text{-}Flank}$	2.384	2.393	2.408	2.424	2.378
t - Flank	0.196	0.223	0.224	0.224	0.207
t– Flank	0.241	0.228	0.226	0.225	0.233
$D_{o\ Intra\text{-}Extra}$	2.358	2.270	2.274	2.303	2.379
t - Intrados	0.243	0.281	0.293	0.282	0.200
t - Extrados	0.204	0.199	0.202	0.205	0.217

Table 4 Geometric characteristics of elbows tested

Segments of Test Specimens		average t (in)	D_o (in)			D_o / t
			average		average	
			Extrados -Intrados	Flank - Flank		
Pipe CM	Elbow	0.22	2.32	2.39	2.35	10.49
	Straight Pipe	0.17	2.37	2.37	2.37	14.25
Pipe OM	Elbow	0.23	2.32	2.40	2.36	10.35
	Straight Pipe	0.16	2.37	2.38	2.38	14.56

4.2 FEA models using ANSYS

4.2.1 Mesh Density and Element Type

As was the case with the straight pipes, for shell models, quarter models were built with double symmetric boundaries even though there were small deviations in side-to-side and end-to-end measurements. Nodal coordinates were defined individually based on measured data, while average measured thicknesses were used in both the elbow portions and the straight tangent portions. Since the end fixture was much stiffer than the pipe, a stiff plate was used to model it. The experiments were displacement controlled and, in the FEA, the displacement was applied at the node located at the center of the rigid plate. Constraining the node at the intrados prevented the rigid body motion. Again, large deformation and the active stress stiffness effects were taken in account.

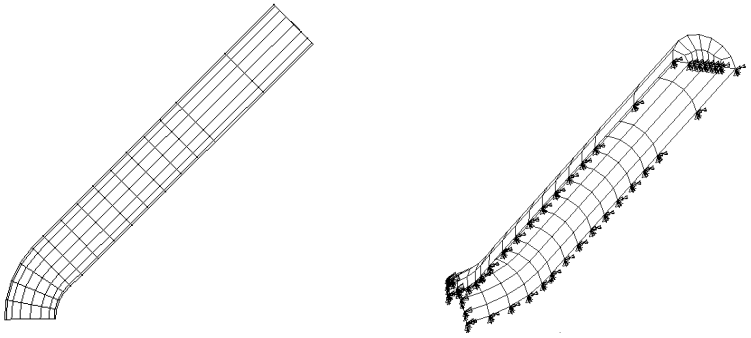

Fig. 12 FEA Model

In Yu's work, four element types-"SHELL43 and SHELL93 from ANSYS, ELBOW31 and S8R5 from ABAQUS-were used."[12]. "While three of them, SHELL43, ELBOW31 and S8R5, give close results [give reasonably consistent results to each other], SHELL93 gives strange results"[12]. In this current study, SHELL43, SHELL181 and PIPE60 of ANSYS, as well as ELBOW31 of ABAQUS were used.

For shell elements, according to Yu's meshing study[12], using 4 half-rings of elements with 8 elements evenly distributed around the semi-circumference in the elbow portions was sufficient. This is consistent with our observation. The FEA models used in both in-plane closing mode and in-plane opening mode are shown in Fig. 12. It was found that the results using SHELL43 and SHELL181 were very close to each other and that SHELL43 was acceptable for this rather thick-walled elbow. See Fig.13 and Fig.14 below. In thinner-walled elbows, it has been necessary to use SHELL181 to obtain convergence.

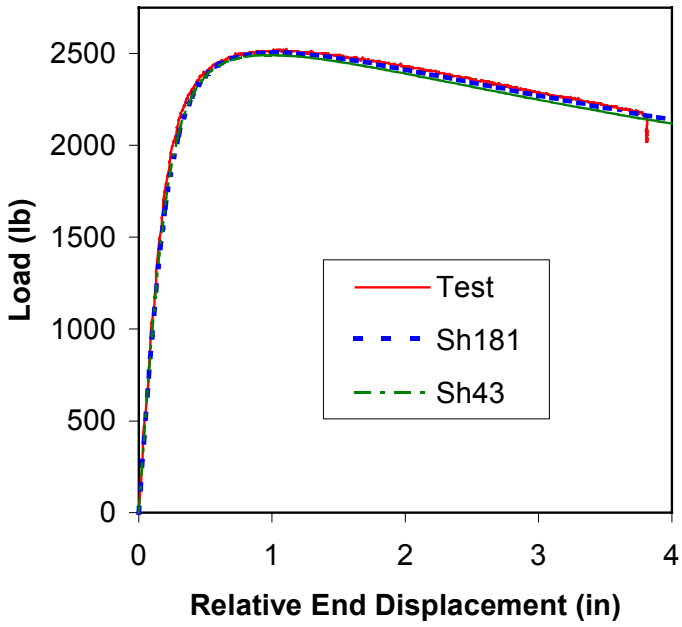

Fig. 13 Shell181 vs. Shell43 for in-plane closing mode

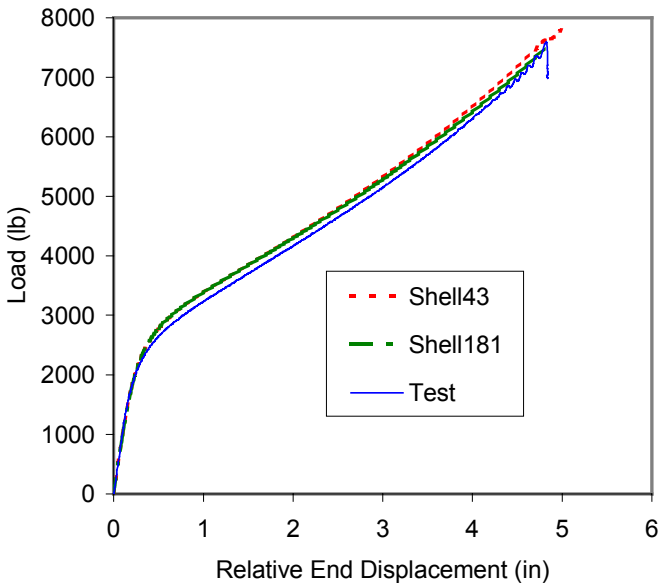

Fig. 14 Shell181 vs. Shell43 for in-plane opening mode

ANSYS 5.4 provides a curved pipe element, PIPE60, and this element was also used. "PIPE60 is a uniaxial element with tension-compression, bending, and torsion capabilities."[18] Its cross-section, however, has no capability of ovalization, and this contributes to the large discrepancy between the FEA predications and test data, as demonstrated in Fig. 15.

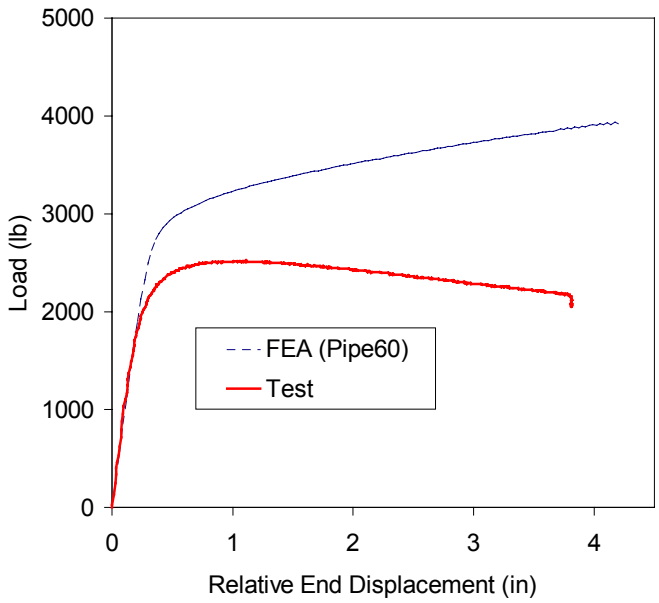

(a)

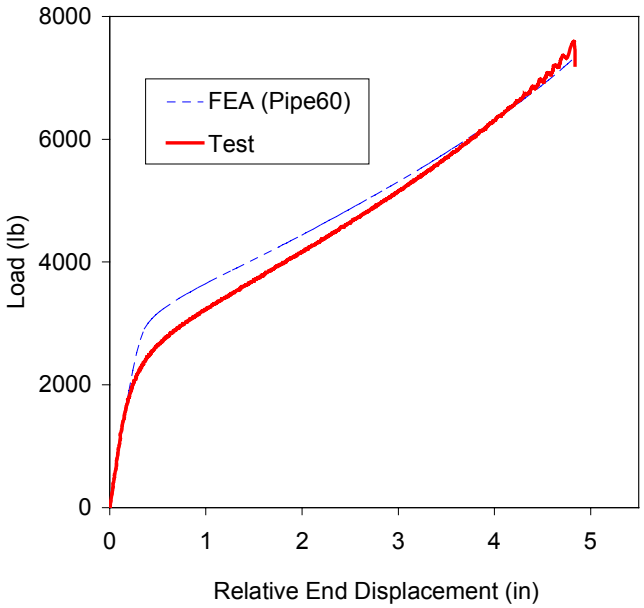

(b)

Fig. 15 Correlation using element PIPE60

4.2.2 Alternate FEA Models

In the investigation mentioned above, all of the FEA models, except those using PIPE60, used measured dimensions for the diameters, but averaged values for the wall thickness both in the elbow and the straight tangent portions. To study the effect of initial out–of-roundness and variation of wall thicknesses, two modified geometric models were investigated. These analyses all used SELL181 elements.

In the first modified model, referred to as 'simplified', it is assumed that the initial cross-sections are everywhere circular with outer diameter equal to the average of the measured values and that the wall thicknesses of the elbow and straight sections are equal to the average values from the respective areas. From the fabricated specimen, it was found that the two tangent sections were not exactly 90^o from each other; the measured angle for Pipe CM was closer to 88 to 89^o. To determine the effect of this slight misalignment, we created two versions of this simplified model, one with the actual measured alignment, labeled "FEA-ActualDeg", and the other using the nominal 90^o angle, labeled "FEA-90Deg". From the results, shown in Fig.16, it can be seen that the correlation between the test data and the FEA data is not as good as when the actual measured diameters were used (see Figs. 13 and 14), and that the slight angular misalignment was of minor significance. The advantage of this model is that using circular cross-sections leads to a much simpler FEA model.

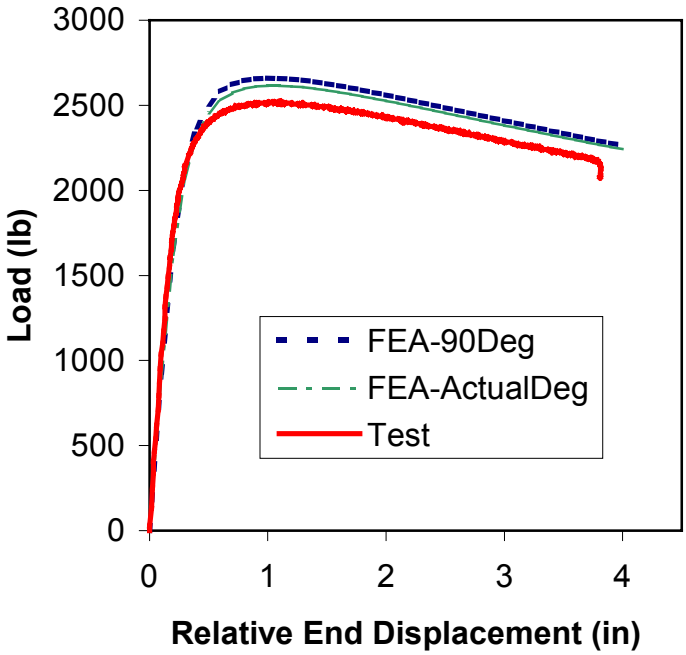

(a)

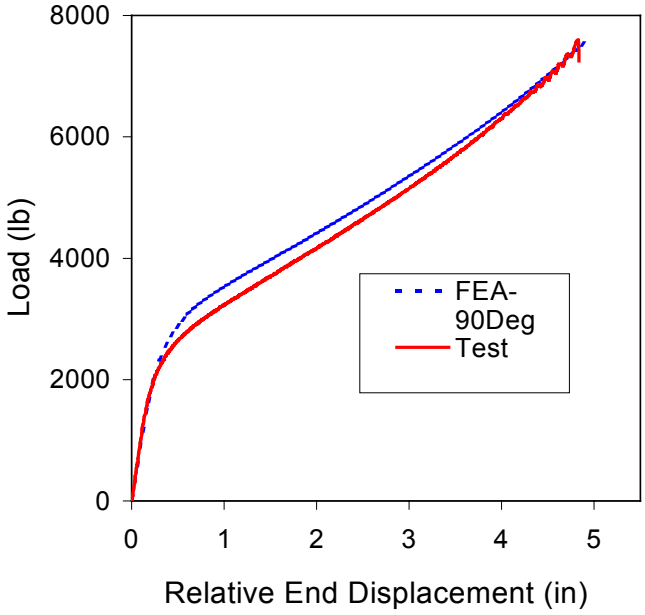

(b)

Fig. 16 Simplified Geometric Model

The second modified model, referred to as 'Detailed' uses not only measured diameters, but also the measured wall thicknesses around the circumference and along the pipe bend radius. The reconciliation results are shown in Fig. 17. Although the correla-

tion is still very good, it is not as good as when the average thickness was used, as shown in Fig. 13 and Fig. 14.

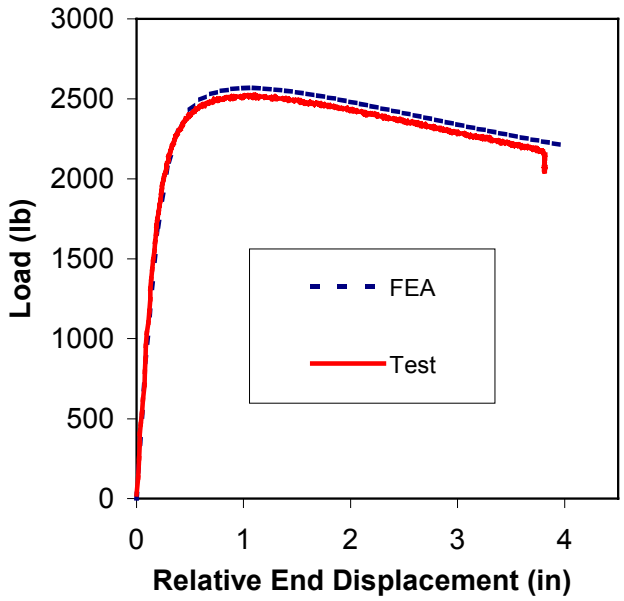

(a)

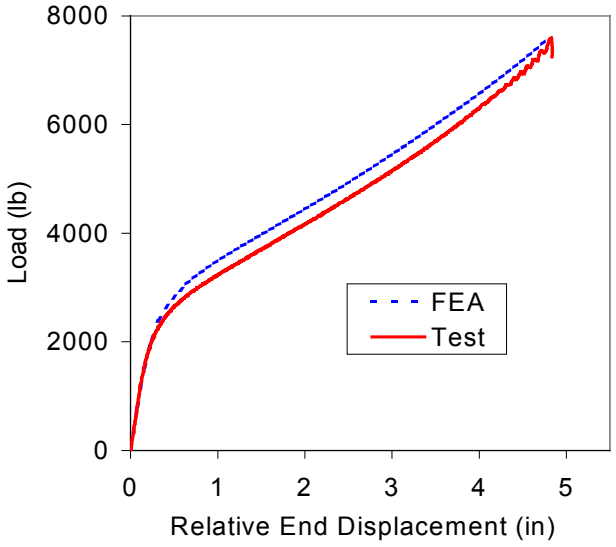

(b)

Fig. 17 Measured Geometric Model

This unexpected result may have been partly caused by an inaccurate measurement of the intrados wall thickness. The probe of the Ultrasonic Thickness Gauge was

flat, and hence could not match the surface curvature of the intrados, as shown schematically in Fig. 18. Because of this, the wall thicknesses of the intrados were probably over-estimated, leading to a stiffer model. Using special probes with contoured faces to match the surface curvature would be needed to obtain an accurate measurement. We speculate that using the average wall thickness minimized the effect of this error. In the following analyses, average wall thicknesses were used in all models.

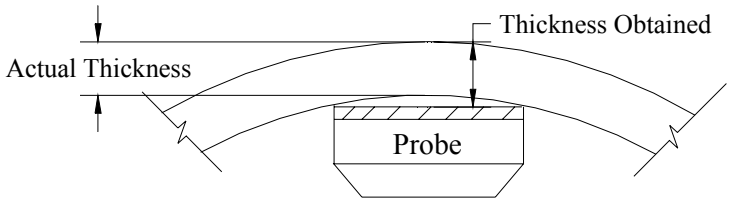

Fig. 18 Measurement of Intrados Wall Thickness

4.3 FEA models using ABAQUS

ABAQUS ELBOW31 were also used to simulate both the elbow tests. Compared with shell models, ABAQUS elbow models are more computationally economic: (1) they are simple space wire models and very easy to construct; (2) the numbers of nodes and elements, therefore the CPU time, are largely reduced. However, there are also some restrictions: the initial cross-sections are circular with uniform wall thickness.

In this section similarly as section 3.3 for straight pipes, again, it is assumed that the initial cross-sections were circular and the average measured wall thicknesses of straight tangent portions and elbow portions were used in each portion respectively. No deformations were allowed for both end cross-sections to simulate the rigid end fixtures of the test specimens. Sixteen ELBOW31 elements were used along the elbow and each straight tangent portion respectively. The selections of material-models are discussed in

the section 4.4 below. The FEA results, compared with measured experimental data and the FEA results using ANSYS SHELL181 assuming all the cross-sections perfectly circular with average wall thicknesses, are illustrated in Fig. 19.

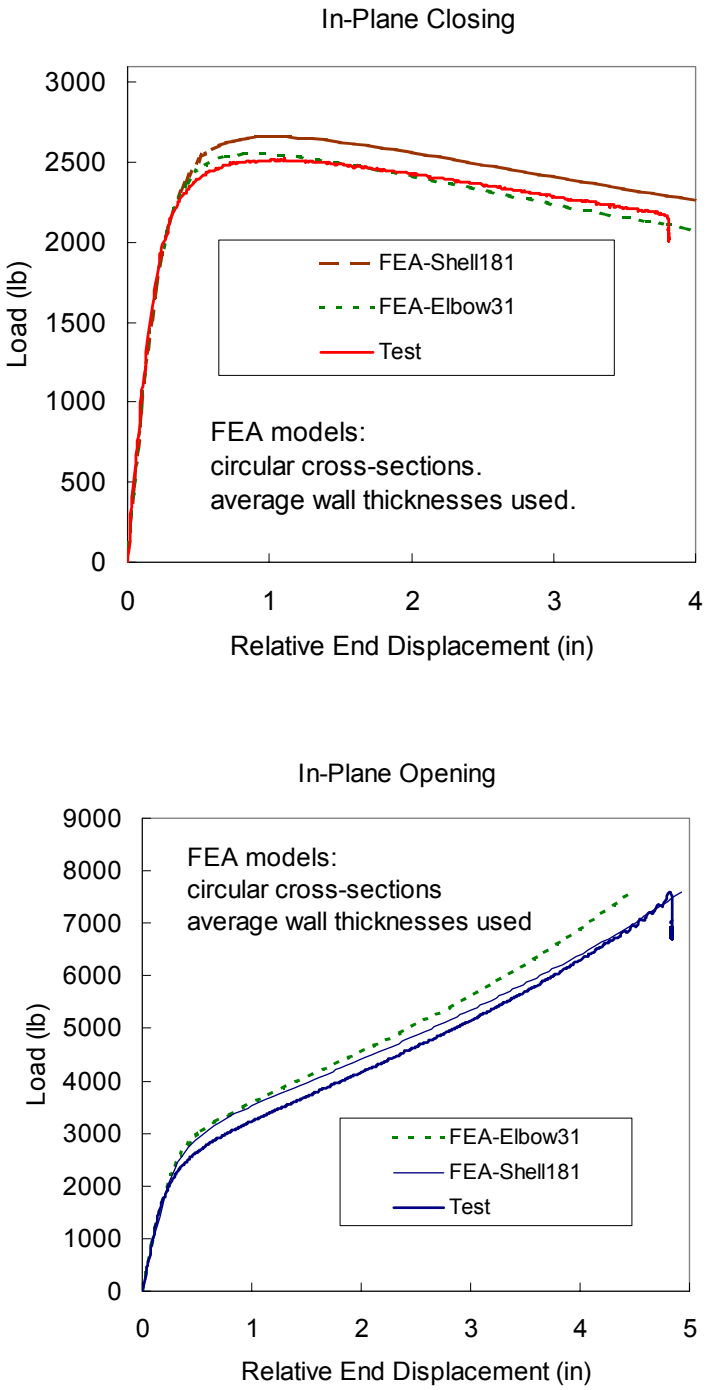

Fig. 19 ABAQUS ELBOW31 vs. Test

4.4 Material models

The elbow reconciliation required that two separate nonlinear stress-strain curves be constructed – one for the straight tangent sections and one for the elbow, since the manufacturer's testing report gave quite different properties for each part. For each one, a multi-linear curve needed to be constructed using the three material parameters (E, S_y and S_u). An ASTM tensile test was performed on a coupon specimen cut from a piece of the straight pipe, which is the same product batch as the straight pipes used in our specimens. The results show close agreement with the manufacturer's report, as shown in Table 5. Hereafter, we refer to this as the ASTM test. Because of the small diameter and thin wall thickness of the elbow and the lack of a readily available small-specimen testing apparatus, however, experimental material properties for the elbow material were not obtained. Instead, two procedures were developed to construct the constitutive model for the elbow portions using only the manufacturer's reported material properties.

Table 5 Material characteristics of shells tested

Segments of Test Specimens		S_y (ksi)	S_u (ksi)	α	
				S_y	S_u
Manufacturer's report	Elbow	37.4	83.0	0.70	0.93
	Straight Pipe	54.0	91.9	/	/
NCSU ASTM test [19]	Straight Pipe	53.2	89.4	1.0	1.0
E=28,300 ksi					

The power curve model due to Ludwik is most frequently employed for the true stress-true strain constitutive model of steel [20]. It is of the form:

$$\sigma = \sigma_o + ke^n \qquad (2)$$

where σ_o, k and n are constants. "In the case of mild steels, the value determined for σ_o is low, or even zero, so that the expression proposed by Hollomon can be used"[12]:

$$\sigma = ke^n \qquad (3)$$

where n is called the strain-hardening exponent.

Based on Eq. (3), Yu derived a procedure to construct a stress-strain curve if E, S_y and S_u are given (see details in [12]). Fig.19 shows the true stress-true strain curve from the ASTM test on the straight pipe. The curve for the elbow, using Yu's method (with parameters from Table 5) is also shown. It is observed that the shape of this curve is quite different from the ASTM curve. When Yu's curve was used to simulate the elbow behavior, it was found that the FEA analysis deviated considerably from the measured data. See Fig. 21. This 2-parameter constitutive model is apparently incapable of accurately describing the sharp knee of the stress-strain curve from the ASTM test.

To obtain a model that more accurately represents the test data, a procedure using linear scaling was developed. The ASTM test curve for the straight pipe was linearly scaled so that it would have the correct modulus, yield stress and ultimate stress for the elbow, but would have the shape of the curve from the ASTM test.

The scaling procedure is as follows:

Step 1: Start with the Engineering stress-strain curve from ASTM test

Step 2: Subtract elastic strain from total strain to get the engineering stress-plastic strain curve of the ASTM test

Step 3: Calculate the following scaling factors. Assume, for the plastic stresses, that

$$\sigma_{elbow} = \alpha(\varepsilon)\, \sigma_{straight\ pipe} \qquad (4)$$

where, $\alpha(\varepsilon)$ is a linear scaling function, $\alpha = a\varepsilon + b$,

with constants a and b found from

$$\alpha = \begin{cases} S_{y,elbow}/S_{y,test} & \text{at} \quad \varepsilon_{plastic} = 0.002 \\ S_{u,elbow}/S_{u,test} & \text{at} \quad \varepsilon_{plastic} = 0.35 \quad \text{(assumed)} \end{cases} \qquad (5)$$

where S_y is defined as the 0.2% offset yield stress. Assume that the engineering plastic strain corresponding to the ultimate stress is 35% (it was approximately this value in our ASTM test.)

Step 4: Use Eq. (4) to get the engineering stress-plastic strain curve of elbow

Step 5: Add the elastic strain to get the engineering stress-total strain curve of elbow and convert to true stress-strain curve.

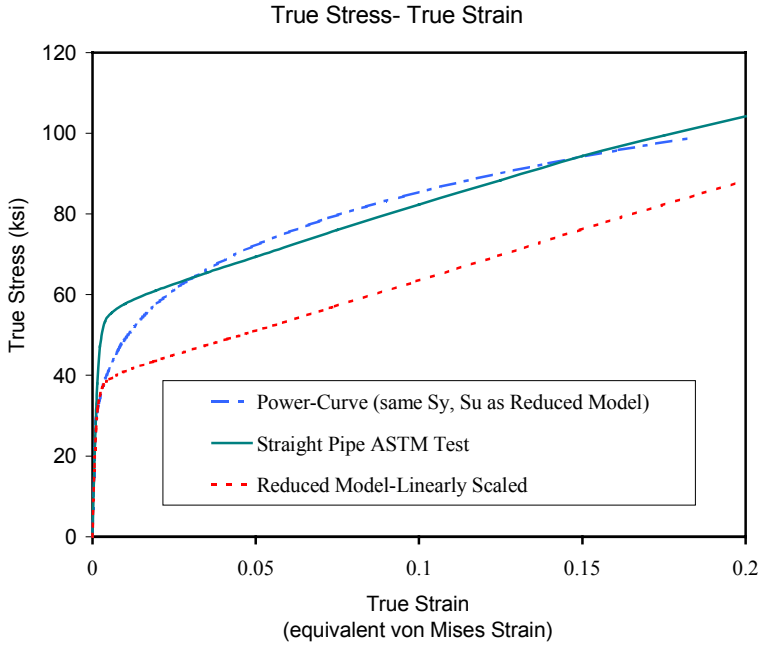

Fig. 20 Stress-Strain Relationship

When this procedure is applied to the elbow, the short-dash curve in Fig. 20, labeled as "Reduced Model-Linearly Scaled" was obtained. The power curve and the Reduced model coincide at S_y and S_u, (S_u not shown in this figure) as well as in the linear region, but deviate significantly elsewhere.

4.5 Correlation of Global Behavior

Fig. 21 (a) and (b) show that FEA, with this new reduced model for the elbow, is able to simulate both the closing mode and opening mode test data very well – in the closing mode, the analytical and test results are virtually indistinguisable. As indicated previously, the FEA results based on the power law are not nearly as good as those from the linearly scaled model.

Since the shell models took the initial out-of-roundness of the cross-sections and variation of the wall thicknesses into account, compared with measured experimental data, the results of shell models were better than those of elbow models in both cases. However, the FEA results of elbow models are still very good and elbow models are much easier to create with higher computational efficiency than shell models.

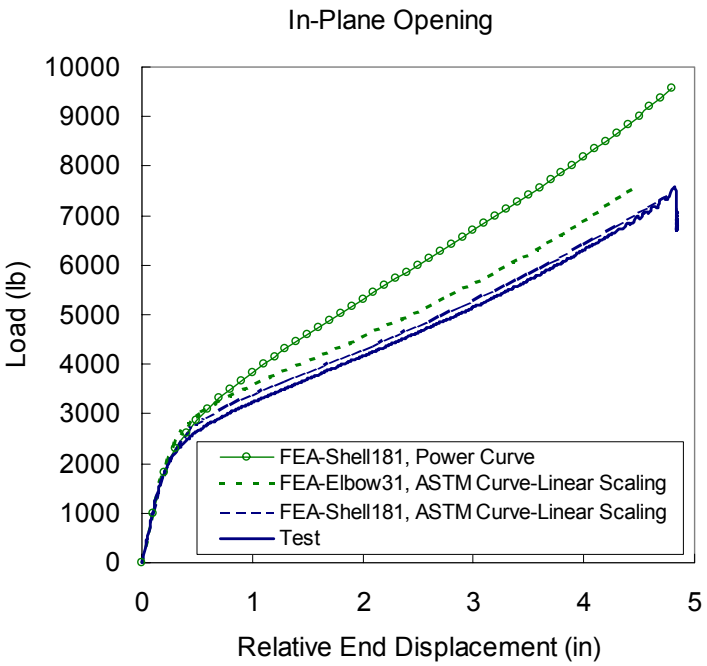

(a)

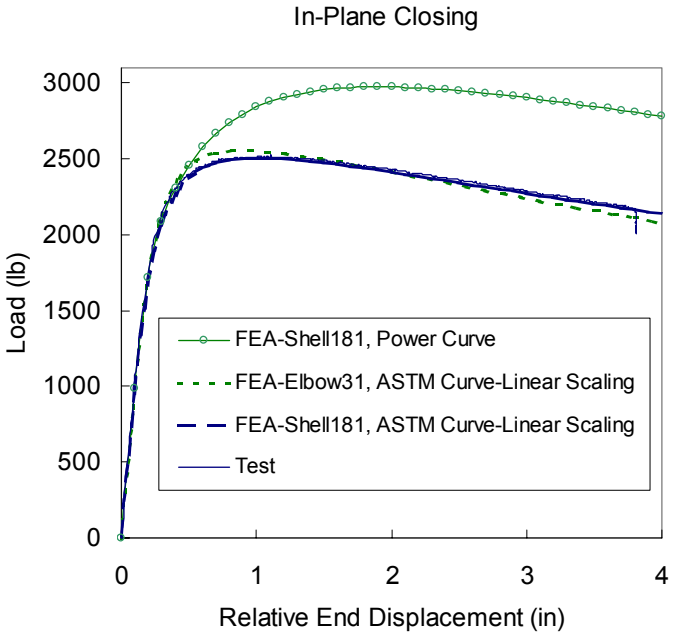

(b)

Fig. 21 Load-Displacement Curves

5. CONCLUSIONS

This part gives a brief review of nonlinear FEA modeling procedures. Four physical tests: two four-point-bending tests on straight Aluminum pipes and two stainless steel elbow tests under in-plane closing mode bending and in-plane opening mode bending, were simulated. The FEA study demonstrates that if element type and mesh density are carefully chosen, and an accurate constitutive material model constructed, under monotonic static loading, then the prediction of straight pipe and elbow global behavior from nonlinear finite element analysis can be very close to physical tests. For thin-wall pipes, the global behavior from FEA can be quite sensitive to wall thicknesses, and there can be significant differences between nominal wall thicknesses and actual specimen thicknesses. Therefore, actual wall thickness should be used when possible for reconciliation work. Preliminary work on 2" schedule 10 elbows indicates that the weld material between the elbow and the tangent pieces may be important in thin-walled elbows.

Later work includes additional in-plane monotonic tests on thin-walled elbows and an out-of-plane monotonic test, also on an elbow. In a second phase of this research, a preliminary experimental and analytical study on an elbow subjected to quasi static cyclic loading is performed.

6. NOMENCLATURE

a,b	=	constants
D_m	=	mean diameter of pipe
D_o	=	outside diameter of pipe
E	=	Young's modulus

k = strength coefficient

L = effective pipe length of the test specimens

M = bending moment

M_o = $S_y D_m^2 t$, theoretical limit moment

n = Ramberg-Osgood hardening parameter / strain hardening exponent

S_y = yield stress

S_u = ultimate stress

t = wall thickness

α = scaling factor

ε = true strain

κ = curvature

κ_1 = t / D_m^2

σ = true stress

σ_y = Ramberg-Osgood yield parameter

7. REFERENCES

1. ASME, 1995. Boiler and Pressure Vessel Code, Section III, Division 1 – Subsection NB. Class 1 Components. American Society of Mechanical Engineers, New York.

2. Mello, R. M., and Griffin, D. S., 1974, "Plastic Collapse Loads for Pipe Elbows Using Inelastic Analysis", J. of Pressure Vessel Technology, p177-183

3. MARC-CDE Nonlinear Finite Element Analysis Program, MARC Analysis Corporation and Control Data Corporation, Minneapolis, Minnesota, 1971

4. Sobel, L. H. and Newman, S. Z., 1980, "Comparison of Experimental and Simplified Analytical Results for the In-Plane Plastic Bending and Buckling of an Elbow", Transactions of the ASME, Vol.102, p400-409

5. Sobel, L.H. and Newman, S. Z., 1986, "Simplified, Detailed, and Isochronous Analysis and Test Results for the In-Plane Elastic-Plastic and Creep Behavior of an Elbow", J. of Pressure Vessel Technology, Vol.108, p297-304

6. Dhalla, A. K., 1987, "Collapse Characteristics of a Thin-Walled Elbow: Validation of an Analytical Procedure", Transactions of the ASME, Vol.109, p394-401

7. Suzuki, N. and Nasu, M., 1989, "Non-linear analysis of welded elbows subjected to in-plane bending", Computers & Structures, Vol, 32, No.3/4, pp871-881

8. Kussmaul, K., Diem, H. K., Uhlmann, D., Kobes, E., 1995, “Pipe bend behaviour at load levels beyond design”, (SMiRT 13), Brazil

9. ABAQUS User’s Manual, Version 4.8, Hibbitt, Karlsson and Sorensen, Inc., 1989

10. SAN, Frderungsvorhaben BMI SR 79, SDK-Report No. 3304 SR 79-01, June 1980

11. Ju, G., 1991 “Bifurcation and Localization Instabilities in Plastic Bending of Cylindrical Shells,” Ph.D. Dissertation, University of Texas at Austin

12. Yu, L., 1998. “Elbow Stress Indices Using Finite Element Analysis,” Ph.D. Dissertation, North Carolina State University

13. ANSYS v5.4, ANSYS, Inc., 1994

14. ANSYS v5.4 Help Manual, 4.181, SHELL181, 1997

15. ANSYS v5.4 Help Manual, 4.43, SHELL43, 1997

16. ABAQUS Help Manual, 3.7.1-1

17. Hassan, T., Bari, S. and Matzen, V.C., "Monotonic In-plane Tests on 2-inch, Schedule 40 Elbows," Data developed at the Center for Nuclear Power Plant Structures, Equipment and Piping, North Carolina State University, 1997-1998

18. ANSYS v5.4 Help Manual, 4.60, PIPE60, 1997

19. Hassan, T., Bari, S., Modlin, M., and Matzen, V.C., "ASTM Coupon Tests on Schedules 40 and 10 Straight Pipe Materials," Data developed at the Center for Nuclear Power Plant Structures, Equipment and Piping, North Carolina State University, 1997-2000

20. “*The book of steel*”, 1996, Editors: Béranger, G., Henry, G., Sanz, G.; Preface by Lacombe, P; Translated from French by Davidson, J. H.; Andover: Intercept, p219

PART IV

CORRELATION OF IN-PLANE BENDING TESTS AND FEA RESULTS FOR THIN-WALLED ELBOWS CONSIDERING WELDS

ABSTRACT

The purpose of this study is to validate a finite element analysis (FEA) simulation methodology to predict the global behavior of thin-walled elbows under in-plane bending. Three in-plane closing mode bending tests and one in-plane opening mode bending test on 2" Schedule 10 elbows were conducted, and a nonlinear FEA procedure was used to simulate the tests. A detailed FEA study was carried out to determine the relative importance of weld size and location, measured wall thicknesses, and original cross-section dimensions. Considering welding effects, the reconciliation results of load-displacement relationships and deformations of mid-elbow sections were excellent. It is concluded that (1) the nonlinear FEA procedure proposed here can simulate the complicated nonlinear behavior of thin-walled elbows within acceptable limits of engineering accuracy; (2) weld joint may have significant effects on the global behavior of thin-wall elbows. Various strains were also simulated, but the results were less conclusive.

1 INTRODUCTION

Piping components such as elbows exhibit significant material and geometric nonlinear behavior when subjected to severe loadings. The ability to simulate this non-

linear behavior is beneficial to the improvement of design codes because the alternative of performing experiments to carry out parametric studies is costly.

In the previous reconciliation study on elbow behavior and analysis [1] (Part III of this dissertation), four physical tests – two four-point-bending tests on straight pipes and two stainless steel (SS) 304, 2" Schedule 40 elbow tests under in-plane closing mode bending and in-plane opening mode bending – were conducted. Using FEA procedures developed in the investigation, the FEA models all gave excellent results compared with experimental data. The study demonstrated that, if element type and mesh density are carefully chosen, and an accurate constitutive material model is constructed, then under monotonic static loading the prediction of the global behavior of straight pipes and elbows using nonlinear FEA can be very close to actual physical behavior. The elbows used in that study had rather thick walls (D/t =10~11). Hassan et al. [2] conducted a set of tests using 2" Schedule 10 elbows (D/t=17~19). An interesting question arose during the reconcilliation phase of this work: what is the effect of the weld geometry? Correlations of tests and numerical results for pipe bends have been attempted by Mello and Griffin [3], Sobel and Newman [4, 5], Dhalla [6], Suzuki and Nasu [7], Kussmaul et al. [8] and Mourad and Younan [9]. But none of the above has addressed the welding effects. In Part III, the effects were neglected because the raised bead had been ground flush with the surrounding pipe and elbow material. In the new tests, the weld bead was left unaltered, as it would be in a power plant. This part presents the results obtained in four in-plane closing and opening bending tests performed on SS304, 2" Schedule 10 elbows. Investigations of welding effects were carried out following the

nonlinear FEA modeling procedures described in Part III. A reconcilliation study on strains was also performed.

2 EXPERIMENTS

Four elbow specimens were tested under monotonic in-plane bending [2]. Three of the specimens, called Pipe_CM (1) ~ Pipe_CM (3), were for in-plane closing mode bending test. Pipe_CM(1) was tested first and the load bearing capacity given by FEA was up to 20% lower than the experiment and we could not figure out the main reason at that time, which turned out to be the welding effects finally. Then Pipe_CM(2) was tested to make sure that the test data obtained were correct. Pipe_CM(3) was tested for correlation of strains. The fourth specimen, called Pipe_OM, was for the in-plane opening mode bending test. Each specimen was a 90°, 2"Sch10, long radius, SS304, seamless elbow, with straight pipe segments about 5 times the outside diameter of the elbow, welded to each end. Fig. 1 illustrates the testing setups. Fig. 2 and Table 1 give the dimensions of test specimens.

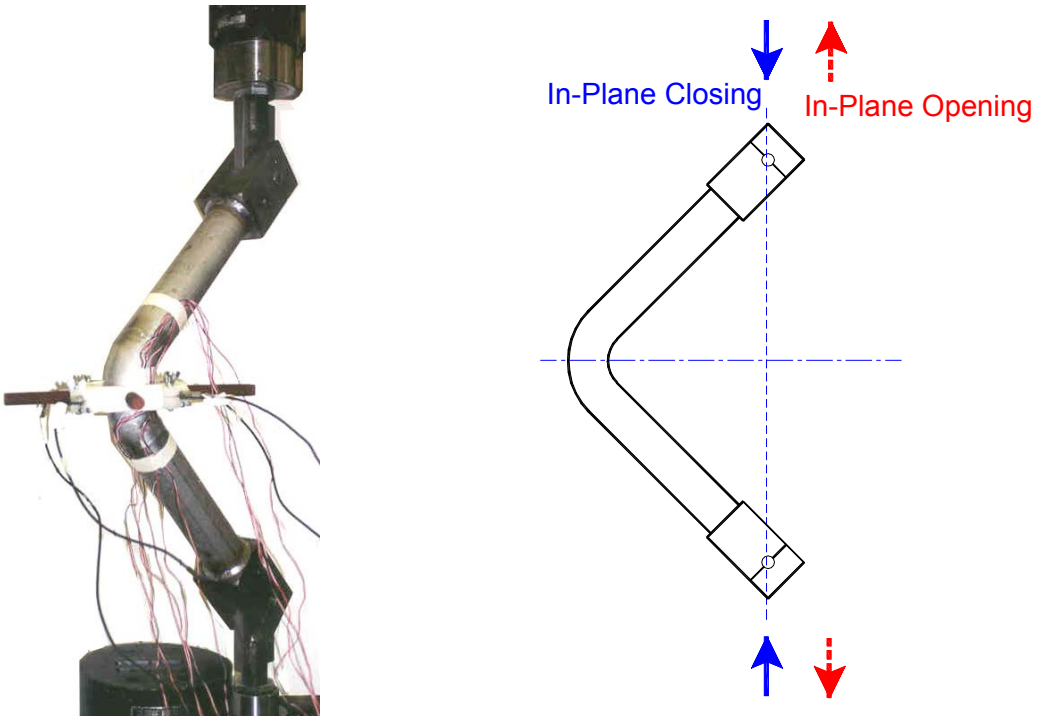

Fig. 1 In-Plane Closing / Opening Mode Testing Setup

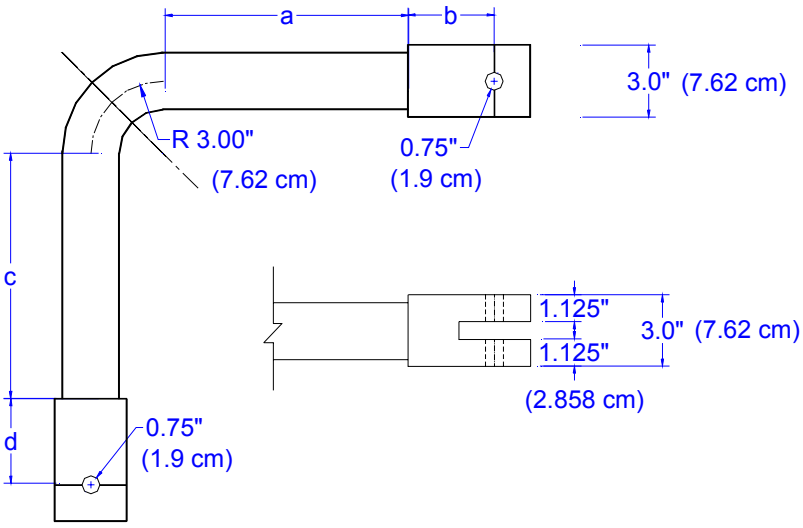

Fig. 2 Measured Dimensions of Test Specimens

Table 1 Measured Dimensions of Specimens

(a, b, c & d correspond to Fig. 2)

	a		b		c		d	
	(in)	(cm)	(in)	(cm)	(in)	(cm)	(in)	(cm)
Pipe_CM (1)	10.00	25.40	3.451	8.766	10.06	25.55	3.412	8.666
Pipe_CM (2)	10.00	25.40	3.475	8.827	10.13	25.72	3.490	8.865
Pipe_CM (3)	10.00	25.40	3.500	8.890	10.00	25.40	3.438	8.733
Pipe_OM	10.00	25.40	3.512	8.920	10.00	25.40	3.468	8.809

Actual outside diameters and pipe wall thicknesses were measured before the tests. For each specimen, five cross-sections along the pipe bend radius, labeled P-1 to P-5 in Fig. 3 (a), were selected for measurement. In each of the cross-sections, wall thicknesses were measured at eight or twelve points around the circumference, as shown in Fig. 3 (b) and (c). The measured data are given in Table 2 through Table 5 for Pipe_CM (1) to Pipe_OM respectively.

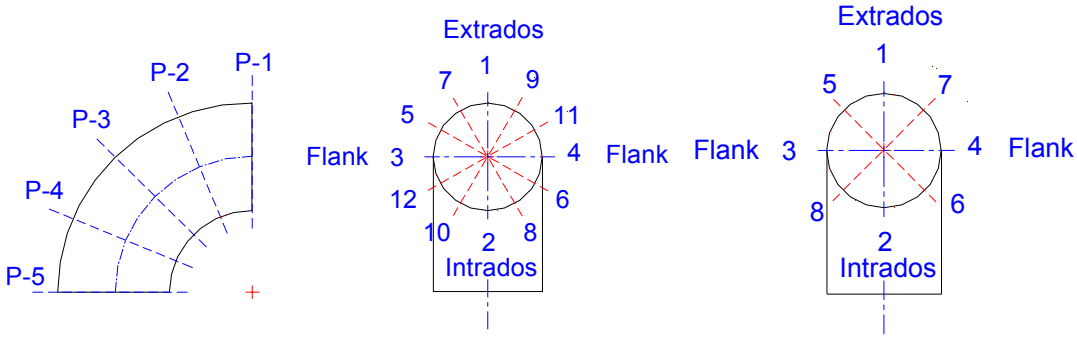

Pipe_CM (1~2), Pipe_OM **Pipe_CM (3)**

(a) (b) (c)

Fig. 3 Measured Cross-Sections

Table 2 Measured outside diameters and wall thicknesses of Pipe_CM (1)

	P-1		P-2		P-3		P-4		P-5	
	(in)	(cm)	(in)	(cm)	(in)	(cm)	(in)	(cm)	(in)	(cm)
$D_{o\ Intra\text{-}Extra}$	2.385	6.058	2.376	6.035	2.389	6.068	2.380	6.045	2.365	6.007

$D_{o\ Flank-Flank}$	2.365	6.007	2.386	6.060	2.372	6.025	2.376	6.035	2.361	5.997
t – 1	0.124	0.315	0.120	0.305	0.120	0.305	0.119	0.302	0.119	0.302
t – 2	0.143	0.363	0.144	0.366	0.144	0.366	0.144	0.366	0.145	0.368
t - 3	0.137	0.348	0.133	0.338	0.135	0.343	0.134	0.340	0.136	0.345
t – 4	0.135	0.343	0.135	0.343	0.136	0.345	0.134	0.340	0.133	0.338
t – 5	0.136	0.345	0.130	0.330	0.128	0.325	0.131	0.333	0.134	0.340
t - 6	0.137	0.348	0.130	0.330	0.150	0.381	0.133	0.338	0.133	0.338
t – 7	0.126	0.320	0.121	0.307	0.124	0.315	0.124	0.315	0.126	0.320
t – 8	0.129	0.328	0.138	0.351	0.138	0.351	0.138	0.351	0.139	0.353
t - 9	0.123	0.312	0.119	0.302	0.120	0.305	0.118	0.300	0.124	0.315
t – 10	0.135	0.343	0.137	0.348	0.138	0.351	0.138	0.351	0.135	0.343
t – 11	0.122	0.310	0.119	0.302	0.120	0.305	0.120	0.305	0.120	0.305
t - 12	0.132	0.335	0.129	0.328	0.130	0.330	0.135	0.343	0.136	0.345

Table 3 Measured outside diameters and wall thicknesses of Pipe_CM (2)

	P-1		P-2		P-3		P-4		P-5	
	(in)	(cm)	(in)	(cm)	(in)	(cm)	(in)	(cm)	(in)	(cm)
$D_{o\ Intra-Extra}$	2.411	6.124	2.380	6.045	2.378	6.040	2.378	6.040	2.398	6.091
$D_{o\ Flank-Flank}$	2.350	5.969	2.379	6.043	2.379	6.043	2.381	6.048	2.359	5.992
t – 1	0.128	0.325	0.120	0.305	0.115	0.292	0.124	0.315	0.125	0.318
t – 2	0.131	0.333	0.134	0.340	0.123	0.312	0.120	0.305	0.144	0.366
t - 3	0.132	0.335	0.139	0.353	0.130	0.330	0.136	0.345	0.130	0.330
t – 4	0.141	0.358	0.134	0.340	0.139	0.353	0.143	0.363	0.142	0.361
t – 5	0.126	0.320	0.123	0.312	0.122	0.310	0.131	0.333	0.135	0.343
t - 6	0.129	0.328	0.135	0.343	0.127	0.323	0.143	0.363	0.146	0.371
t – 7	0.133	0.338	0.130	0.330	0.117	0.297	0.134	0.340	0.137	0.348
t – 8	0.121	0.307	0.124	0.315	0.123	0.312	0.139	0.353	0.136	0.345
t - 9	0.120	0.305	0.116	0.295	0.122	0.310	0.122	0.310	0.125	0.318
t – 10	0.139	0.353	0.125	0.318	0.124	0.315	0.144	0.366	0.145	0.368
t – 11	0.135	0.343	0.136	0.345	0.135	0.343	0.121	0.307	0.127	0.323
t - 12	0.126	0.320	0.134	0.340	0.137	0.348	0.143	0.363	0.145	0.368

Table 4 Measured outside diameters and wall thicknesses of Pipe_CM (3)

	P-1		P-2		P-3		P-4		P-5	
	(in)	(cm)	(in)	(cm)	(in)	(cm)	(in)	(cm)	(in)	(cm)
$D_{o\ Intra-Extra}$	/	/	2.375	6.033	/	/	/	/	2.375	6.033
$D_{o\ Flank-Flank}$	/	/	/	/	/	/	/	/	2.410	6.121
t – 1	0.119	0.302	0.117	0.297	0.115	0.292	0.115	0.292	0.122	0.310
t – 2	0.181	0.460	0.180	0.457	0.178	0.452	0.180	0.457	0.190	0.483
t - 3	0.131	0.333	0.128	0.325	0.132	0.335	0.128	0.325	0.127	0.323
t – 4	0.139	0.353	0.136	0.345	0.139	0.353	0.136	0.345	0.139	0.353
t – 5	0.119	0.302	0.119	0.302	0.117	0.297	0.119	0.302	0.124	0.315
t - 6	0.156	0.396	0.161	0.409	0.163	0.414	0.158	0.401	0.154	0.391
t – 7	0.151	0.384	0.166	0.422	0.173	0.439	0.171	0.434	0.159	0.404
t – 8	0.129	0.328	0.123	0.312	0.120	0.305	0.126	0.320	0.130	0.330

Table 5 Measured outside diameters and wall thicknesses of Pipe_OM

	P-1		P-2		P-3		P-4		P-5	
	(in)	(cm)	(in)	(cm)	(in)	(cm)	(in)	(cm)	(in)	(cm)
$D_{o\ Intra-Extra}$	2.387	6.063	2.370	6.020	2.360	5.994	2.377	6.038	2.389	6.068
$D_{o\ Flank-Flank}$	2.360	5.994	2.380	6.045	2.377	6.038	2.391	6.073	2.350	5.969
t – 1	0.119	0.302	0.116	0.295	0.111	0.282	0.115	0.292	0.121	0.307
t – 2	0.134	0.340	0.127	0.323	0.133	0.338	0.132	0.335	0.133	0.338
t - 3	0.138	0.351	0.128	0.325	0.129	0.328	0.130	0.330	0.134	0.340
t – 4	0.138	0.351	0.136	0.345	0.126	0.320	0.121	0.307	0.130	0.330
t – 5	0.128	0.325	0.125	0.318	0.120	0.305	0.136	0.345	0.131	0.333
t - 6	0.137	0.348	0.129	0.328	0.137	0.348	0.116	0.295	0.137	0.348
t – 7	0.124	0.315	0.122	0.310	0.114	0.290	0.136	0.345	0.124	0.315
t – 8	0.135	0.343	0.133	0.338	0.136	0.345	0.136	0.345	0.135	0.343
t - 9	0.123	0.312	0.119	0.302	0.115	0.292	0.116	0.295	0.121	0.307
t – 10	0.135	0.343	0.135	0.343	0.137	0.348	0.131	0.333	0.133	0.338
t – 11	0.130	0.330	0.123	0.312	0.123	0.312	0.123	0.312	0.130	0.330
t - 12	0.135	0.343	0.139	0.353	0.136	0.345	0.132	0.335	0.135	0.343

The average wall thicknesses and average outside diameters of each specimen are shown in Table 6.

Table 6 Geometric Characteristics of Elbows Tested

Segments of Test Specimens			average t	D_o			D_o / t
				average		average	
				Extrados -Intrados	Flank - Flank		
Pipe_CM (1)	Elbow	(in)	0.131	2.378	2.374	2.376	18.14
		(cm)	0.333	6.040	6.030	6.035	
	Straight Pipe	(in)	0.107	/	/	2.378	22.22
		(cm)	0.272	/	/	6.040	
Pipe_CM (2)	Elbow	(in)	0.131	2.389	2.370	2.380	18.17
		(cm)	0.333	6.068	6.020	6.045	
	Straight Pipe	(in)	0.110	/	/	2.380	21.64
		(cm)	0.279	/	/	6.045	
Pipe_CM (3)	Elbow	(in)	0.143	2.375	2.410	2.393	16.73
		(cm)	0.363	6.033	6.121	6.078	
	Straight Pipe	(in)	0.106	/	/	2.379	22.44
		(cm)	0.269	/	/	6.043	
Pipe_OM	Elbow	(in)	0.128	2.377	2.373	2.374	18.55
		(cm)	0.325	6.038	6.027	6.030	
	Straight Pipe	(in)	0.112	/	/	2.376	21.21
		(cm)	0.284	/	/	6.035	

The attached straight tangent portions were butt-welded to the elbows. In the previous reconciliation study in Part III, welds had been grounded smooth before the tests, but in this study, welds were kept as applied. To investigate the welding effects in correlations of FEA and the tests, the size of weld bead was measured. The height of weld bead on the outer surface was obtained by subtracting the outside diameters of the welding regions from the outside diameters of the adjacent pipe. On the internal surface, weld bead was observed. We assumed that the profile of the welds on the inside was the same as on the outside of the specimens. Since welds were non-uniform, only the average welding dimensions could be obtained, as illustrated in Fig. 4.

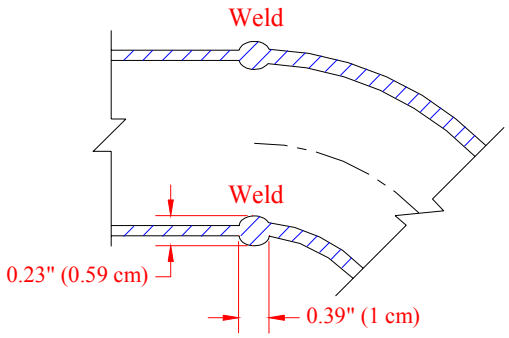

Fig. 4 Average Welding Dimensions for Testing Specimens

3 FINITE ELEMENT ANALYSIS USING ANSYS

3.1 Geometric Models

In this work, ANSYS version 5.5 was used. To improve computing efficiency, taking advantage of approximate double symmetry, quarter models were built with double symmetric boundaries using element SHELL181. Nodal coordinates and wall thicknesses along the circumference and along the pipe bend radius were carefully defined by measured data. Since the end fixture was much stiffer than the pipe, a stiff plate was used to model it. The experiments were displacement controlled; and, in the FEA, the displacement was applied at the node located at the center of the rigid plate. The rigid body motion was prevented by constraining the node at the intrados. Large deformation and the active stress stiffness effects were taken into account.

Based on the meshing study in Part III, using 4 half-rings of elements with 8 elements evenly distributed around the semi-circumference in the elbow portions was sufficient. This is consistent with our observation in this current study. The FEA models of both in-plane closing mode and in-plane opening mode are shown in Fig. 5. To

study the welding effects in reconciliation, three cases were considered. One model, shown in Fig. 5 (a), ignores welds. Another model includes welds but assumes that the location of the welds is entirely in the straight tangent regions, this is obviously not true but it makes the FEA models simpler. The corresponding mesh is shown in Fig. 5 (b). The third model also includes the weld, but assumes that the weld is half in the straight tangent region and half in the elbow region, as shown in Fig. 5 (c). This may be the best guess, since the weld metal was fused and merged into the abutting components and it is impossible to obtain the actual positions of welds. For the cases with welds, it is assumed that the welds were uniform along the circumference and were 0.23" (0.59 cm) high and 0.33" (0.85 cm) wide. This width is 85% of the measured width of 0.39" (1 cm). This reduction was included because the actual welds were not rectangular in cross-section. The reduction factor was selected by observation and using engineering judgement. In the corresponding FEA models, a half ring of shell elements with uniform width and thickness was used to simulate the weld beads.

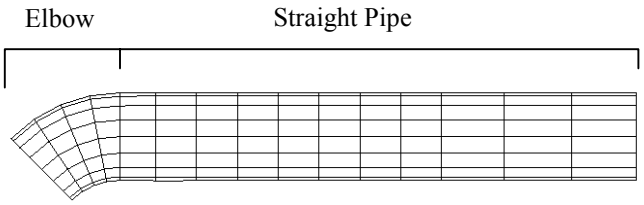

(a) Mesh without Welds

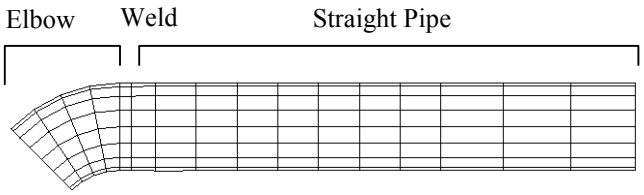

(b) Mesh with Welds All in Straight Tangent Regions

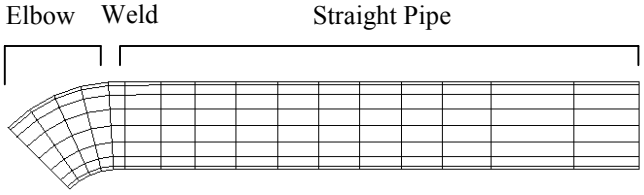

(c) Mesh with Welds Half in Elbow Regions and Half in Straight Tangent Regions

Fig. 5 FEA Models used in Weld Study

3.2 Material Models

The elbow reconciliation required that at least two separate nonlinear stress-strain curves be constructed – one for the straight tangent pieces and one for the elbow, since the manufacturer's testing report gave quite different properties for each part. For each one, a multi-linear curve needed to be constructed using the three material parameters (E, S_y and S_u). Two ASTM tensile tests were performed on two coupon specimens, called 2"Sch10 Coupon A and B, cut from a piece of straight pipe, which is the

same product batch as the straight pipes used in our specimens. The experimental engineering stress-engineering strain curves are shown in Fig. 6. The results show close agreements with the manufacturer's report, as given in Table 7. Hereafter, we refer to these data as the ASTM tests.

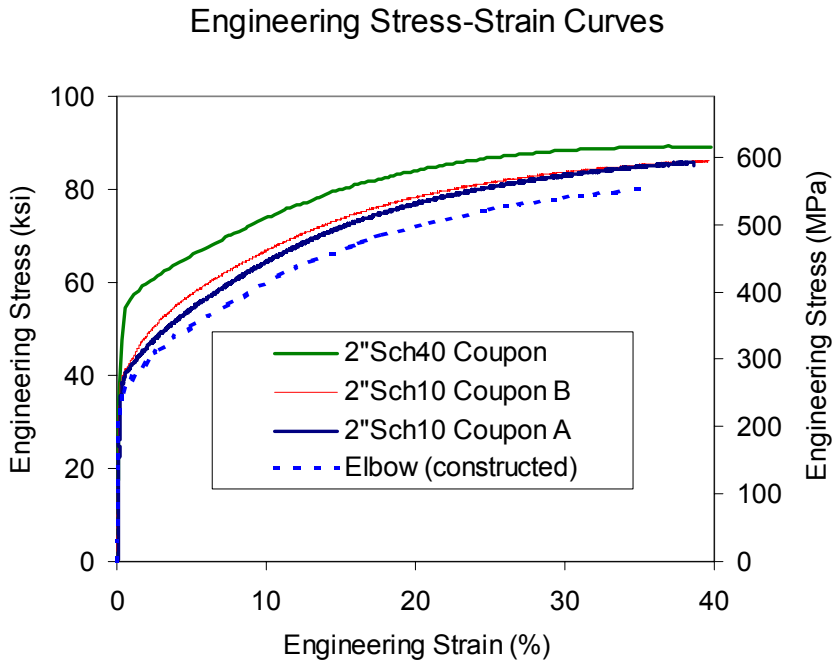

Fig. 6 ASTM material curves

Table 7 Material characteristics of shells tested

			S_y		S_u		E	
Segments of Test Specimens			(ksi)	(MPa)	(ksi)	(MPa)	(ksi)	(GPa)
Manufacturer's report	Elbow		35.4	244	81.0	558	N/A	N/A
	Straight Pipe		39.5	272	82.2	567	N/A	N/A
NCSU ASTM test	Straight Pipe	2"Sch10 Coupon A	38.4	265	85.8	592	29000	200
		2"Sch10 Coupon B	39.4	272	86.1	594	29300	202
		2"Sch40 Coupon	53.2	367	89.4	616	N/A	N/A

For the straight tangent portions, the constitutive ASTM curve of 2"Sch10 Coupon A was used directly. That of 2"Sch10 Coupon B was not used in our FEA studies

because data in the initial part of 2”Sch10 Coupon B curve contained too much noise to allow an accurate determination of the proportional limit.

Because of the small diameter and wall thickness of the elbow and the lack of a readily available small-specimen testing apparatus, experimental material properties for the elbow were not obtained. Instead, the procedure developed in Part III was used to construct the constitutive model for elbow regions using only the manufacturer’s reported material properties in Table 7. The ASTM stress-strain curve of 2”Sch10 Coupon A was used thereafter as the base curve. The resulting curve for the elbow is labeled “Elbow (constructed)” in Fig. 6.

The material properties of weld metal could not be obtained experimentally. There is little information of the actual welding material properties available. According to ASME B31.3 Code, K328.2.1 [10], the yield strength of weld material is required to be no lower than “the minimum yield strength for the base metals joined” [10]. Herein, in our analyses, its yield strength is considered to be equal to or greater than that of the straight tangent pieces, 38.4ksi (265 MPa) (See Table 7). So there are two choices. One is to assume that the filler metal has the same mechanical material properties as the straight tangent portions. Then the stress-strain curve of 2”Sch10 Coupon A could be used for welds. The other choice is to assume that the weld metal has higher yield strength than the straight tangent portion. If so, one more nonlinear stress-strain curve for welds is needed. In our previous reconciliation study as described in Part III, it happened that one ASTM stress-strain curve of a SS304 coupon cut from a piece of 2”Sch40 straight pipe was readily available, as shown in Fig. 6. It has higher yield strength than 38.4 ksi (265Mpa), as shown in Table 7, which satisfied our assumptions

mentioned above. Our choice was to use this higher value, although other assumptions might be equally valid.

3.3 Correlation of Overall Behavior

Using the FEA procedure illustrated above in this part, three to four models were used for each test. In each case, the measured dimensions were used in the models. The simplest one neglects welds. It is labeled as "FEA-No Weld" in Fig. 7, Fig. 8 and Fig. 10. The second model includes the welds and uses the assumption that welds are located entirely in straight tangent portions and the weld material properties were the same as the straight tangent portions, labeled as "FEA-Weld Only in Straight Pipe (a)" in Fig. 7. A third model also includes welds and assumes that the welds are located only in straight tangent portions but the weld material properties are the same as the 2"Sch40 Coupon, labeled as "FEA-Weld Only in Straight Pipe (b)" in Fig. 7, Fig. 8 and Fig. 10. The final model with welds assumes that the welds are located half in straight tangent portions and half in elbow portions and the weld material properties are the same as the 2"Sch40 Coupon. In Fig. 7, Fig. 8, 9 and Fig. 10, they are labeled as "FEA-Weld Half in Elbow (b)". The entire load-displacement curves of FEA results against test data are plotted in Fig. 7, Fig. 8, 9 and Fig. 10 for Pipe_CM(1~3) and Pipe_OM respectively. It is clearly demonstrated that, without consideration of the welds, the FEA results under-predicted in both in-plane closing and in-plane opening bending modes compared with experimental data. In our cases, the weld effects are more significant in in-plane closing mode than in in-plane opening mode. Taking welds into account, the FEA results are much closer to the test data. It is concluded that considering welding effects is necessary

in correlation study of tests and FEA results in some situations, for example, for thin-wall piping components where the thicknesses of welds are much thicker than the adjacent regions without welds.

Comparing the curves of “FEA-Weld only in straight pipe (a)” and “FEA-Weld only in straight pipe (b)” in Fig. 7 (a), the only difference in these two cases is the material properties of welds. It is illustrated that if the welds have higher strengths, the specimen has higher strength in global behavior and the effects are not negligible in our cases.

Comparing the curves of “FEA-Weld only straight pipe (b)” and “FEA-Weld Half in Elbow (b)” in Fig. 7, Fig. 8 and Fig. 10, those assuming welds to be located half in elbow regions and half in straight-tangent regions give better results than those assuming welds to be entirely located in straight pipe regions.

The initial parts of load-displacement curves are plotted in Fig. 7-(b), Fig. 8-(b), 9-(b) and Fig. 10-(b). Evidently, in all four cases, if taking welds into account, assuming that welds were located half in elbow regions and half in straight tangent regions, and the weld material properties were the same as the 2”Sch40 Coupon, the FEA results are excellent.

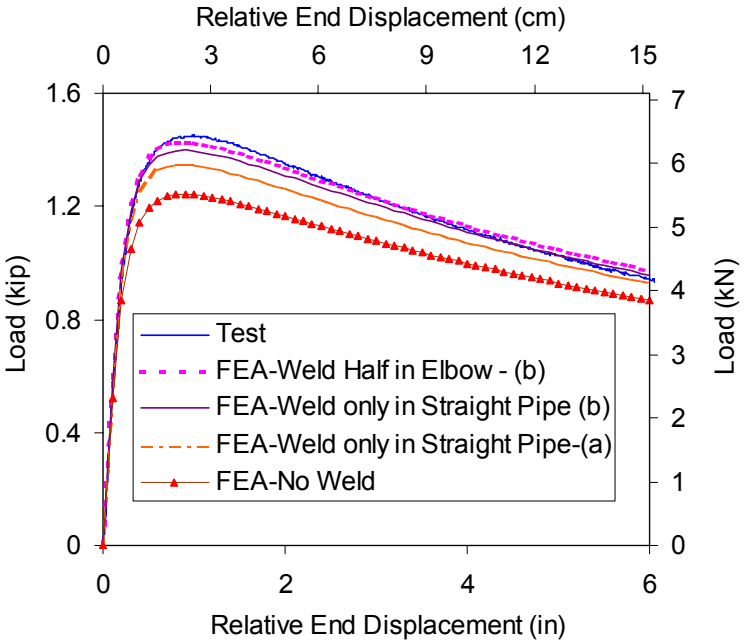

(a) Pipe_CM(1)

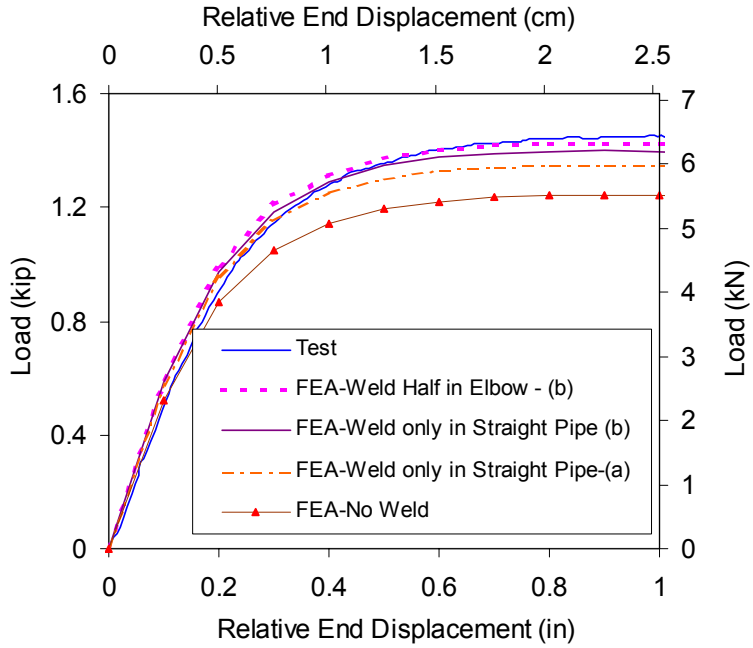

(b) Pipe_CM(1), enlarged scale

Fig. 7 Pipe_CM(1), Load-Displacement Curves

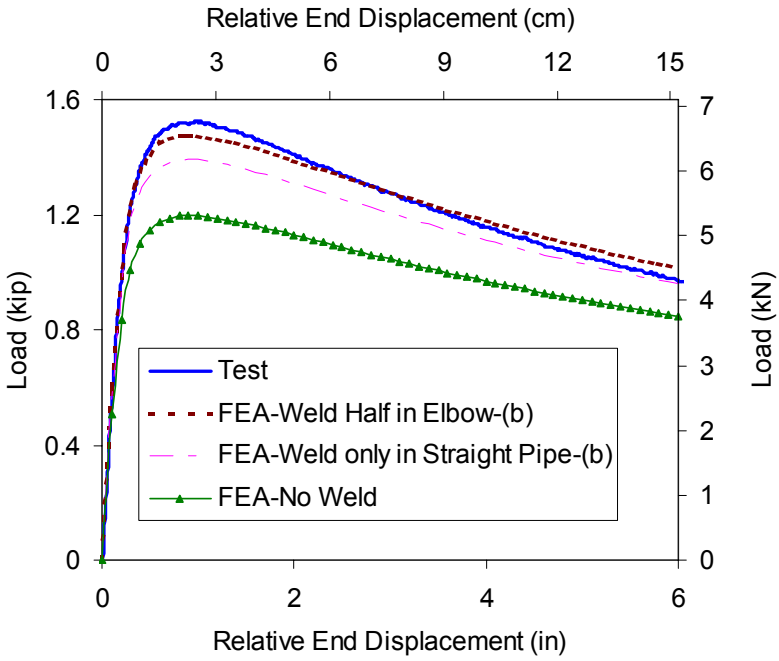

(a) Pipe_CM(2)

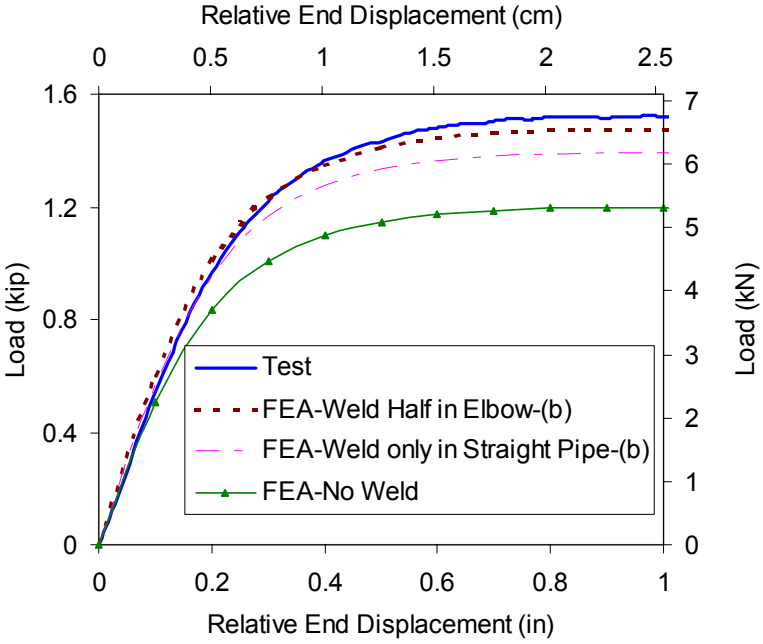

(b) Pipe_CM(2), enlarged scale

Fig. 8 Pipe_CM(2), Load-Displacement Curves

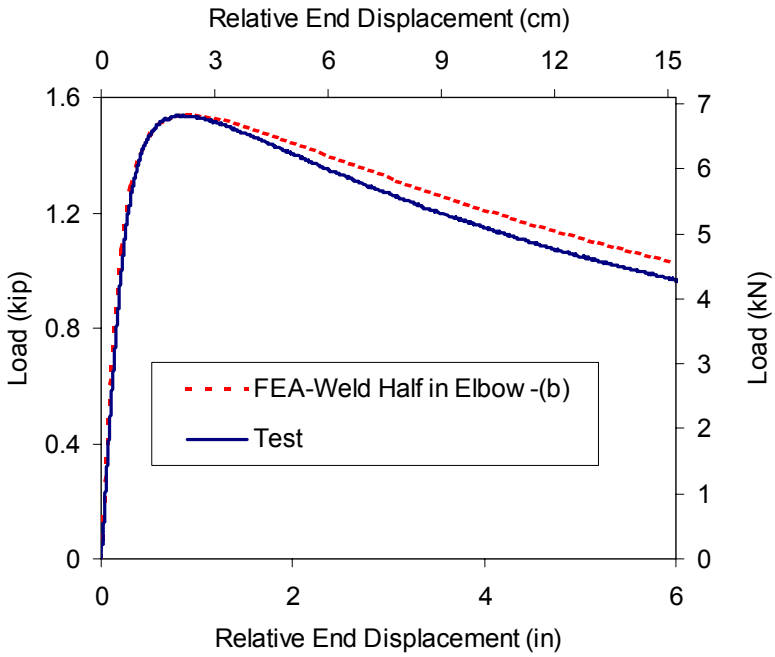

(a) Pipe_CM(3)

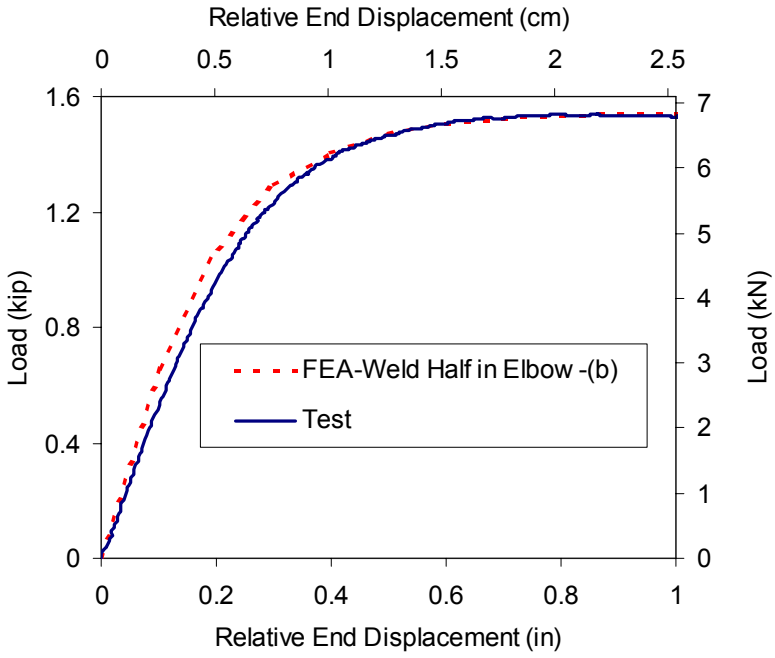

(b) Pipe_CM(3), enlarged scale

Fig. 9 Pipe_CM(3), Load-Displacement Curves

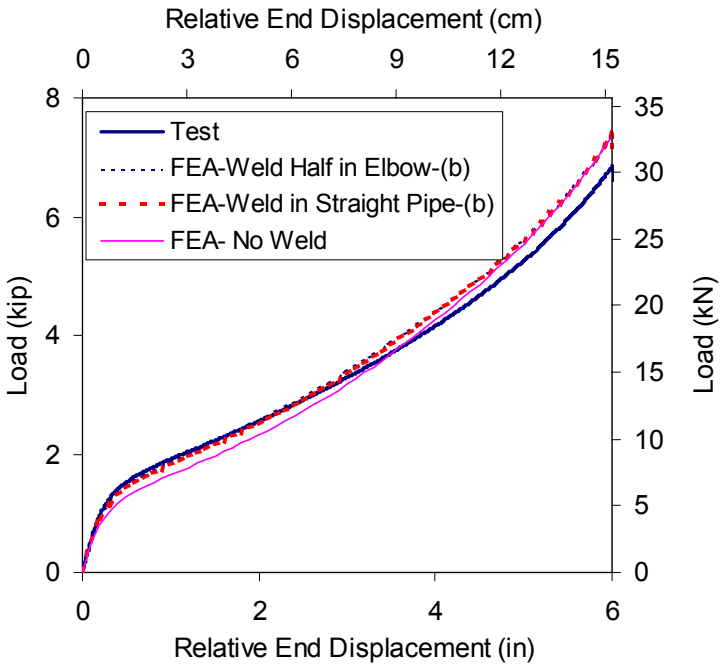

(a) Pipe_OM

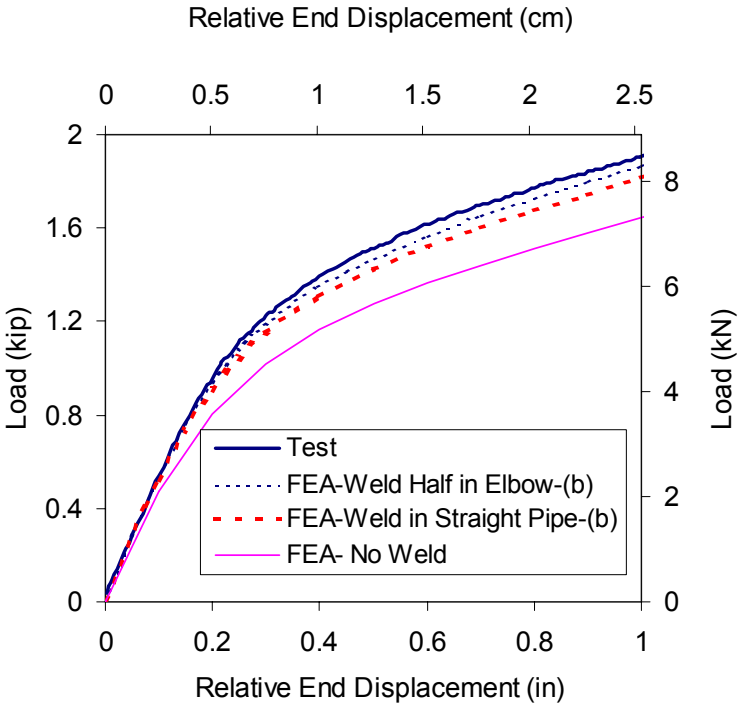

(b) Pipe_OM, englarged scaled

Fig. 10 Pipe_OM Load-Displacement Curves

In addition to the investigations on the welding effects described above, the effects of including the variation of the cross-sectional radius and wall thickness were also studied, as illustrated in Fig. 11. The solid line at the bottom, labeled "FEA-No Weld-Measured-Avg Thick" shows the results using measured piping diameters but with uniform wall thickness. The dash line labeled "FEA-No Weld-Round + Avg Thick" indicate the results utilizing circular cross sections with uniform wall thickness. These two show close agreements with each other, which reveals that the effects of the initial out-of-roundness of the specimen tested is negligible.

Comparing the two sets of curves, i.e., "FEA-Weld-Measured" and "FEA-Weld-Measured-Avg Thick", "FEA-No Weld-Measured" and "FEA-No Weld-Measrued-Avg Thick", the variations of the wall thickness for the tested elbow are evidently significant, whether welds are taken into account or not.

Reviewing these results, it is concluded that, for the elbows tested in this work: (1) the variation of piping diameters is negligible; (2) the variation of wall thickness has quite significant effects on the FEA load-displacement calculations; (3) to get the best correlation between tests and FEA, considering the actual wall thickness along the pipe bend and circumferential directions is highly recommended.

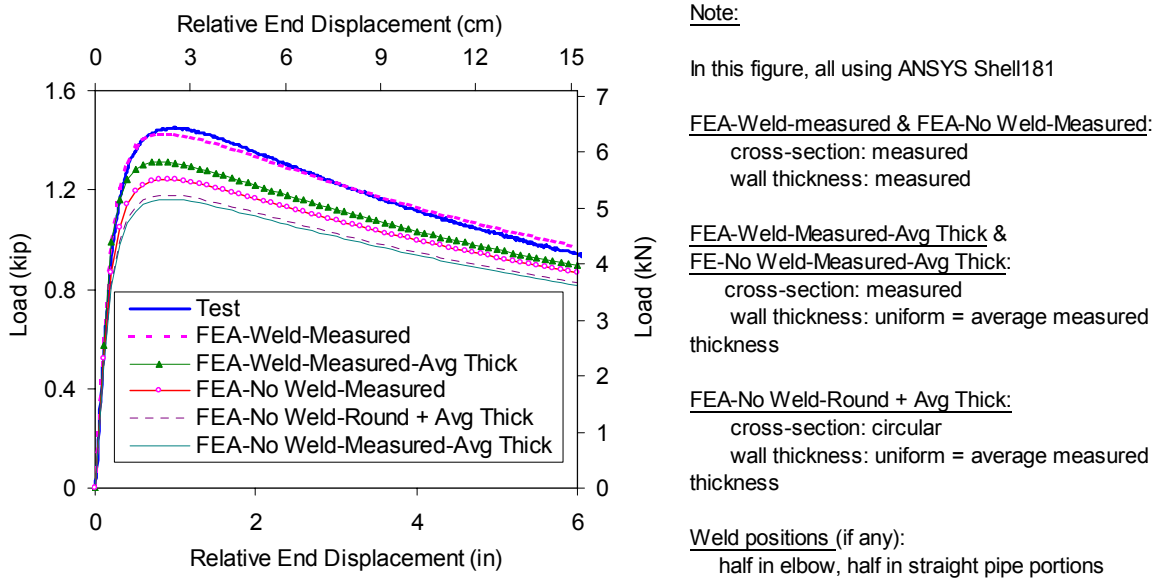

Fig. 11 Load-Displacement Curves using different FEA Geometric Models

Hereafter, the procedure using detailed measured geometric models and considering welds half in elbows and half in straight tangent portions was used in all FEA correlation studies.

3.4 Correlation of Ovalization

Under monotonic in-plane bending, the elbows underwent severe geometric and material nonlinearities. The cross-sections of elbows were increasingly ovalized, as illustrated schematically in Fig. 12 (a) (not drawn in scale). In each physical test, four Linear Variable Differential Transformers (LVDT) were attached to the specimens to measure the changes in outside diameters of the mid-section of elbow, which lies in the symmetric plane of the elbow, as illustrated in Fig. 12 (b). From these measruements, the deformations in intrados-extrados and flank-flank outside diameters were obtained. To better illustrate the correlation, FEA results are plotted against the experimental data

in Fig. 13, with the magnitude of changes in outside diameters as the horizontal axis and load as the vertical axis. The correlation in both intrados-extrados and flank-flank directions of these tests are less satisfactory than the correlations for global end-to-end displacements. The reason for the difference of correlation quality is not yet understaood. These agreements further verify the FEA procedures described above.

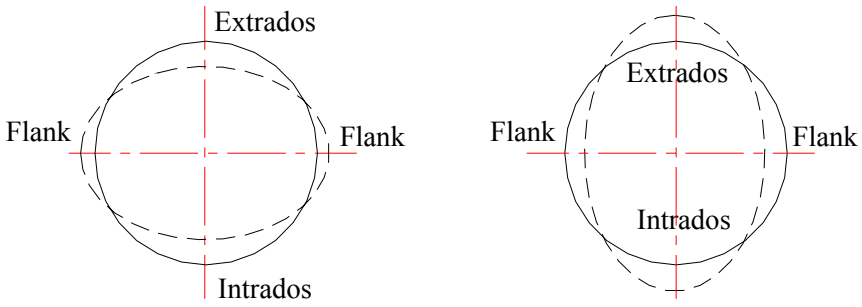

In-Plane Closing Mode In-Plane Opening Mode

(a)

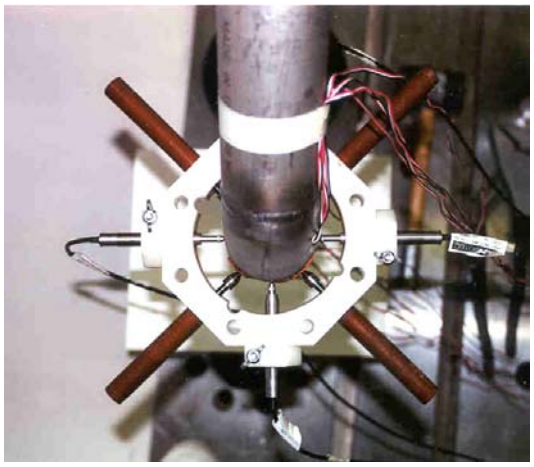

(b)

Fig. 12 Ovalization

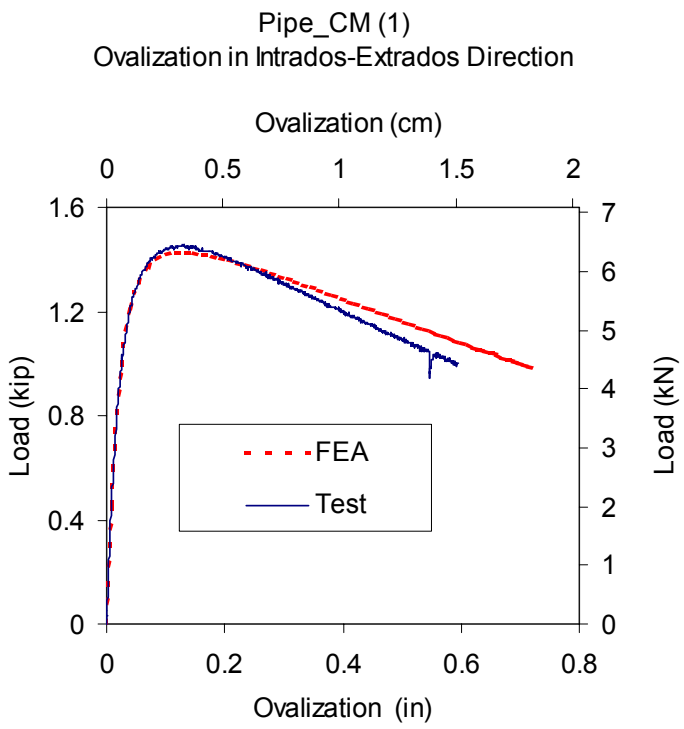
Pipe_CM (1)
Ovalization in Intrados-Extrados Direction
Ovalization (cm)
0
0.5
1
1.5
2
1.6
1.2
0.8
0.4
0
7
6
5
4
3
2
1
0
Load (kip)
Load (kN)
FEA
Test
0
0.2
0.4
0.6
0.8
Ovalization (in)

(a)

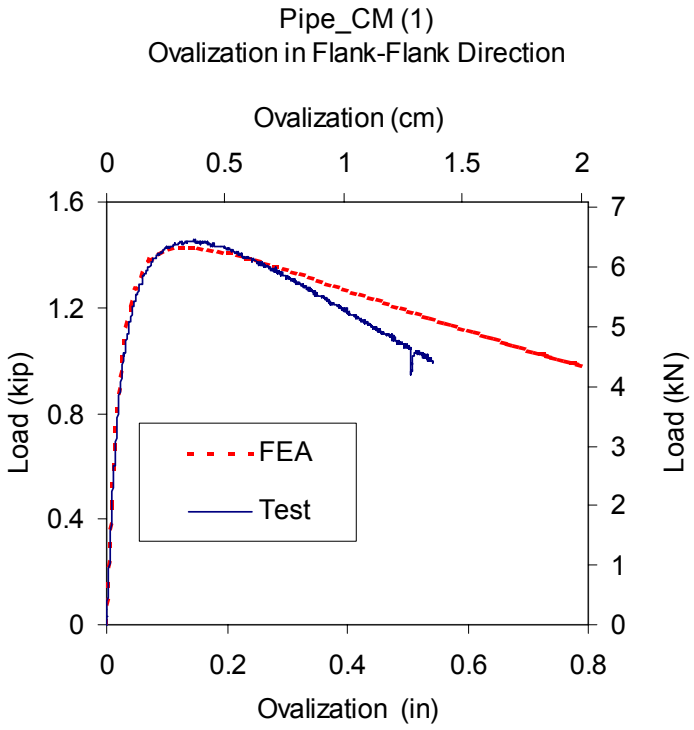
Pipe_CM (1)
Ovalization in Flank-Flank Direction
Ovalization (cm)
0
0.5
1
1.5
2
1.6
1.2
0.8
0.4
0
7
6
5
4
3
2
1
0
Load (kip)
Load (kN)
FEA
Test
0
0.2
0.4
0.6
0.8
Ovalization (in)

(b)

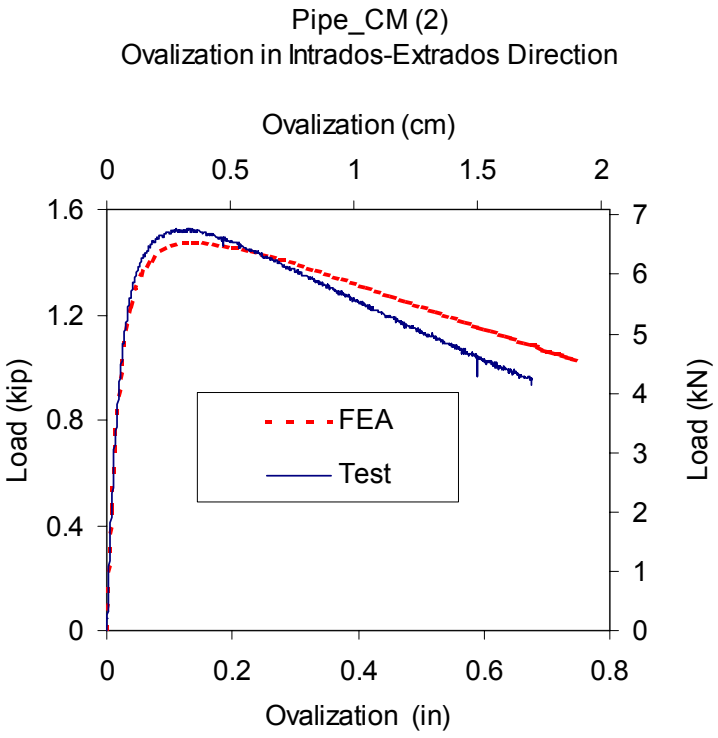
Pipe_CM (2)
Ovalization in Intrados-Extrados Direction
Ovalization (cm)
0
0.5
1
1.5
2
1.6
1.2
0.8
0.4
0
7
6
5
4
3
2
1
0
Load (kip)
Load (kN)
FEA
Test
0
0.2
0.4
0.6
0.8
Ovalization (in)

(c)

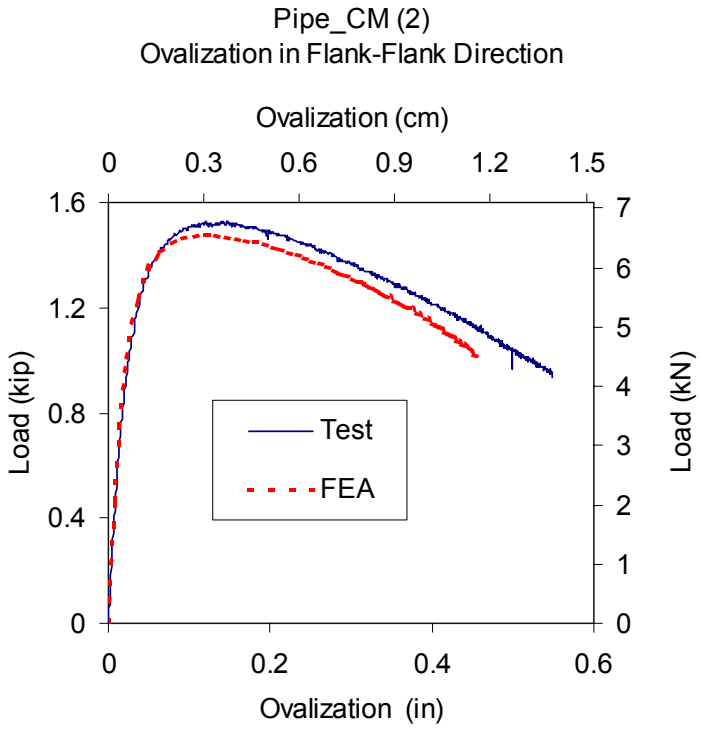
Pipe_CM (2)
Ovalization in Flank-Flank Direction
Ovalization (cm)
0
0.3
0.6
0.9
1.2
1.5
1.6
1.2
0.8
0.4
0
7
6
5
4
3
2
1
0
Load (kip)
Load (kN)
Test
FEA
0
0.2
0.4
0.6
Ovalization (in)

(d)

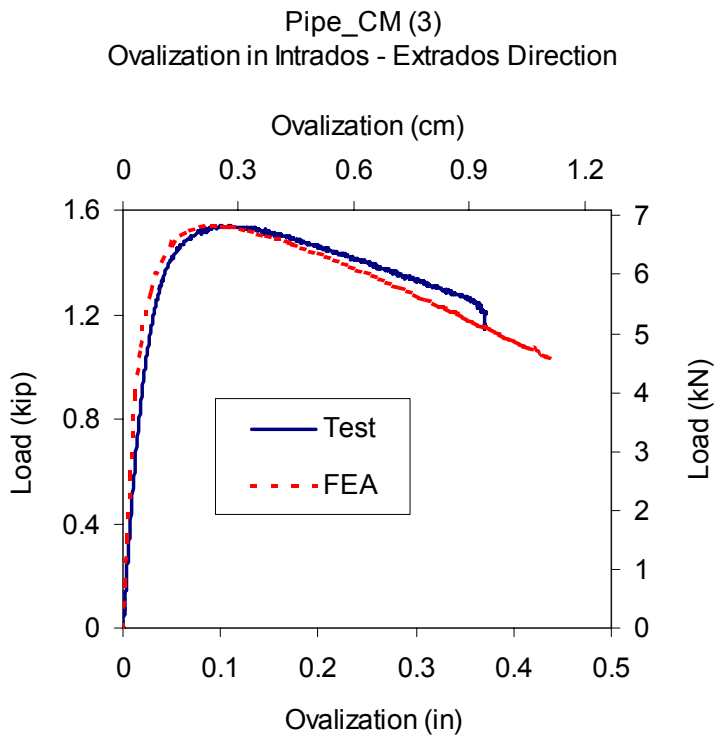
Pipe_CM (3)
Ovalization in Intrados - Extrados Direction
Ovalization (cm)
0
0.3
0.6
0.9
1.2
1.6
1.2
0.8
0.4
0
Load (kip)
7
6
5
4
3
2
1
0
Load (kN)
Test
FEA
0
0.1
0.2
0.3
0.4
0.5
Ovalization (in)

(e)

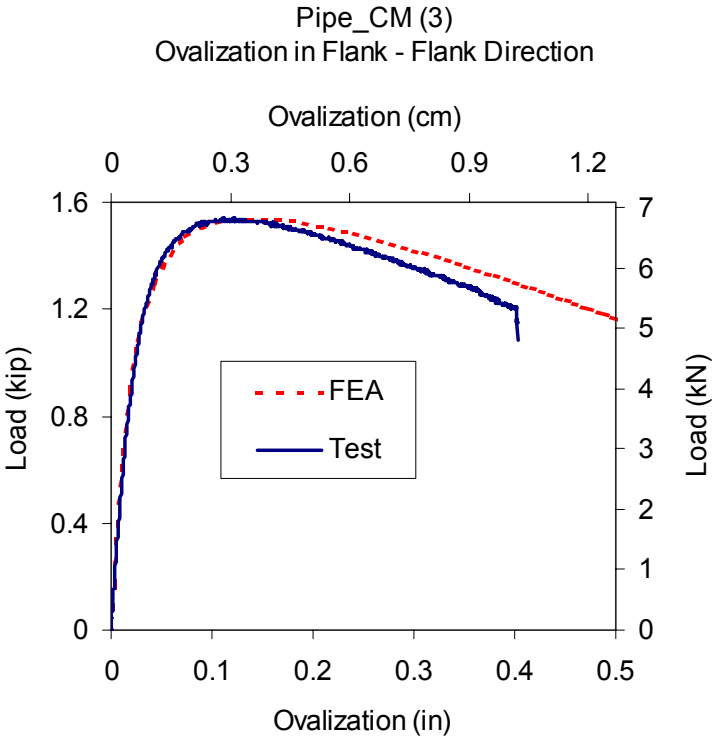
Pipe_CM (3)
Ovalization in Flank - Flank Direction
Ovalization (cm)
0
0.3
0.6
0.9
1.2
1.6
1.2
0.8
0.4
0
Load (kip)
7
6
5
4
3
2
1
0
Load (kN)
FEA
Test
0
0.1
0.2
0.3
0.4
0.5
Ovalization (in)

(f)

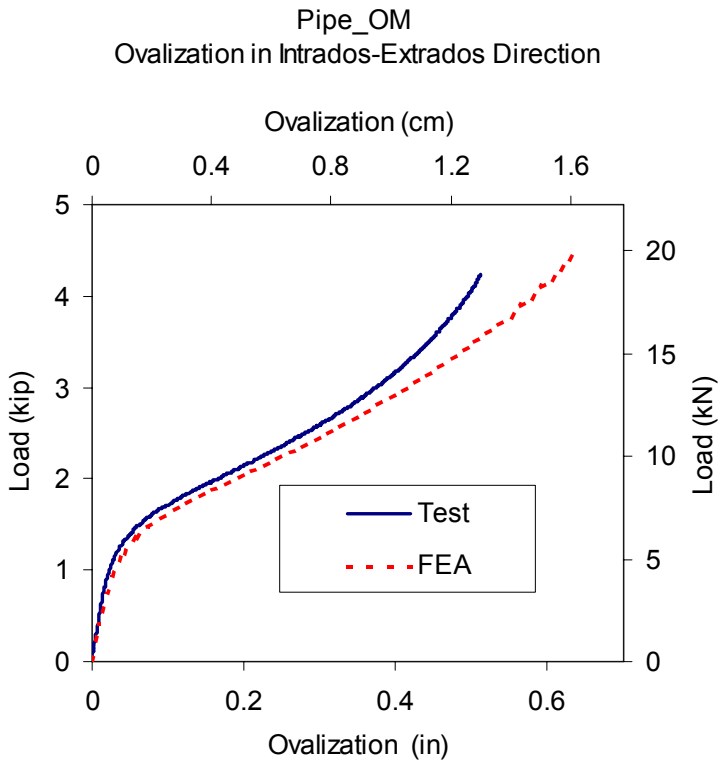

(g)

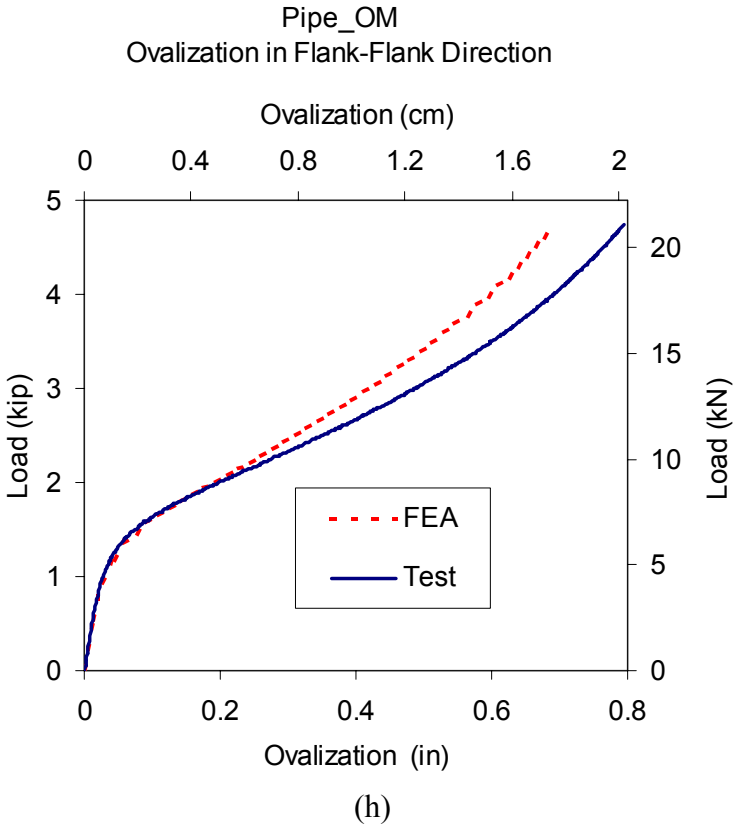

(h)

Fig. 13 Reconciliation of Ovalization

3.5 Correlation of Strains

The FEA procedure described above works quite well in simulating the overall behavior of elbows. How are the simulations of strains? Pipe_CM (3) was designed to perform this investigation. Before the test, five positions, where an FEA run indicated that strains would be relatively large, were selected as the strain gage locations, as shown in Fig. 14 (a). They are called "position 1" through "position 5" respectively hereafter. At each position, a planar T-gage was applied at the outer surface to measure the longitudinal and hoop strains of the area, as illustrated in Fig. 14 (b).

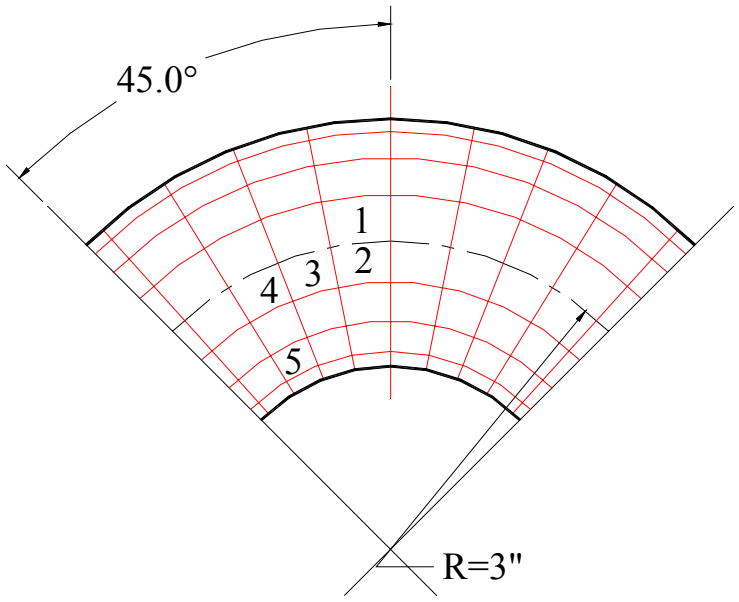

(a)

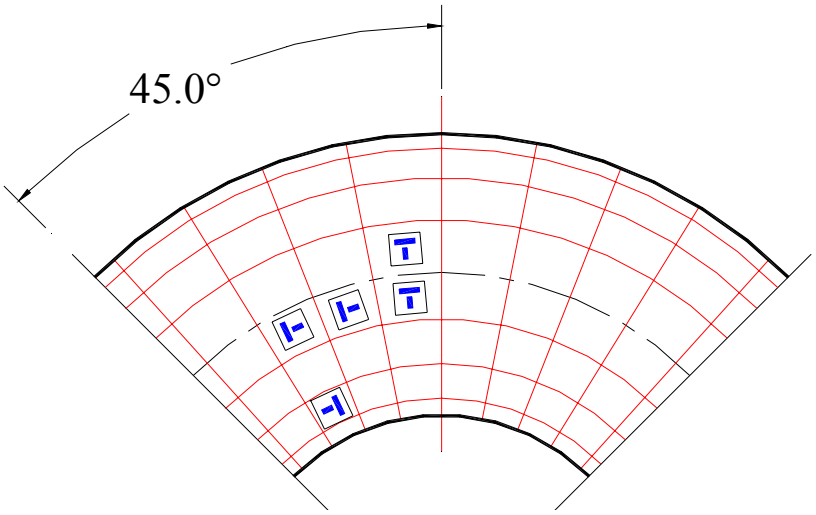

(b)

(c)

Fig. 14 Pipe_CM (3), Strain Gages Layout

The grids in Fig. 14 (b) are actually the FEA elements shown in Fig. 5 (c). This mesh density was the first one used in the FEA study. The calculated strains turned out to be not very accurate compared with experimental data, and a refined FEA mesh was created to improve the correlation. The element automatic mesh refined technique provided by ANSYS was applied to obtain local finer meshes for Strain Gages 01 to 05, as illustrated in Fig. 15. Again, all the nodal coordinates and element wall thicknesses

were generated based on measured data shown in Table 4. This time the computed results were greatly improved and showed good agreement with the measurement in general, except the hoop strains at position 2, 3 and longitudinal strains at position 2, as demonstrated in Fig. 16.

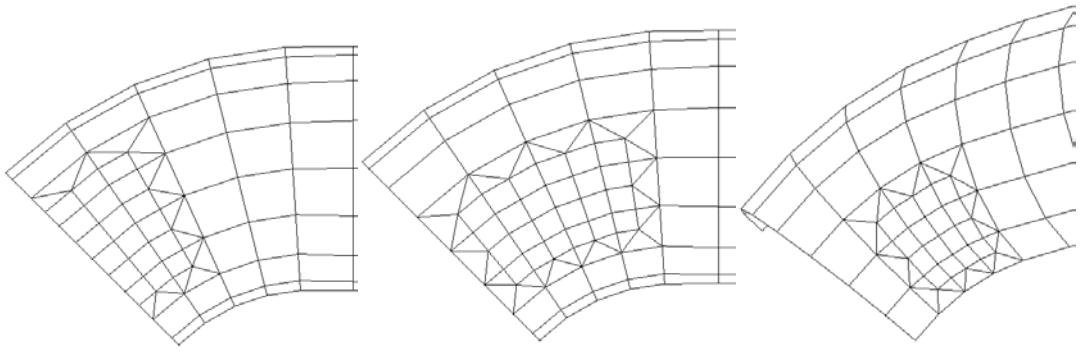

(a) Positions 1 & 2 (b) Positions 3 & 4 (c) Position 5

Fig. 15 Local Mesh for Strains Reconciliation Study of Pipe_CM(3)

As illustrated in Fig. 16 (d) and (f), the hoop strains given by FEA at position 2 and 3 agreed pretty well with the test data up to 0.4% and then deviated significantly. It is probably because that the strain gages partly peeled off during the test, which was reflected by sharp changes in the slopes of the test curves.

For longitudinal strains of position 2, although the computed curve shape was the same of the test, the magnitude did not agree with the measurement very well. Fig. 18 (a) illustrates the longitudinal strain distributions along the circumference at the areas, labeled as "Line 1" in Fig. 17. It shows that the longitudinal strain changes sharply at that region, which indicates that a small change of the position at that area along the circumference will cause a significant change in the computed strains. Although the strain gages alignments were performed as carefully as possible during specimen preparations, it is not easy to apply the gage at exactly the right location and orientation for

the small diameter elbow. Under such circumstances, a small discrepancy between the actual and FEA location of position 2 may cause considerably larger discrepancy in strains.

In the regions where strain distributions change gradually, the strains are not so sensitive to the positional discrepancy and the reconciliation results should be better. To demonstrate this, longitudinal and hoop strain distributions were plotted along four lines, two in circumferential directions, labeled “Line 1” and “Line 2”, and the other two in pipe bend directions, labeled “Line 3” and “Line 4” ” in Fig. 17. The strain distributions given by FEA are presented in Fig. 18. Since the gage length of each T gage is around 4mm, (0.1-0.2”), it accounts for approximately 8° along the circumference and 3° along the pipe bend. This is the measured area of each gage and is illustrated by a band area between two straight lines and labeled as “position 2” etc. in Fig. 18 (a) to (d). Even though “Line 3” and “Line 4” are very close to each other, as shown in Fig. 17, the values of longitudinal strains have very big differences, because those of “Line 3” and “Line 4” along the circumference change substantially as shown in Fig. 18 (a) and (c). The longitudinal strains of position 2 in Fig. 16 (c) are not simply obtained from Fig. 18 (e) or (g) alone and the influence of cirumferential distribution has significant effect in the determination. To clarify this, in Fig. 18 (e) to (h), the measured regions were labeled by “position 2 area” instead of “position 2”. It’s the same so for “position 3 (area)” and “position 4 (area)” in Fig. 18 (e) to (h).

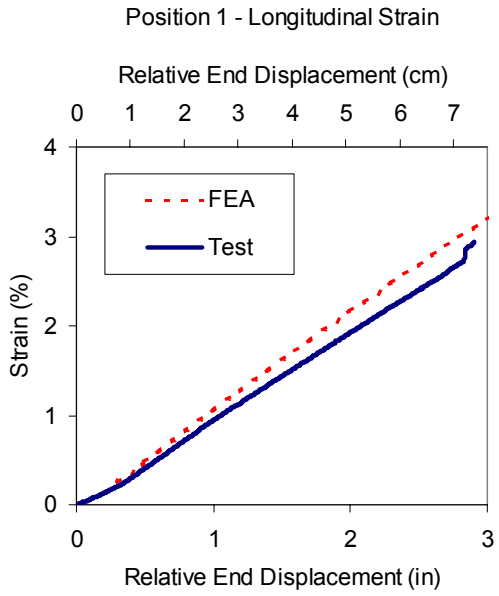
Position 1 - Longitudinal Strain
Relative End Displacement (cm)
0 1 2 3 4 5 6 7
4
3
2
1
0
Strain (%)
FEA
Test
0 1 2 3
Relative End Displacement (in)

(a)

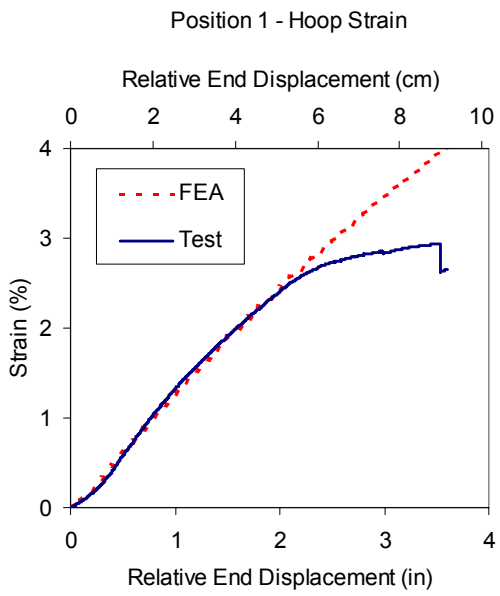
Position 1 - Hoop Strain
Relative End Displacement (cm)
0 2 4 6 8 10
4
3
2
1
0
Strain (%)
FEA
Test
0 1 2 3 4
Relative End Displacement (in)

(b)

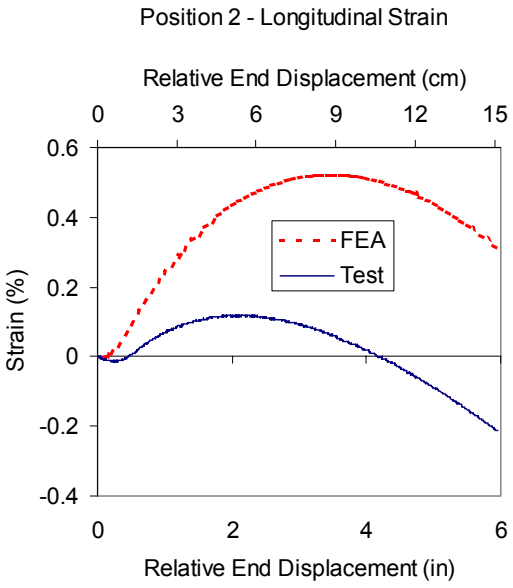
Position 2 - Longitudinal Strain
Relative End Displacement (cm)
0 3 6 9 12 15
0.6
0.4
0.2
0
-0.2
-0.4
Strain (%)
FEA
Test
0 2 4 6
Relative End Displacement (in)

(c)

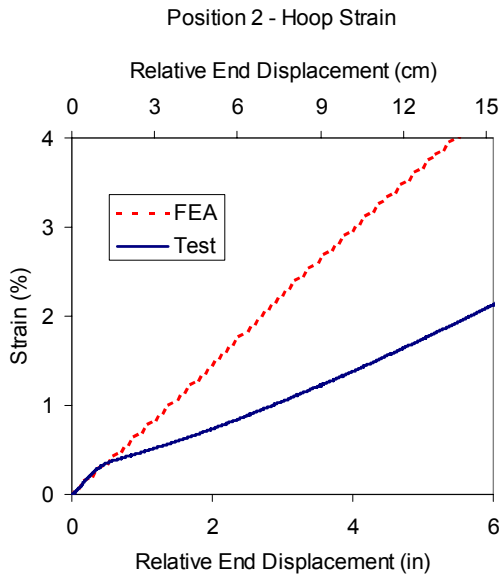
Position 2 - Hoop Strain
Relative End Displacement (cm)
0 3 6 9 12 15
4
3
2
1
0
Strain (%)
FEA
Test
0 2 4 6
Relative End Displacement (in)

(d)

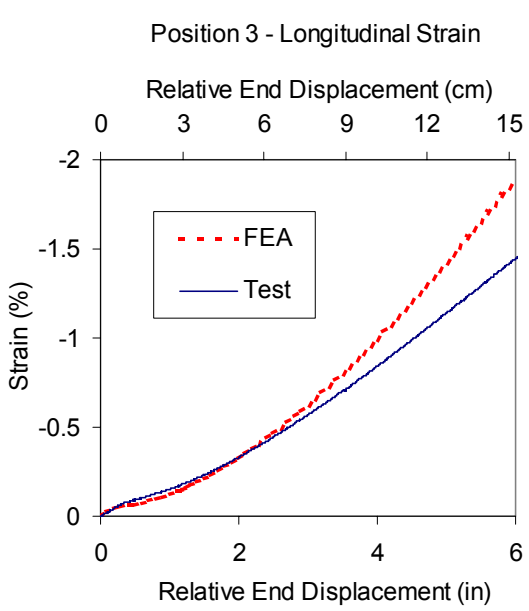
Position 3 - Longitudinal Strain
Relative End Displacement (cm)
0 3 6 9 12 15
-2
-1.5
-1
-0.5
0
Strain (%)
FEA
Test
0 2 4 6
Relative End Displacement (in)

(e)

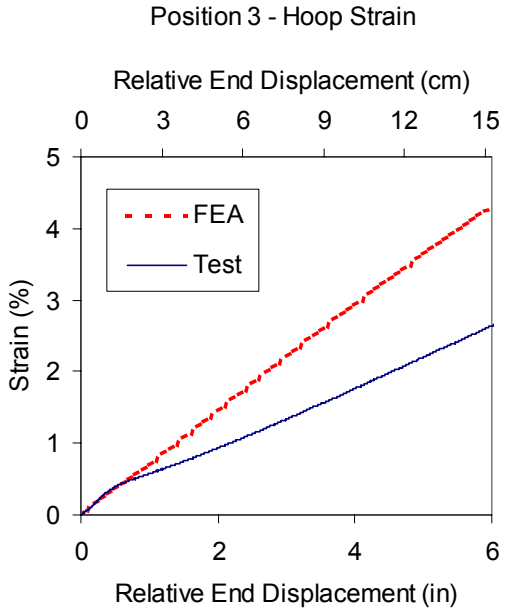
Position 3 - Hoop Strain
Relative End Displacement (cm)
0 3 6 9 12 15
5
4
3
2
1
0
Strain (%)
FEA
Test
0 2 4 6
Relative End Displacement (in)

(f)

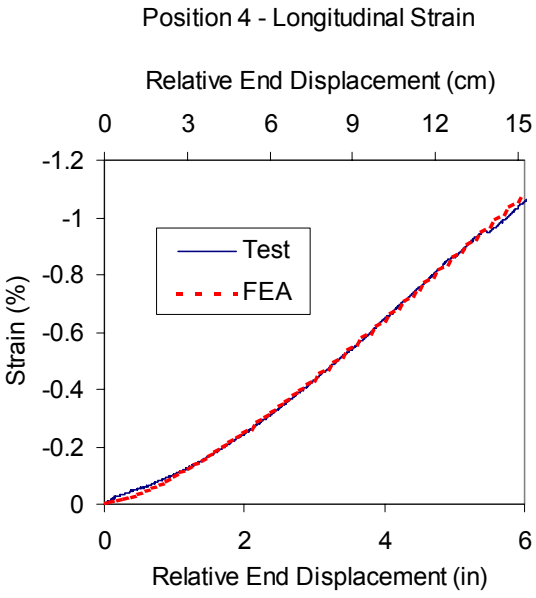
Position 4 - Longitudinal Strain
Relative End Displacement (cm)
0 3 6 9 12 15
-1.2
-1
-0.8
-0.6
-0.4
-0.2
0
Strain (%)
Test
FEA
0 2 4 6
Relative End Displacement (in)

(g)

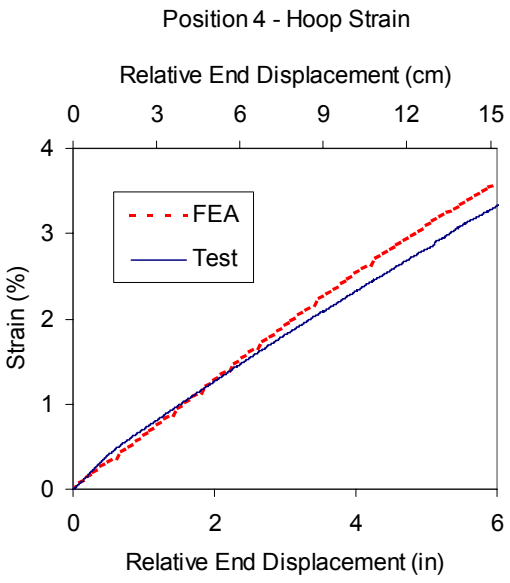
Position 4 - Hoop Strain
Relative End Displacement (cm)
0 3 6 9 12 15
4
3
2
1
0
Strain (%)
FEA
Test
0 2 4 6
Relative End Displacement (in)

(h)

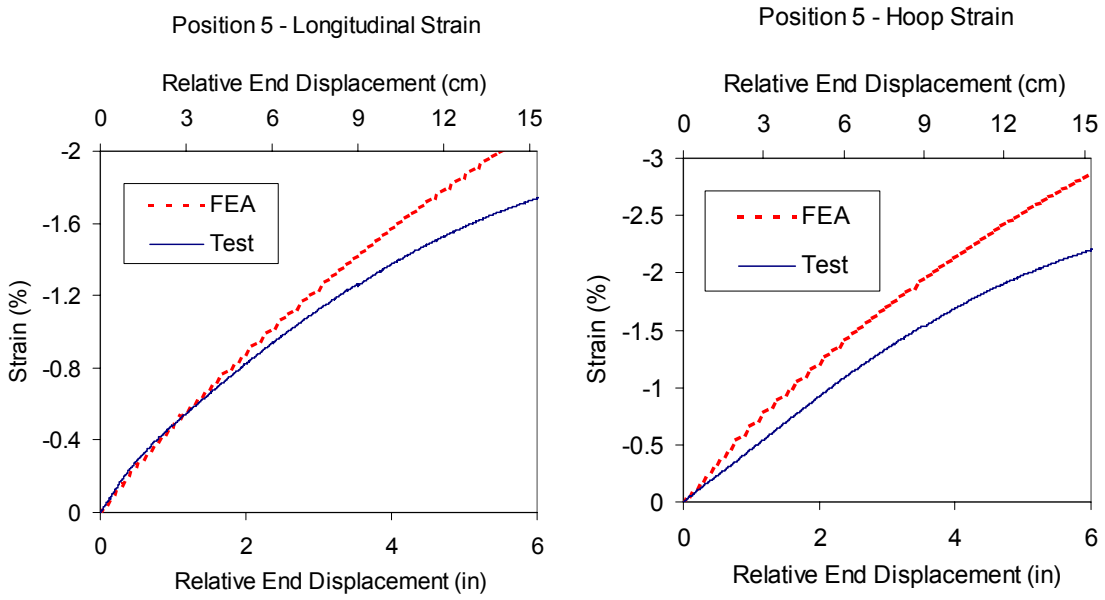

Fig. 16 Strain-Displacement Curves

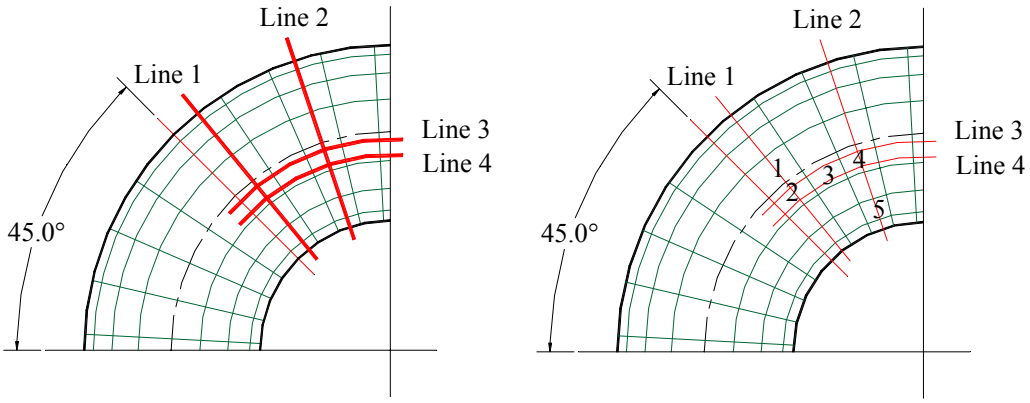

Fig. 17 Strain Distributions Layouts

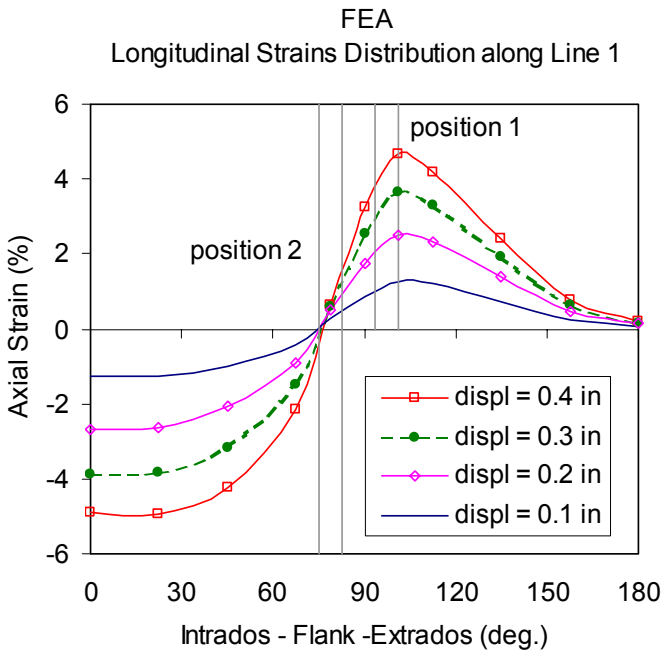
FEA
Longitudinal Strains Distribution along Line 1
position 1
position 2
Axial Strain (%)
6
4
2
0
-2
-4
-6
0
30
60
90
120
150
180
Intrados - Flank -Extrados (deg.)
displ = 0.4 in
displ = 0.3 in
displ = 0.2 in
displ = 0.1 in

(a)

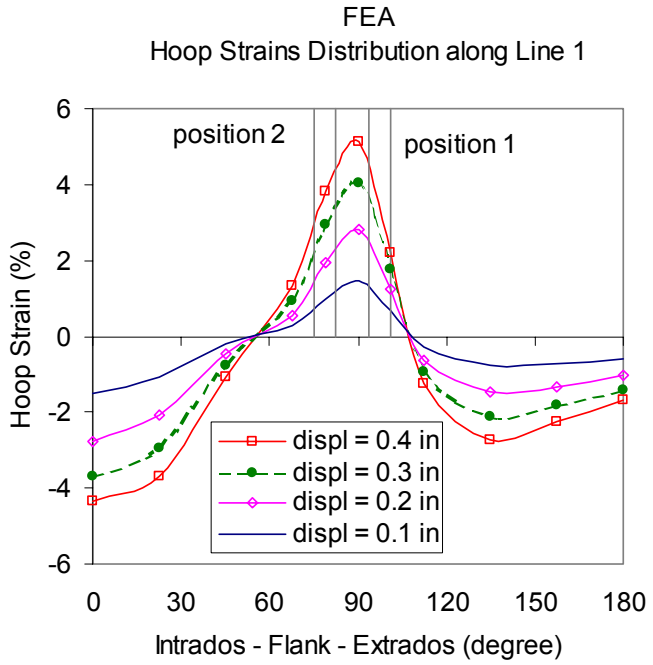
FEA
Hoop Strains Distribution along Line 1
position 2
position 1
Hoop Strain (%)
6
4
2
0
-2
-4
-6
0
30
60
90
120
150
180
Intrados - Flank - Extrados (degree)
displ = 0.4 in
displ = 0.3 in
displ = 0.2 in
displ = 0.1 in

(b)

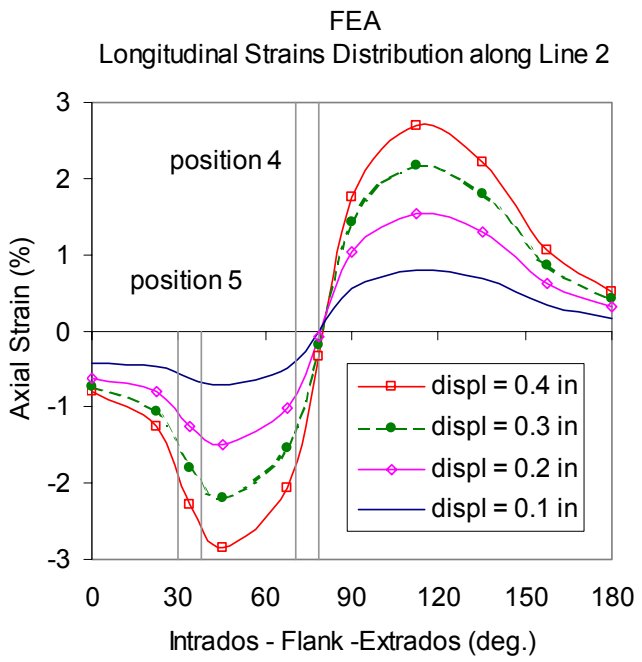
FEA
Longitudinal Strains Distribution along Line 2
Axial Strain (%)
position 4
position 5
displ = 0.4 in
displ = 0.3 in
displ = 0.2 in
displ = 0.1 in
Intrados - Flank -Extrados (deg.)

(c)

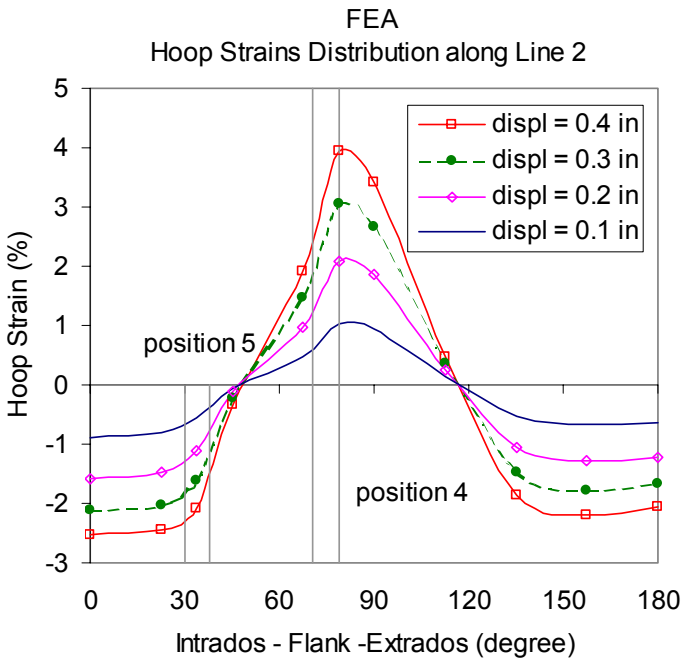
FEA
Hoop Strains Distribution along Line 2
Hoop Strain (%)
displ = 0.4 in
displ = 0.3 in
displ = 0.2 in
displ = 0.1 in
position 5
position 4
Intrados - Flank -Extrados (degree)

(d)

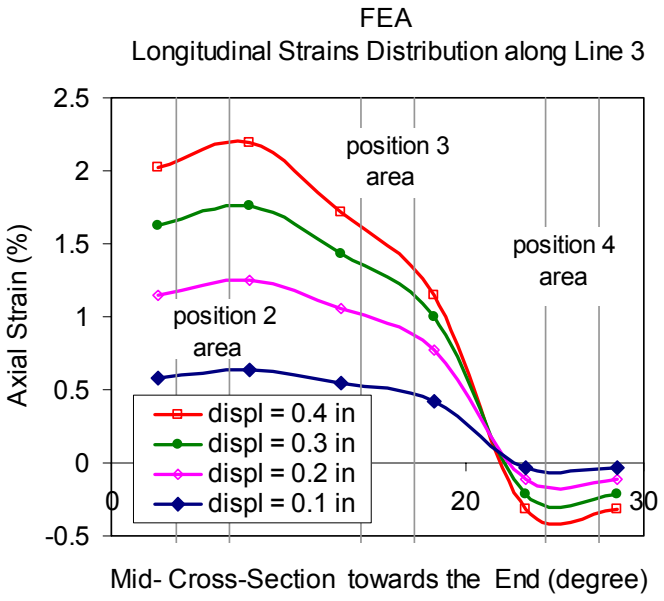
FEA
Longitudinal Strains Distribution along Line 3
Axial Strain (%)
2.5
2
1.5
1
0.5
0
-0.5
0
20
30
position 3 area
position 4 area
position 2 area
displ = 0.4 in
displ = 0.3 in
displ = 0.2 in
displ = 0.1 in
Mid- Cross-Section towards the End (degree)

(e)

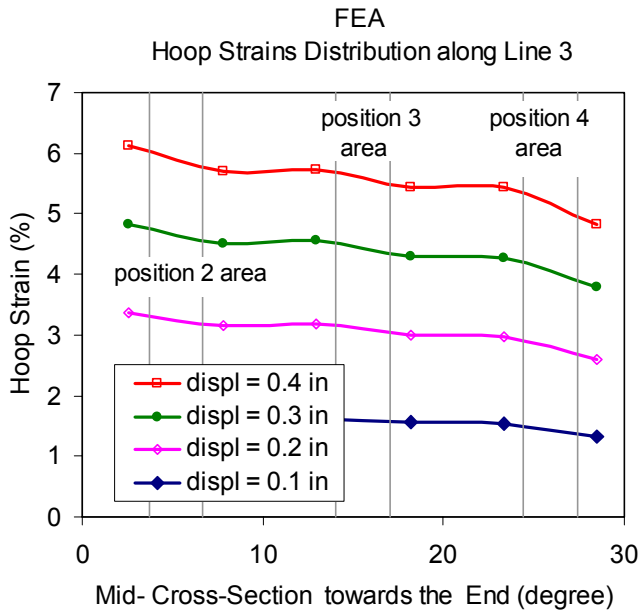
FEA
Hoop Strains Distribution along Line 3
Hoop Strain (%)
7
6
5
4
3
2
1
0
0
10
20
30
position 3 area
position 4 area
position 2 area
displ = 0.4 in
displ = 0.3 in
displ = 0.2 in
displ = 0.1 in
Mid- Cross-Section towards the End (degree)

(f)

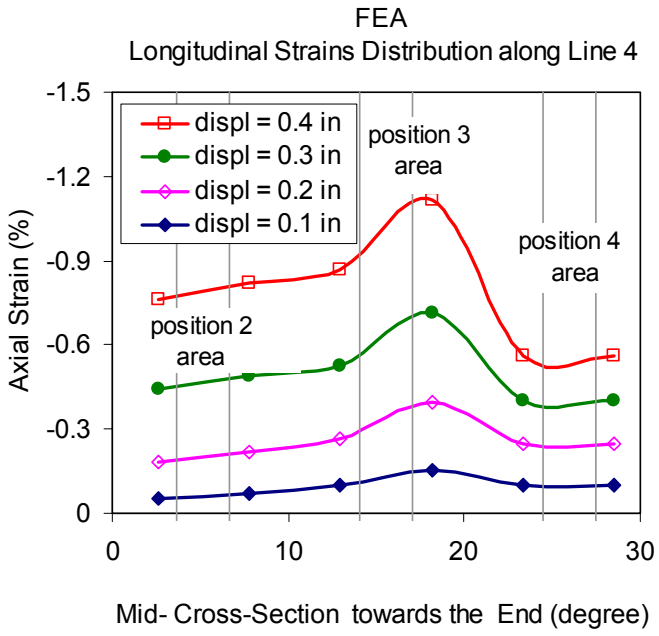

(g)

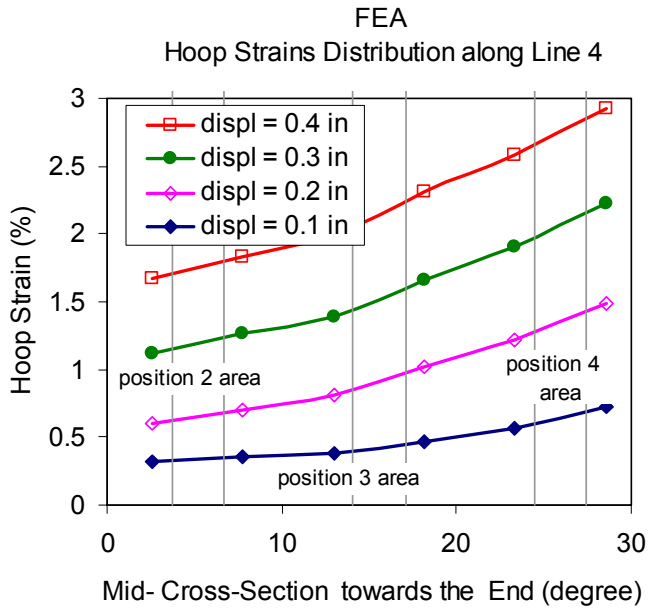

(h)

Fig. 18 Strains Distributions by FEA of Pipe_CM (3)

The study shown above and other results not included led to the conclusions that, (1) mesh density should be sufficiently fine for evaluating strains with good accu-

racy, (2) strain distributions are quite sensitive to the element wall thicknesses used and actual wall thicknesses should be used if possible, (3) in the high strain gradient regions, a small difference in the position may result in significant discrepancy in the reconciliation of FEA and tests.

4 FINITE ELEMENT ANALYSIS USING ABAQUS

In this section, ABAQUS Elbow models (element ELBOW31) were used to simulate the experiments on Pipe_CM (1) and Pipe_OM. The material models utilized are the same as presented in section 3.2 above.

At first, the FEA results neglecting the welds were obtained, as shown in Fig. 20 (a), labeled "FEA-Elbow31-No Weld". To compare with ANSYS SHELL181, a corresponding ANSYS shell model without considering welds was constructed, which used the same assumptions as ELBOW31, i.e. circular initial cross-sections and uniform pipe wall thickness with the value of average measured data. The results are also shown in Fig. 20 (a), labeled "FEA-Shell181-No Weld". It is demonstrated that these two curves agree with each other closely.

To illustrate the effects of welds, an ELBOW31 model taking welds into account was constructed, as shown in Fig. 19 below. It is assumed that the welds are located half in the elbow portions and half in straight tangent portions. ELBOW31 elements were utilized to simulate a welding ring on each end, with the element thicknesses equal to the average measured weld region thickness.

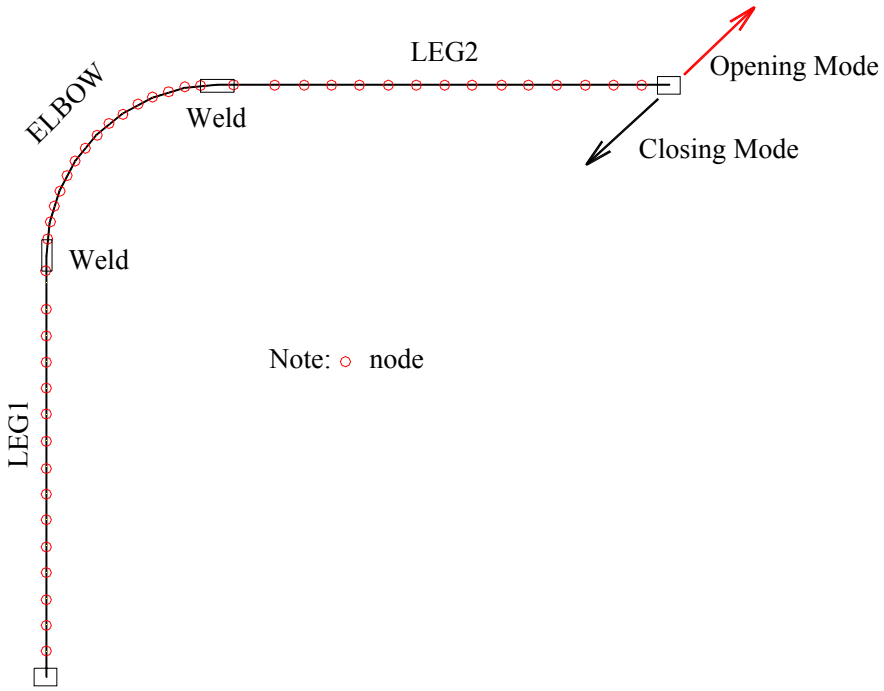

Fig. 19 ABAQUS ELBOW31 Models

The ELBOW31 results considering welds are shown as a fine solid line, labeled "FEA-Elbow31-Weld" in Fig. 20 (a) and (b). It is observed that, for the elbow investigated, the welding effects are significant, which can lead to 12% difference in the load bearing capacity. Even with the welds taken into account, the ELBOW31 results are still up to 5-6% lower than the measured test data. To investigate the possible reasons, the results from ANSYS SHELL181 using the detailed measured geometric models are plotted in Fig. 20 (b) also. It is shown that the models considering the actual cross-sections diameters and wall thickness gave better predictions than using simplified geometric models (initial round cross-sections and uniform wall thickness). For the elbow tested, these actual geometric dimensions do matter to some extent.

For the in-plane opening bending test, the load-displacement history responses, plotted against the measured experimental data and FEA results from ANSYS Shell models (considering variation of wall thickness, initial out-of-roundness of the cross-

sections and welds half in straight tangent parts and half in elbow portions), are illustrated in Fig. 20 (c).

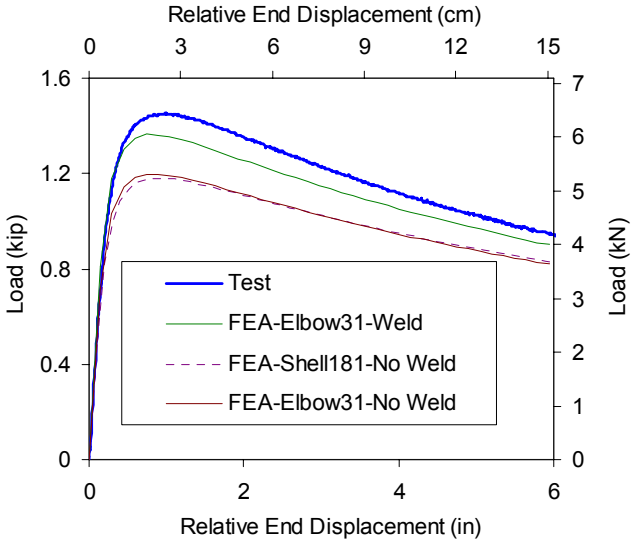

Note:

In this figure,

Shell181 models & **Elbow31 models**:
cross-section: circular
wall thickness: uniform,
average measured value
Weld positions:
half in elbow, half in straight pipe portions

(a) Pipe_CM (1)

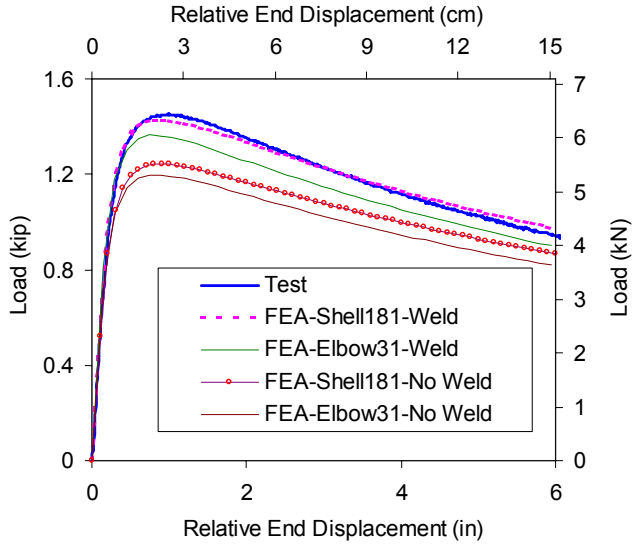

Note:

In this figure,

Shell181 models:
cross-section: measured
wall thickness: measured

Elbow31 models:
cross-section: circular
wall thickness: uniform,
average measured value
Weld positions (for both):
half in elbow, half in straight pipe portions

(b) Pipe_CM (1)

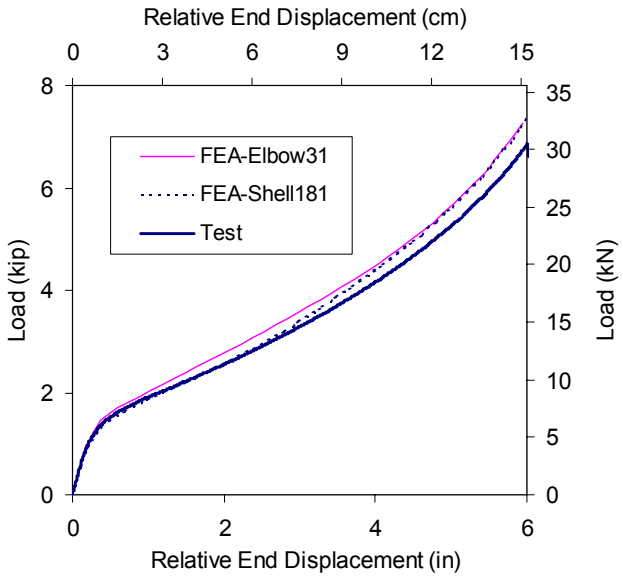

(c) Pipe_OM

Fig. 20 Correlation of Overall Behaviors

In general, for the specimens tested, ELBOW31 gave very good load-displacement predictions and compared with measured test data presented above, the discrepancy is less than 6%. However, it is observed that Elbow31 under-predicted the load capacity for the in-plane closing test Pipe_CM (1) and over-predicted the in-plane opening test for Pipe_OM. It is very likely due to the implementation approaches of ELBOW31, which assume that the initial cross sections are circular and the pipe walls are uniform.

5 CONCLUSIONS

Following the nonlinear FEA modeling procedures described in Part III, this part focuses on investigating weld joint effects and evaluating strains in reconciliation work. Four stainless steel elbow specimens subjected to in-plane closing loading and in-plane opening loading were simulated. The FEA models all give quite good results compared

with test data with global end-to-end displacement correlation being the best and cross-sectional distortion and strain correlation being less good. As was the case in Part III, this study also demonstrates that under monotonic static loading, the finite element procedure is capable of providing quite accurate predictions of pipe bend behavior. For thin-walled pipes, the global behavior from FEA can be quite sensitive to welding conditions if welds are not ground off. There can be significant differences between neglecting and considering welding effects. If possible, the existence of welds, the welding material properties and the geometric positions of welds should be taken into account in reconciliation work. For the elbows investigated, the variations of cross-sectional diameters are negligible, while the variation of the wall thickness is not. Considering the actual wall thickness distributions is recommended in FEA simulations. In general, the simulation of strains will not be as good as of load-displacement relationships, and wall thicknesses and mesh density are critical for such simulation.

6 NOMENCLATURE

a, b, c, d = measured dimensions of specimens

D_o = outside diameter of pipe

E = Young's modulus

S_y = yield stress

S_u = ultimate stress

t = wall thickness

7 REFERENCES

1. Tan, Y. and Matzen, V. C., "Correlation of test and FEA results for the nonlinear behavior of elbows", PVP, vol. 407, Pressure Vessel and Piping Codes and Standards-2000, pp307-314, July 2000

2. Hassan, T., Modlin, M. and Matzen, V.C., "Monotonic In-plane Tests on 2-inch, Schedule 10 Elbows," Data developed at the Center for Nuclear Power Plant Structures, Equipment and Piping, North Carolina State University, 1999-2001

3. Mello, R. M., and Griffin, D. S., 1974, "Plastic Collapse Loads for Pipe Elbows Using Inelastic Analysis", J. of Pressure Vessel Technology, p177-183

4. Sobel, L. H. and Newman, S. Z., 1980, "Comparison of Experimental and Simplified Analytical Results for the In-Plane Plastic Bending and Buckling of an Elbow", Transactions of the ASME, Vol.102, p400-409

5. Sobel, L.H. and Newman, S. Z., 1986, "Simplified, Detailed, and Isochronous Analysis and Test Results for the In-Plane Elastic-Plastic and Creep Behavior of an Elbow", J. of Pressure Vessel Technology, Vol.108, p297-304

6. Dhalla, A. K., 1987, "Collapse Characteristics of a Thin-Walled Elbow: Validation of an Analytical Procedure", Transactions of the ASME, Vol.109, p394-401

7. Suzuki, N. and Nasu, M., 1989, "Non-linear analysis of welded elbows subjected to in-plane bending", Computers & Structures, Vol, 32, No.3/4, pp871-881

8. Kussmaul, K., Diem, H. K., Uhlmann, D., Kobes, E., 1995, "Pipe bend behaviour at load levels beyond design", (SMiRT 13), Brazil

9. Mourad, H. M. and Younan, Y. A., "The effect of modeling parameters on the predicted limit loads for pipe bends subjected to out-of-plane moment loading", PVP-Vol. 399, ASME 2000, p131-138

10. ASME Code For Pressure Piping, B31, An American National Standard, ASME B31.3-1999 Edition, v.22, pp140

PART V

CORRELATION OF TESTS AND FEA RESULTS FOR ELBOWS SUBJECTED TO OUT-OF-PLANE LOADING

ABSTRACT

The main purpose of this study is to validate a finite element analysis (FEA) simulation methodology to predict the out-of-plane behavior of piping elbows. Two out-of-plane elbow experiments and the corresponding FEA shell and elbow element models are presented. For load-displacements curves, all the FEA predictions showed excellent agreements with measured experimental results. For the correlation of strains, only shell models were used and the computed results turned out to match the measured strain responses closely. It is concluded that the FEA procedure can simulate elbow behaviors subjected to out-of-plane loading very well.

1 INTRODUCTION

In our foregoing reconciliation work, described in Parts III and IV, the FEA procedures developed have successfully simulated eight physical tests: two four-point-bending tests on straight pipes, four in-plane closing bending tests and two in-plane opening bending tests on 90° long-radius elbows. The purpose of this study is to determine if out-of-plane loading can be equally well simulated.

2 BACKGROUND

The study of pipe bends started with von Karman [1] in 1911. Since then Hovgaard [2] in 1930, Turner and Ford [3] in 1957, developed comprehensive theories for

curved tubes under in-plane bending. Beskin [4] in 1945 extended von Karman's theory and Smith [5] in 1967 adapted Turner and Ford's analysis to deal with out-of-plane bending. All the studies above were based on elastic and small-deflection assumptions.

In addition to theoretical study, extensive experimental investigations have been performed. Smith and Ford [6] in 1967 carried out an experimental investigation on three individual pipe bends subjected to three-dimensional loading, one for in-plane bending, one for out-of-plane bending and one for combined bending. Deflections, cross-sectional distortions and strains were measured. In 1978, twenty elbow tests were shown in Greenstreet's report [7], in which five were out-of-plane tests with or without internal pressure. Deflection and strain data were shown. Imazu et al. [8] in 1979 tested one thin-walled stainless steel 304 elbow at 600°C under out-of-plane moment. In Prost et al.'s 1983 experimental study [9] three out-of-plane elbow tests were conducted at room temperature with or without internal pressure and one at elevated temperature (340°C). Hilsenkopf et al. [10] in 1988 presented the results of two series tests performed on 90° large-radius elbows, among which six were out-of-plane tests. Each series includes three tests respectively. One was out-of-plane bending at room temperature without internal pressure, one was without internal pressure but at 120°C temperature, and one was at room temperature but with internal pressure. The moment-rotation relationships and the ovalization modes were recorded and illustrated. All of the work cited above was based on experiments; FEA simulation was not involved.

Natarajan, R. and Mirza, S. [11] in 1981 developed a finite element scheme for the analysis of a piping system subjected to out-of-plane moments. In 1993, Basavaraju

and Lee [12] utilized ANSYS, a commercial FEA computer program, to study stress intensification factors and the C_2 stress index (the B_2 index is related to the C_2 index [13]) for in-plane and out-of-plane moment, in which linear elastic analysis was used. To determine the stress for an elbow which has a stiffener closer than one pipe radius from the elbow, Machida, H. et al. [14] in 1995 carried out elastic stress analyses using FEA for a 90° elbow subjected to out-of-plane moment. Mourad and Younan [15] in 2000 using ABAQUS (a commercial FEA package) and taking geometric and material nonlinearities into account, performed nonlinear analysis of elbows subjected to out-of-plane moment and internal pressure. All the works above focused exclusively on FEA study and the computed results were not confirmed by experimental data.

Some reconciliation works were conducted to bridge the experimental and FEA investigations. Fujimoto, T. and Soh, T. [16] in 1988 analyzed very thin-walled pipe bends under in-plane or out-of-plane moments and compared their FEA stress distributions with experimental measurements. The experimental values are less than their FEA data by 13-21% for out-of-plane forces [16] and they attributed the discrepancies to "the geometric irregularities of the test models". In 1995, Kussmaul et al. [17] reported a 90° elbow subjected to out-of-plane bending without internal pressure, and a finite element analysis using ABAQUS element ELBOW31 to simulate the test. Their computed loads differed up to 15-20% compared with experimental results. They attributed the discrepancies to inaccurate material properties. Although Mourad and Younan [18] concentrated on the effect of FEA modeling parameters for pipe bends subjected to out-of-plane moment and internal pressure, they verified their FEA models by comparing the computed results to the measured test data reported by Greenstreet [7], 1978. In their study, it's

clearly demonstrated that using "closest in properties to a real elastic-plastic strain-hardening material"[18] is very important for correlations between FEA and tests.

As mentioned in the foregoing, though volumes of research have been performed on elbows under out-of-plane bending, the correlation of test and FEA results has not been fully solved. To further validate the FEA developed in Parts III and IV, the procedure was verified by two out-of-plane elbow tests in the present work.

3 EXPERIMENTS

3.1 Pipe-1

The first test used to verify our FEA procedure is an out-of-plane bending test on 6" Sch40 long radius carbon steel elbow, reported by Greenstreet [7], (called Test No. PE – 3 in [7], called Pipe-1 hereafter). The test information is illustrated in Fig. 1. Measured specimen dimensions were not available and only nominal dimensions were reported in [7]. They are shown in Table 1.

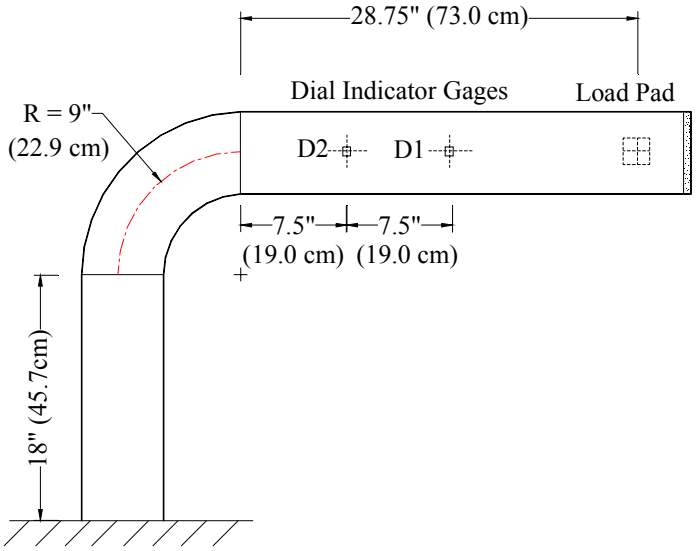

Fig. 1 Test Setup [7], Fig.2

Table 1 Nominal Specimen Dimensions [7], Table 1

D_o		t		D_o / t
(in)	(cm)	(in)	(cm)	
6.625	16.83	0.280	0.711	23.7

3.2 Pipe-2 [19]

At NCSU, one specimen, called Pipe-2, was tested under out-of-plane loading, as shown in Fig. 2. The specimen was a 2"Sch10, 90° long radius, stainless steel 304 L, seamless elbow, with segments of straight pipes welded to both ends, as illustrated in Fig. 3. The lengths of the straight tangent portions were about 5 times the outside diameter of the elbow, which were long enough to eliminate the end effects according to Yu [20].

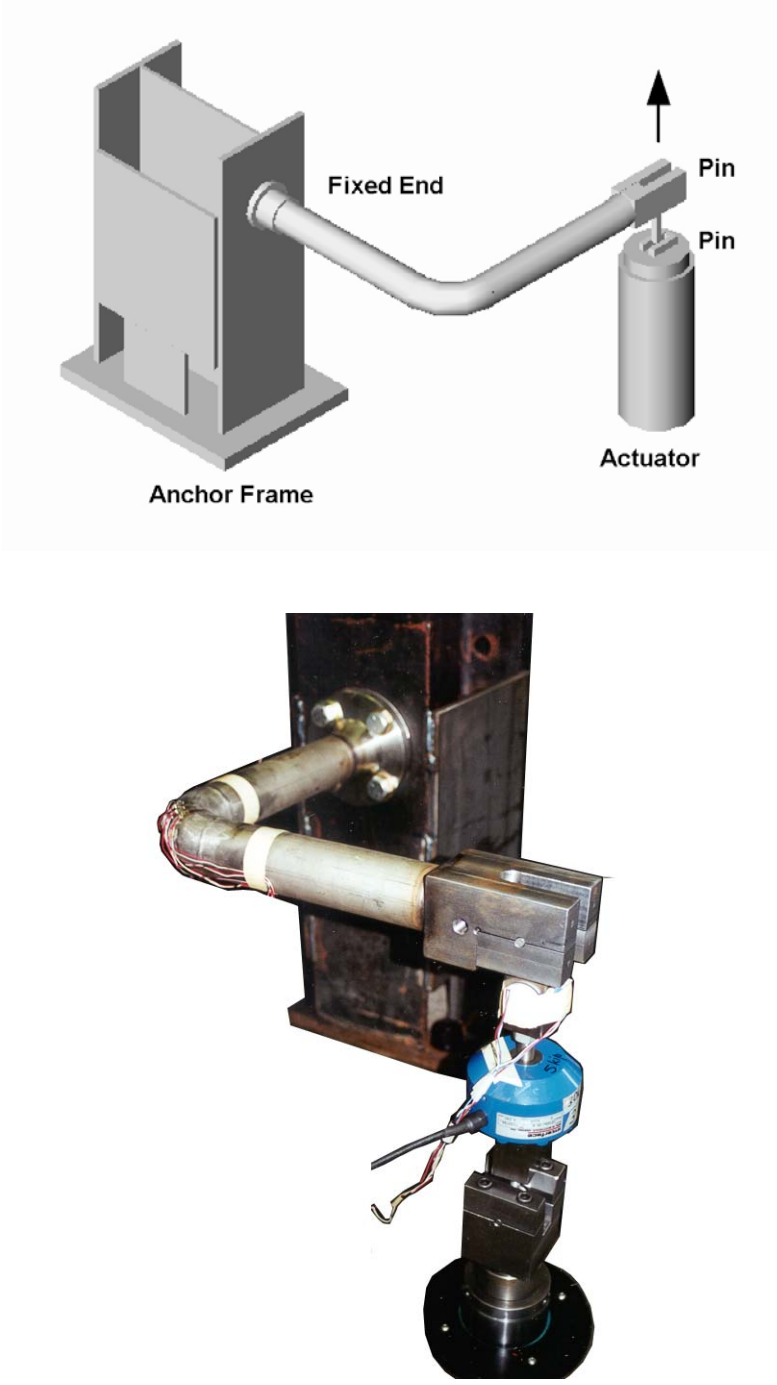

Fig. 2 Test Setups

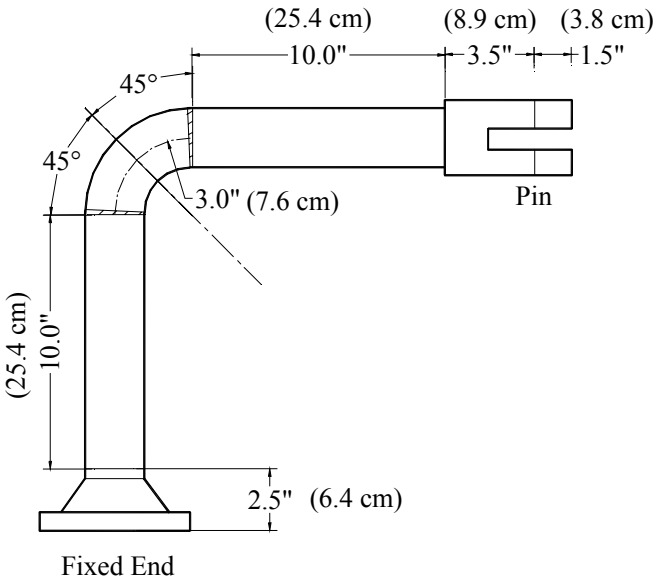

Fig. 3 Specimen Dimensions

Actual geometrical dimensions and pipe wall thicknesses were measured before the test. Five cross-sections along the pipe bend radius, labeled P-1 to P-5 in Fig. 4 (a), were picked as planes to measure. In each plane, the wall thicknesses at extrados, intrados and flanks were measured as shown in Fig. 4 (b). The measured data are given in Table 2 and the average wall thicknesses and average outside diameters are provided in Table 3.

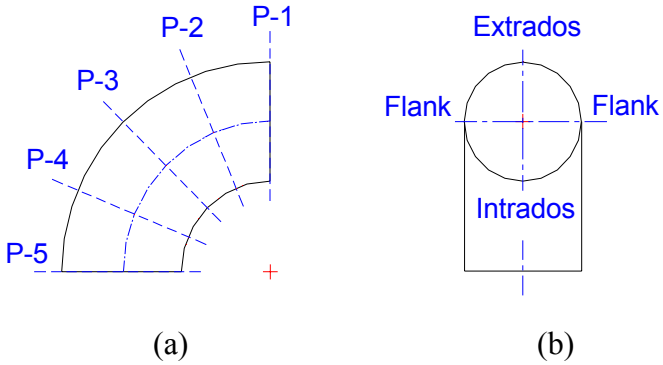

Fig. 4 Measured Cross-Sections

Table 2 Measured outside diameters and wall thicknesses

Plane No.	P-1		P-2		P-3		P-4		P-5		average	
unit	(in)	(cm)	(in)	(cm)	(in)	(cm)	(in)	(cm)	(in)	(cm)	(in)	(cm)
$D_{o\ Flank\text{-}Flank}$	2.380	6.045	2.385	6.058	2.376	6.035	2.382	6.050	2.380	6.045	2.381	6.047
t -Flank	0.132	0.335	0.130	0.330	0.130	0.330	0.130	0.330	0.132	0.335	0.131	0.332
t -Flank	0.135	0.343	0.131	0.333	0.135	0.343	0.138	0.351	0.142	0.361	0.136	0.345
$D_{o\ Intra\text{-}Extra}$	2.375	6.033	2.365	6.007	2.370	6.020	2.377	6.038	2.377	6.038	2.373	6.027
t -Intrados	0.131	0.333	0.141	0.358	0.139	0.353	0.141	0.358	0.128	0.325	0.136	0.345
t -Extrados	0.119	0.302	0.120	0.305	0.117	0.297	0.119	0.302	0.120	0.305	0.119	0.302

Table 3 Average outside diameters and wall thicknesses

Segments of Test Specimens		average t	D_o			D_o / t
			average		average	
			Extrados -Intrados	Flank - Flank		
Elbow	(in)	0.133	2.373	2.381	2.377	17.9
	(cm)	0.338	6.027	6.047	6.038	
Straight Pipe	(in)	0.110	/	/	2.375	21.6
	(cm)	0.279	/	/	6.033	

4 FINITE ELEMENT ANALYSIS

In this study, ANSYS version 5.6 and ABAQUS version 6.1were used. Two types of FEA models, one using shell elements and the other using elbow elements, were tried. For the FEA shell models, ANSYS SHELL43, SHELL181and ABAQUS S8R5 were utilized. For FEA elbow element models, ABAQUS ELOW31 was used. Nominal dimensions were used in elbow models and the shell models for Pipe-1, while in the shell models for Pipe-2, nodal coordinates and wall thicknesses along the circumference and along the pipe bend radius were carefully defined by measured data. In all cases, large deformations were taken into account.

4.1 Material Models

FEA requires the non-linear stress-strain curves for the tested specimens, but none were available for any of the specimens tested. However, the values of the three material parameters (E, S_y and S_u) were provided in Ref. [7] for Pipe-1 and in the manufacturer's report for Pipe-2, as shown in Table 4 and Table 5 below respectively. In the current study, the procedure described in Part III was used to construct the specimen stress-strain curves based on these three parameters and other available stress-strain curves of the same type of material.

For Pipe-1, a uniaxial tensile test stress-strain curve for SA106 Grade B published in [21], as illustrated in Fig. 5, was used as the base curve and it is assumed that the engineering ultimate strain corresponding to the ultimate stress was 20% and the proportional limit was 35 ksi. For Pipe-2, an ASTM type tensile test was performed on a coupon specimen cut from a piece of straight pipe, which is the same product batch as the straight pipes used in our specimens. The experimental engineering stress-engineering strain curve is shown in Fig. 6 as a solid line, and labeled as "2"Sch10 Coupon". The measured stress-strain data show close agreements with the manufacturer's report, as given in Table 5. Since the manufacturer's testing report gave different properties for the elbow and straight tangent pipes, two separate nonlinear stress-strain curves were needed in the FEA model – one for the straight tangent pieces and one for the elbow. For the straight tangent portions, the stress-strain curve of 2"Sch10 coupon was used directly. For the elbow portion, a new stress-strain curve was constructed using the curve of 2"Sch10 coupon as the base curve, as illustrated by a dash line, labeled

"Elbow (constructed)" in Fig. 6. Since the welds of Pipe-2 specimen were ground off before the test, the welds were assumed to be negligible in the FEA model.

Table 4 Material Properties of Pipe-1

Carbon Steel SA106 Grade B	S_y		S_u		E		e_y	e_u
	(ksi)	(MPa)	(ksi)	(MPa)	(ksi)	(GPa)	(%)	(%)
Pipe -1 [7], Table 1	50.0	345	73.6	507	30100	208	N/A	N/A
Base Curve [21], Table 3	42.5	293	69.7	480	42922	296	0.2	20

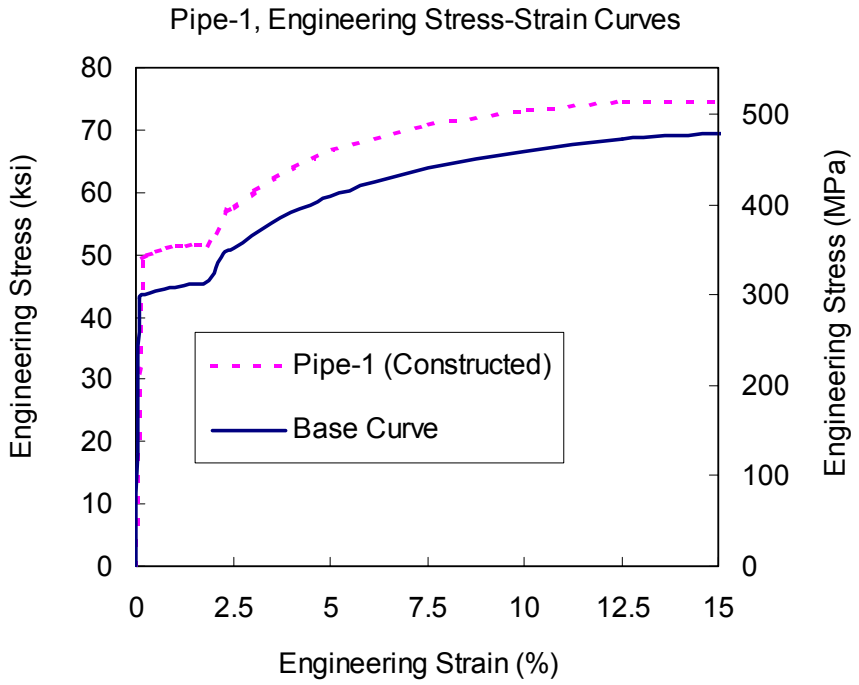

Fig. 5 Material Curves of Pipe-1

Table 5 Material Properties of Pipe-2

Stainless Steel 304		S_y		S_u		E	
Segments of Test Specimens		(ksi)	(MPa)	(ksi)	(MPa)	(ksi)	(GPa)
Manufacturer's report	Elbow	35.4	244	81.0	558	N/A	N/A
	Straight Pipe	39.5	272	82.2	567	N/A	N/A
NCSU ASTM test	Straight Pipe	38.4	265	85.8	592	29000	200

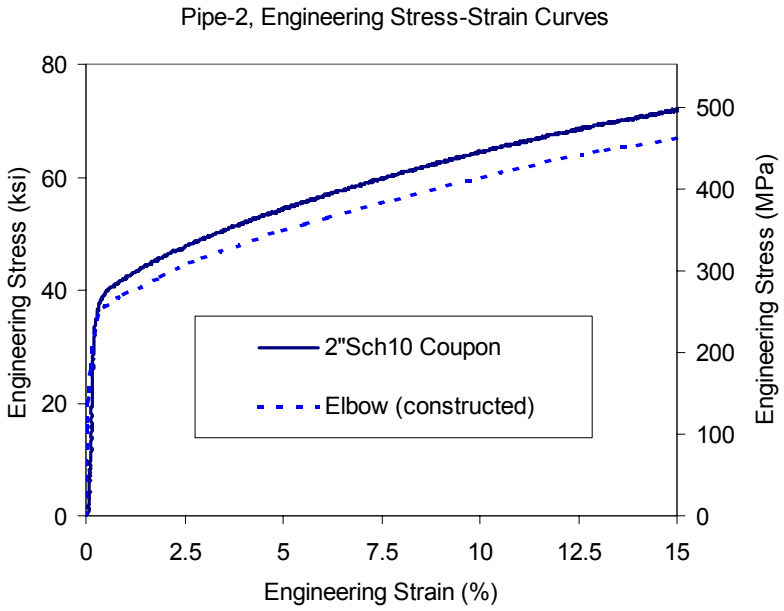

Fig. 6 Material Curves of Pipe-2

4.2 Correlation of Overall Behavior

For Pipe-1, the experimental load-displacement curves, schematically published in Ref. [7], were digitized and are plotted in Fig. 7. The circular marks show the test data of load-displacements at Dial Gage 1 and the triangles were those of load-displacement at Dial Gage 2. The positions of the two dial gages were illustrated in Fig. 1. To demonstrate the accuracy of FEA simulations, the FEA results were plotted against the measured experimental data in Fig. 7. The thin dash lines show the results using ANSYS shell element SHELL43. The solid lines show the results using ABAQUS Elbow31. The dot-dash lines present the results of ANSYS SHELL181 and the thick dash lines show those of ABAQUS shell element S8R5. These four models gave essentially the same predictions and they all matched the experimental data very well up to 7000 pounds. Then, the three models using ANSYS SHELL181, ABAQUS S8R5 and

ABAQUS ELBOW31 still agreed with each other and the experimental results closely. However, ANSYS SHELL43 gave a little higher load bearing prediction than the experiment and the other three FEA models.

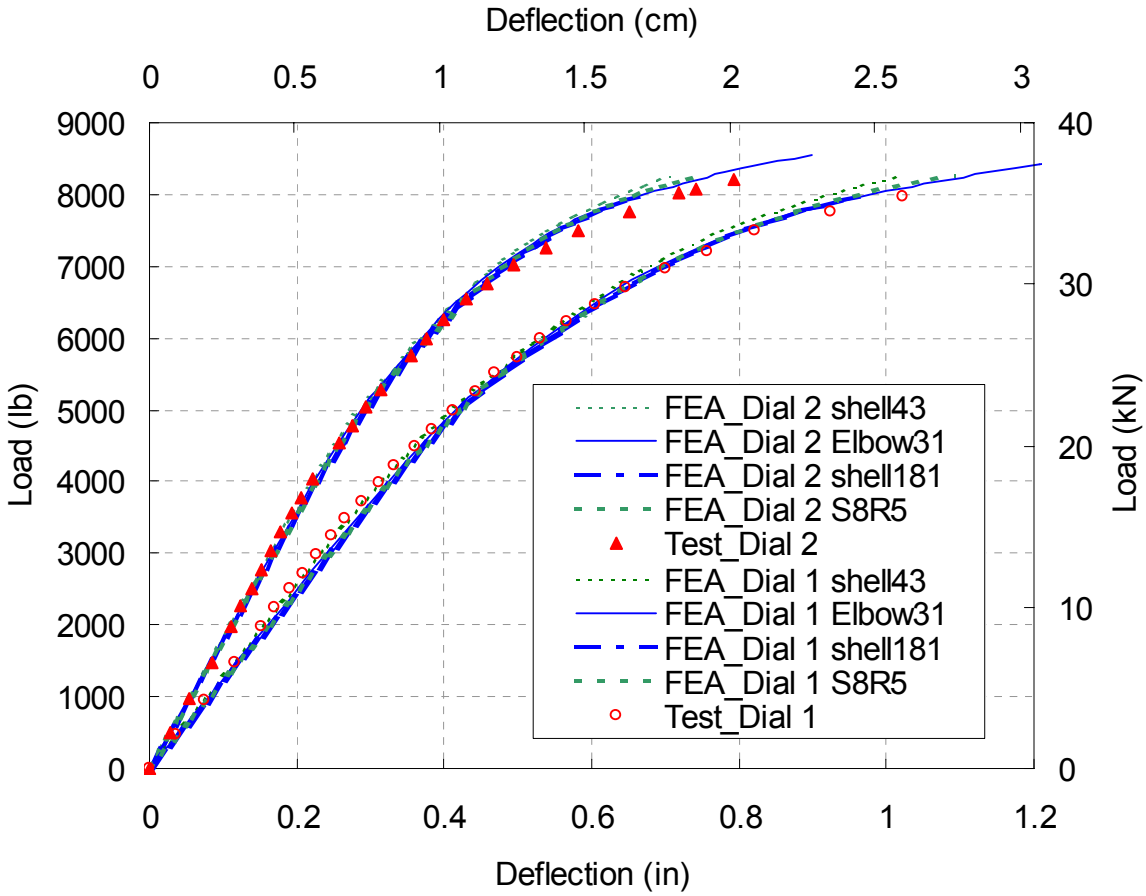

Fig. 7 Load-Displacement Curves of Pipe-1

For Pipe-2, an ABAQUS elbow model using ELBOW31 and two ANSYS shell models using SHELL43 and SHELL181 respectively were constructed to simulate the experiment. The thin dash line ending at 4" (10 cm) in Fig. 8 shows the results of ANSYS SHELL43. The dash line ending at 4.5" (11.4 cm) is for ANSYS SHELL181 and the thin solid line is for ABAQUS ELBOW31. Again, in general, they all match the experiment very well. All the three FEA models gave almost identical predictions up to

3” (7.6 cm). Then the computed curve using ABAQUS ELBOW31 agrees with the test curve perfectly until the end of the test, while those of ANSYS SHELL43 and SHELL181 gave a little higher load bearing predictions than the experiment and ABAQUS ELBOW31. For the shell models, convergence difficulties were encountered at 4” (10 cm) end displacement for SHELL43 and at 4.5” (11.4 cm) end displacement for SHELL181. For elbow model, no convergence problems were encountered. The reason for this lack of convergence is not yet understood.

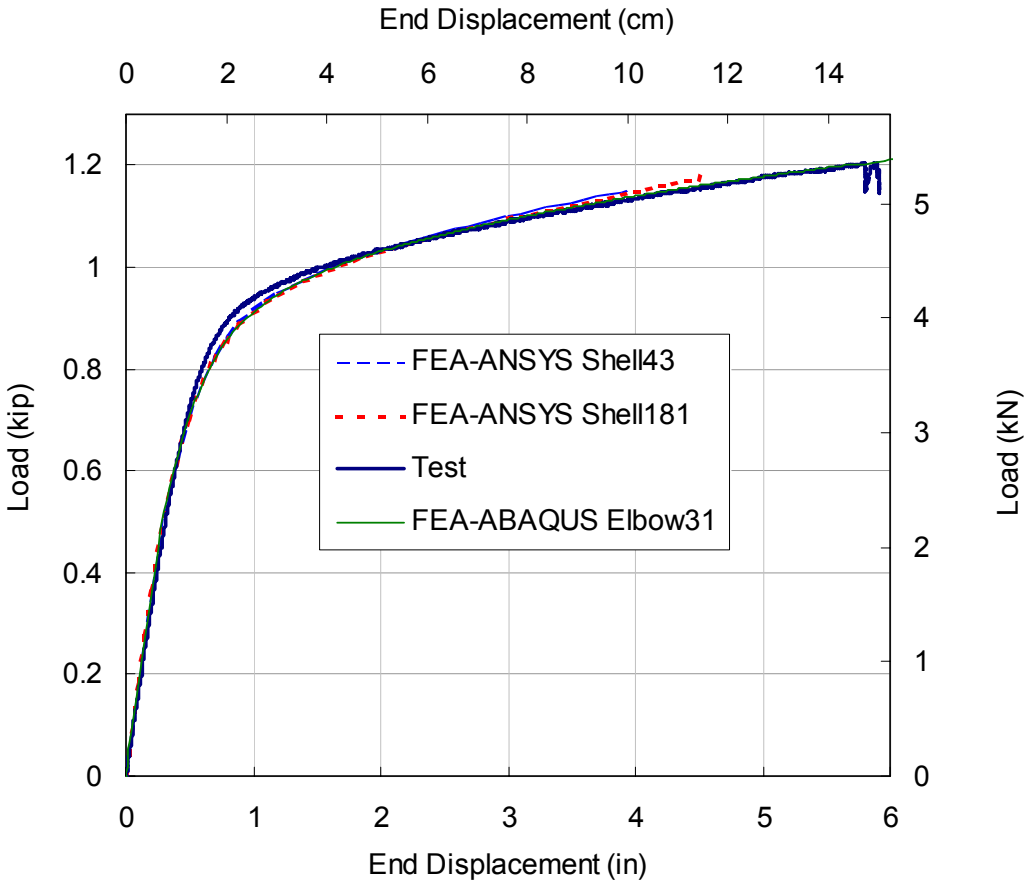

Fig. 8 Load-Displacement Curve for Pipe-2

From the correlation of the two experiments shown above, it is concluded that both shell models and elbow models can provide quite accurate predictions of elbow

behaviors subjected to out-of-plane bending. Compared with shell models, the elbow model is much easier to construct and has higher computing efficiency without decreasing the computing accuracy. Therefore, when only the overall elbow behaviors is needed, the elbow element model may be a better choice.

4.3 Correlation of Strains

In Ref. [7], the measured response curves for strain gages SG00 and SG01 (as named in [7]) were illustrated. They were digitized and are shown in Fig. 10 and Fig. 11 below respectively. To simulate these strains, a shell model, using ANSYS SHELL181, was created, with the mesh refined locally at the strain gages locations, as illustrated in Fig. 9. The FEA results are plotted as solid lines in Fig. 10 and Fig. 11. It is seen that the FEA responses followed the experimental results closely for SG01, while there is some deviation between FEA and test data for a portion of the SG00 σ-ε curve. The reason for the deviation is not clear.

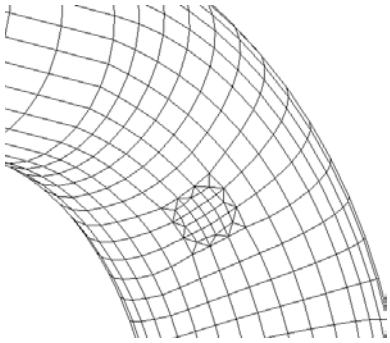

Fig. 9 Local Mesh for Strain Gage Location for SG01, Pipe-1

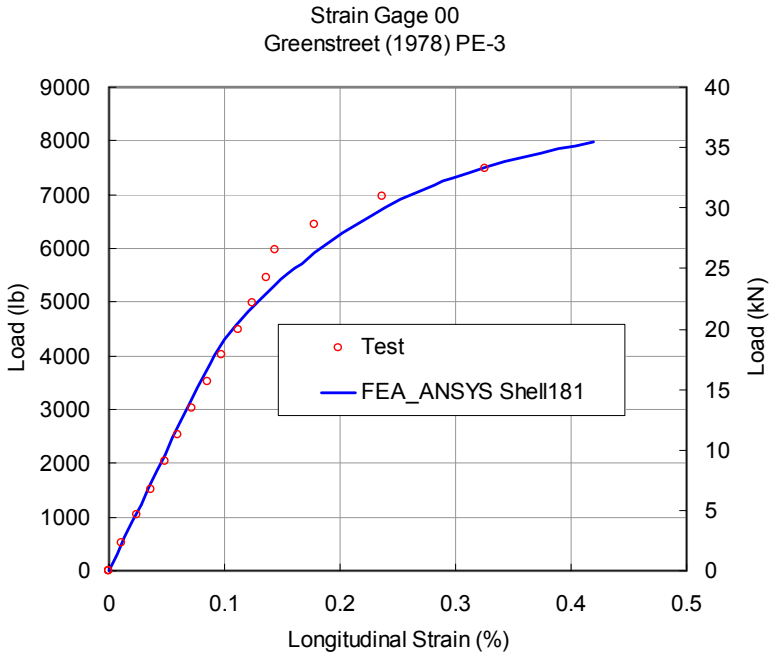

Fig. 10 SG00 Strain Responses for Pipe-1

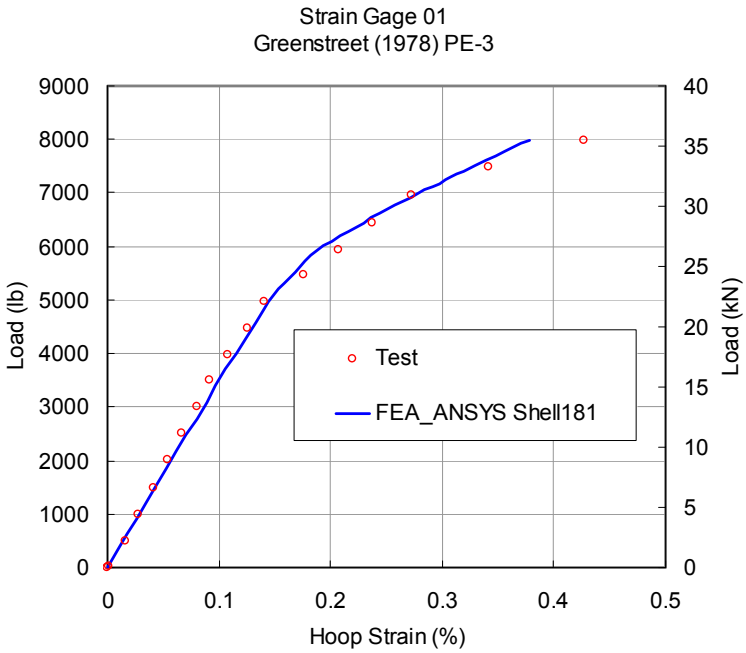

Fig. 11 SG01 Strain Responses for Pipe-1

For Pipe-2, five T strain gages, called SG01 to SG05 hereafter as illustrated in Fig. 12 below, were mounted on the specimen. These positions were in the high-strain regions given by FEA predictions and were selected in order to verify our FEA ap-

proach. For each gage, longitudinal and hoop strains were recorded except for the hoop strain at SG04, where the hoop element was broken.

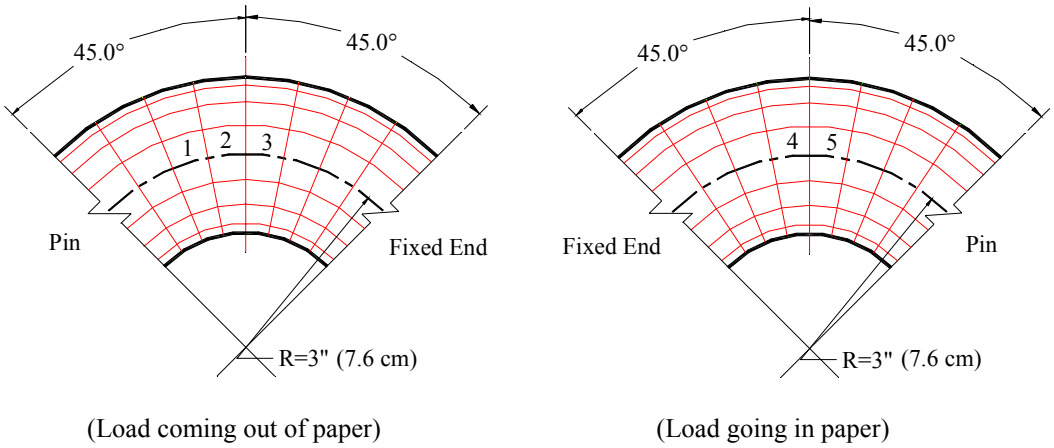

(Load coming out of paper) (Load going in paper)

(a) SG01-05

(b) SG01-03

Fig. 12 Strain Gages Locations for Pipe-2

A shell model using ANSYS SHELL181 was created similar to Pipe-1 to simulate these responses. The local meshes at strain gage regions were refined, as shown in Fig. 13. The FEA results plotted against the measured experimental data are shown in Fig. 14. In general, the FEA predictions match all the experimental responses very well. The discrepancies, which are reasonably small are likely a result of the interpolation of the strain data from the FEA postprocessor. In this study, the FEA results were obtained

by using the average element strains at the gage regions. The discrepancy between the actual gage areas and those defined in FEA will unavoidably introduce some error.

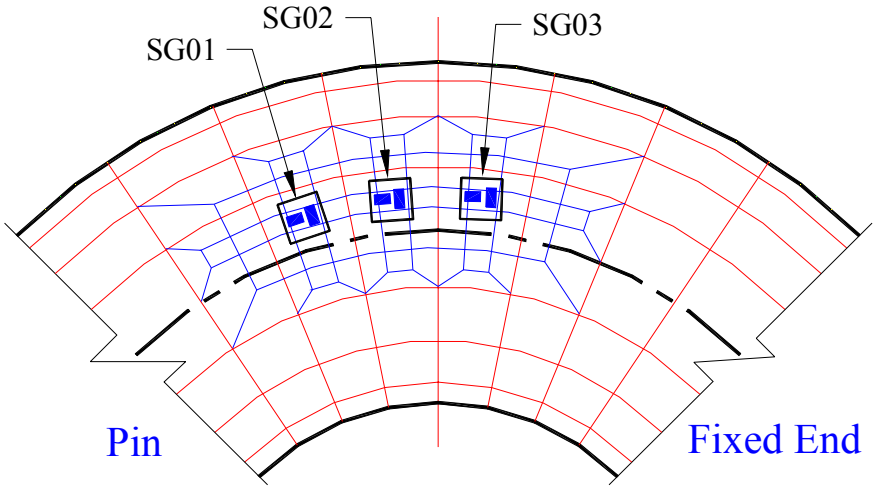

(a) Gages sizes, location and orientations and FEA Local Mesh for SG01-03

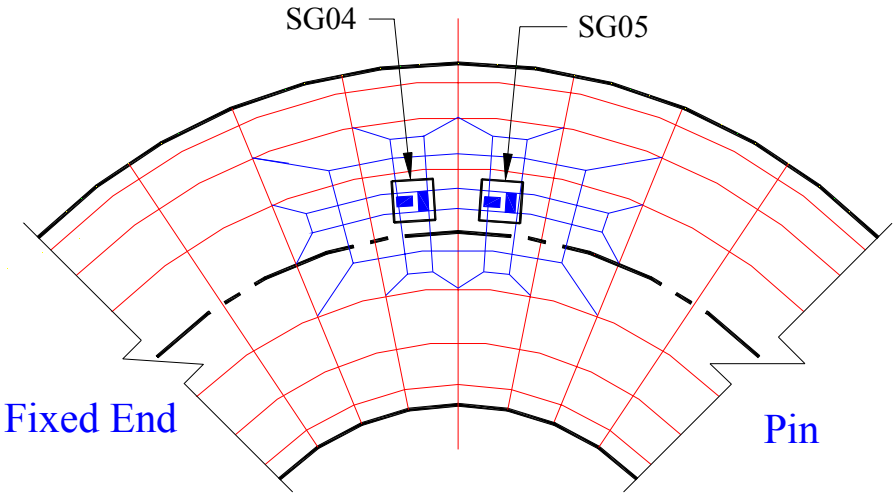

(b) Gages sizes, location and orientations and FEA Local Mesh for SG04-05

Fig. 13 Local Mesh for Strain Gage Locations for Pipe-2

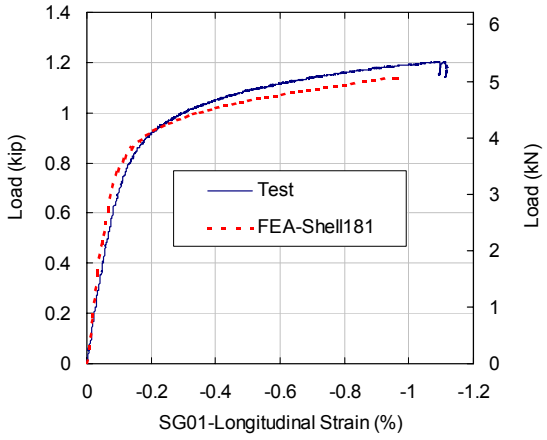

(a) SG01 Longtitudinal Strain

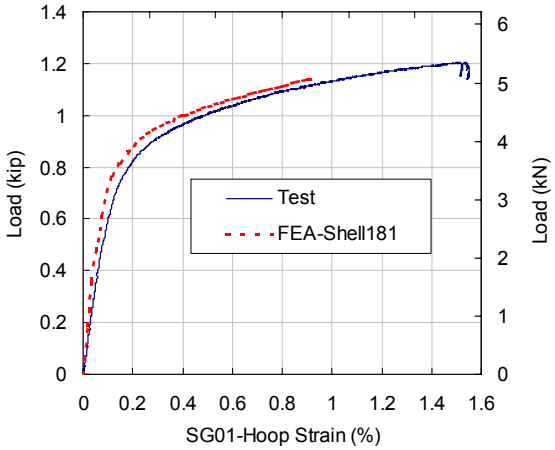

(b) SG01 Hoop Strain

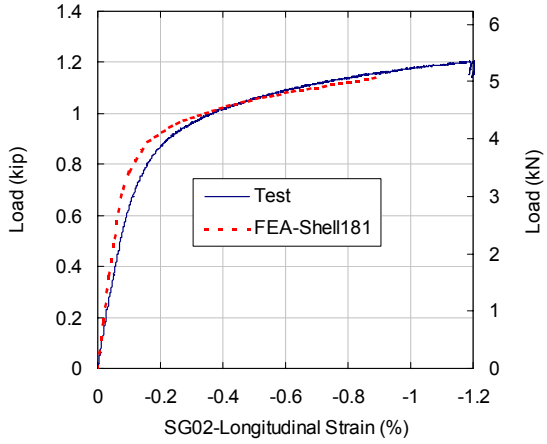

(c) SG02 Longtitudinal Strain

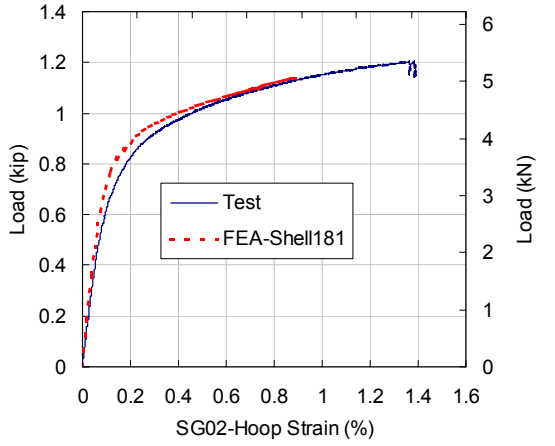

(d) SG02 Hoop Strain

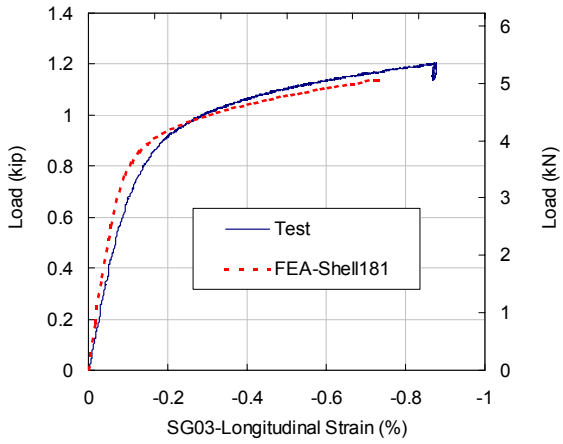

(e) SG03 Longtitudinal Strain

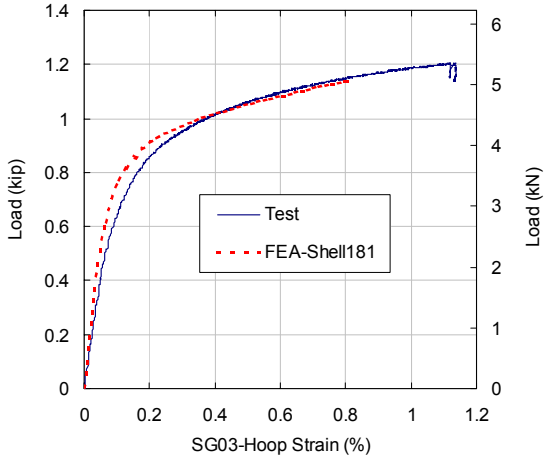

(f) SG03 Hoop Strain

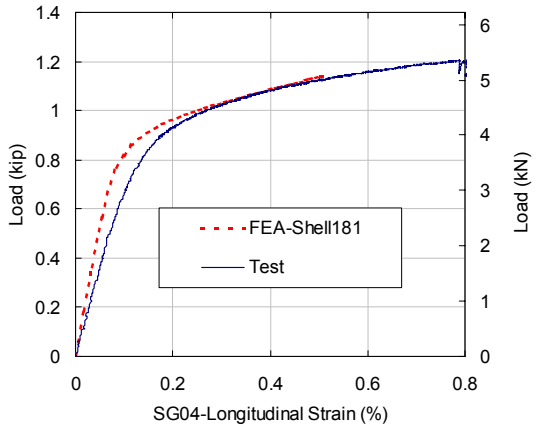

(g) SG04 Longtitudinal Strain

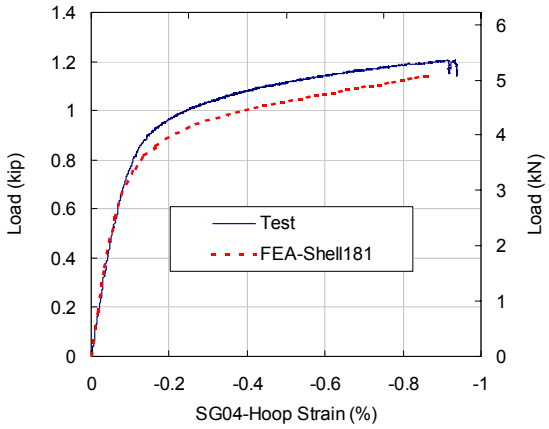

(h) SG04 Hoop Strain

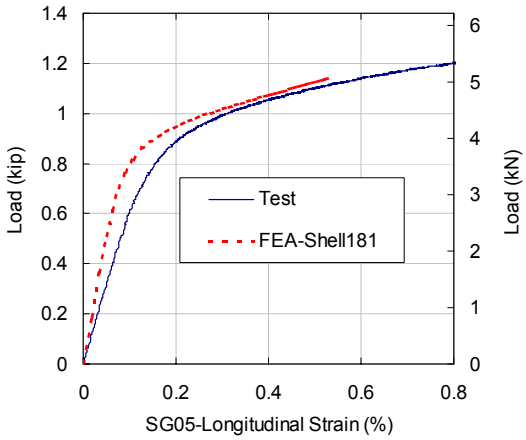

(i) SG05 Longtitudinal Strain

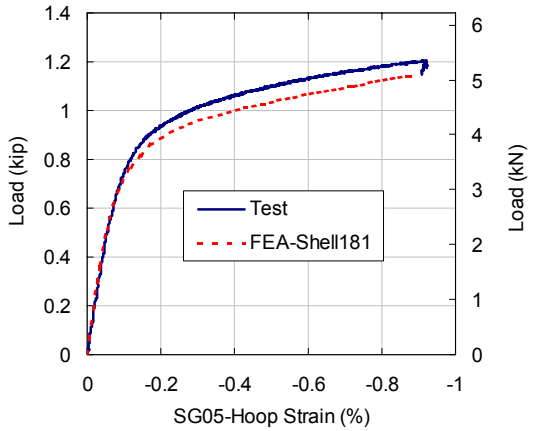

(j) SG05 Hoop Strain

Fig. 14 Strain Responses for Pipe-2

5 CONCLUSIONS

This part briefly presents two elbow experiments under out-of-plane loadings and the nonlinear FEA procedures to simulate them. FEA shell models and elbow models were used and they all give excellent results compared with measured testing load-displacement responses and strain responses. In addition to our foregoing reconciliation work in Parts III and IV, this study further demonstrates that the FEA procedures can provide quite accurate predictions of elbow behaviors under monotonic static loadings.

When only the global elbow behaviors are expected, elbow element models may be a better choice than shell models.

6 NOMENCLATURE

D_o = outside diameter of pipe

E = Young's modulus

e_u = uniaxial engineering ultimate strain

e_y = uniaxial engineering yield strain

S_y = yield stress

S_u = ultimate stress

t = wall thickness

7 REFERENCES

1. von Karman, T. "Über die Formänderung dünnwandiger Rohre, insbesondere federnder Ausgleichrohre," Zeitschrift des Vereines deutscher Ingenieure, Vol. 55, 1911, pp. 1889-1895.

2. Hovgaard, W., "Bending of curved pipes", Proc. Of the 3rd international Congress for Applied Mechanics, Stockholm, Sweden, vol. 2, 1930, pp331-341

3. Turner, C. E. and Ford, H. "Examination of the theories for calculating the stresses in pipe bends subjected to in-plane bending", Proc. Instn mech. Engrs, 1957

4. Beskin, L., "Bending of thin curved tubes", J. of Applied Mechanics, Trans. ASME, vol.67, 1945, ppA-1

5. Smith, R. T., "Theoretical analysis of the stresses in pipe bends subjected to out-of-plane bending", J. of mechanical engineering science, vol.9, No.2, 1967, p115-123

6. Smith, R. T. and Ford, H., "Experiments on pipelines and pipe bends subjected to three-dimensional loading", J. of mechanical engineering science, vol.9, No 2., 1967, p124-137

7. Greenstreet, W. L., "Experimental Study of Plastic Responses of Pipe Elbows", ORNL/NUREG-24, 1978

8. Imazu, A., Sakakibara, Y., Nagata, T. and Hashimoto, T., "Plastic instability test of elbows under in-plane and out-of-plane bending", Trans. of the 5th International Conference on SMiRT., 1979, Berlin, Germany, E6/5

9. Prost, J. P., Taupin Ph. and Delidais, M., "Experimental Study of Austenitic Stainless Steel Pipes and Elbows Under Pressure and moment Loadings", 7th SMiRT Conference, 1983, Chicago, G/F 5/5

10. Hilsenkopf, P., Boneh, B. and Sollogoub, P., "Experimental Study of Behavior and Functional Capability of Ferritic Steel Elbows and Austenitic Stainless Steel Thin-Walled Elbows", Int. Journal of Pres. Ves. & Piping, 0308-0161/88, 1988

11. Natarajan, R. and Mirza, S., "Stress Analysis of Curved Pipes with End Restraints Subjected to Out-of-Plane Moments", Proceedings of SMiRT Conference, F2/8, 1-9, Paris, 1981

12. Basavaraju, C. and Lee, R. L., "Stress distribution in elbow due to external moments using finite-element methodology", PVP, vol. 249, ASME 1993, p103-112

13. Matzen, V. C. and Tan, Y. , "The history of the B_2 stress index and a new margin-consistent procedure for its calculation", PVP-vol.399, Design and Analysis of Pressure Vessels and Piping-2000, pp251-258, July 2000

14. Machida, H., Kamishima, Y., Ueta, M. and Dozaki, K, "Stress index of 45 and 90 degree elbow subjected to in-plane and out-of-plane moment", Transactions of the 13th International Conference on Structural Mechanics in Reactor Technology (SMiRT 13), Brazil, August 13-18, 1995, pp377-382

15. Mourad, H. M. and Younan, M. Y. A., "Nonlinear Analysis of Pipe Bends Subjected to Out-of-Plane Moment Loading and Internal Pressure", PVP-Vol. 399, Design and Analysis of Pressure Vessels and Piping, ASME 2000, pp123-129

16. Fujimoto, T. and Soh, T., "Flexibility factors and stress indices for piping components with D/T>=100 subjected to In-Plane or Out-of-Plane moment", Journal of Pressure Vessel Technology, Nov. 1988, vol.110, pp374-386

17. Kussmaul, K., Diem, H. K., Uhlmann, D., Kobes, E., 1995, "Pipe bend behaviour at load levels beyond design", (SMiRT 13), Brazil, pp187-198

18. Mourad, H. M. and Younan, M. Y. A., "The Effect of Modeling Parameters on The Predicted Limit Loads for Pipe Bends Subjected to Out-of-Plane Moment Loading

and Internal Pressure", PVP-Vol. 399, Design and Analysis of Pressure Vessels and Piping, ASME 2000, pp131-148

19. Wilkins, K., Tan, Y. and Matzen, V.C., "Monotonic Out-of-plane Tests on 2-inch, Schedule 10 Elbows," Data developed at the Center for Nuclear Power Plant Structures, Equipment and Piping, North Carolina State University, 2000-2001

20. Yu. L., "Elbow Stress Indices Using Finite Element Analysis", Ph.D. dissertation, Dec. 1998, NCSU

21. Gosselin, S. R. and Wais, E. A., "A Case Study Comparison of ASME Section III Appendix F and Proposed Code Case N-584 Criteria in Carbon Steel and Stainless Steel Pipes", PVP-vol. 383, ASME 1999, p13-22

PART VI

CORRELATION OF TEST AND FEA RESULTS FOR ELBOWS UNDER QUASI STATIC CYCLIC LOADING

1. INTRODUCTION

During an earthquake, a component will be subjected to some number of cyclic excitations, some in the elastic range but others perhaps in the nonlinear, inelastic range. There are several possible outcomes. There could be, with a sufficient number of cycles, the initiation of or a complete through-wall crack, there could be some permanent local deformation, or there could be global deformation that is sufficiently large that the component is considered to be "collapsed". It is this last failure mode that is considered in this part of the research.

In 2000, the Code was modified to accommodate reversing dynamic loading – a loading for which fatigue ratcheting may be a failure mode. The following design equation for Level D loading, an extremely low probability event, was approved:

$$B'_1 \frac{P_D D_o}{2t} + B'_2 \frac{D_o}{2I} M_E \le 3.0 \cdot S_m \qquad (1)$$

where M_E is the amplitude of the resultant moment due to the inertial loading from the earthquake, other reversing type dynamic events and weight, and P_D is the pressure occurring coincident with the reversing dynamic load.

The interesting thing about this equation is that it still contains B type indices, which are used elsewhere in the Code only for monotonic loading. Because the failure

modes for monotonic loading will in general be quite different from those for cyclic loading, it would seem as though the indices for this equation should have their own definition based on the failure mode associated with the equation. This part of the 1995 Code was not accepted by the NRC, and the ASME Code committees are still working on the appropriate form for design equations for reversing dynamic loading.

In the past, it was generally expected that "plastic collapse does not occur under seismic excitation and that the failure mode is ratcheting or combined fatigue and ratcheting." [1]. Unfortunately, based on the experimental investigations by BNL[1], the University of Liverpool and EPRI[2], some elbows, when subjected to high-level seismic input, have collapsed, meaning there is excessive deformations of the inertia arm. Slagis[2] concluded that "Uniform wall thickness straight pipe and straight pipe with elbows, without large added weight, can withstand extreme levels of seismic loading without failure. High weigh stresses (0.5 S_m), however, can lead to large permanent bending deformations. Collapse is a possible failure mode for certain configurations, but the common failure mode is fatigue."[2]

Based on the information described above, Hassan [3] and Gurdal et al. [4] suggested that a study of the B_2' stress index under cyclic loading would seem to be worthwhile. In this case it would be necessary to redefine what is meant by collapse that may occur after several cycles of loading, and then use this definition in the calculation of a B_2' stress index.

[1] Berkeley Nuclear Laboratories
[2] Electric Power Research Institute

As will be seen in the following section, there have been no detailed studies on the nature of collapse of a piping component following one or more cycles of near-collapse behavior. A full investigation of this topic is beyond the scope of this current project as it would require extensive testing and analysis to determine the relationship between ratcheting, fatigue and collapse. Such analyses would require constitutive models that can accurately simulate the ratcheting behavior. Although much progress has been made in recent years in this area [Hassan and Bari [5, 6]], the best models are still not capable of simulating the full range of material behavior. An experimental program to investigate this topic completely is possible, but would be prohibitively expensive.

Our approach in this preliminary investigation of cyclic collapse involves two experiments and a limited amount of analysis. It has been undertaken (a) to illustrate those aspects of the behavior that differ significantly from the monotonic behavior, (b) to make an initial attempt to define a collapse load for cyclic behavior and then (c) to use this information in a newly defined cyclic B_2' stress index.

Each test to be conducted and simulated consists of three quarters of a full hysteretic loop. The elbow component was subjected to an in-plane opening displacement to the point of Code-defined collapse, and then closed until actual collapse occurred. This experimental approach to understanding cyclic collapse is similar to the one taken by Greenstreet [7] in his definitive experimental work on monotonic collapse. Our tests, the corresponding FEA, and the constitutive models utilized are described in the following sections.

2. BACKGROUND

A large volume of work has been carried out on the seismic response of piping. Most of this work has been associated with ratcheting or combined fatigue and ratcheting. Because this type of behavior may be related to collapse associated with cyclic loading, a brief review of this literature will be presented.

Diem and Müller [8] and Kussmaul et al. [9] describe experiments on piping systems containing a pipe bend, with internal pressure and subjected to cyclic in-plane bending. They concluded that, for cyclic bending, thin-walled elbows fail due to longitudinal cracks starting at the inside of the flank region, while thick-walled elbows failed as a result of a circumferential crack initiating on the outside wall of the intrados. All of the failure modes are through-wall cracks leading to leakage.

Diem et al. [10] reported four cyclic tests on 60° and 90° elbows with constant internal pressure and both in-plane and out-of-plane bending. The objective was to determine the failure modes (location and orientation of the crack, leak or break) and the number of cycles to failure [10]. They observed that "in all four tests, the piping elbows have failed in the form of a leak after a high number of loading cycles (between 7980 and 17,260)". [10]

Fujiwaka et al. [11] investigated the strength of piping components due to seismic loading. In their work, fifteen static-cyclic and fifteen dynamic tests with and without internal pressure were conducted on elbows, tees and straight pipes. The material test results from monotonic tensile tests, cyclic stress-strain tests and ratchet fatigue tests, at

room temperature and elevated temperature, are reported. Their static cyclic tests were from 53 to 1050 cycles. A typical experimental steady state load-displacement relationship from their set of experiments under static cyclic loading has been digitized and is shown in Fig. 1 below. In this figure, the stiffnesses of the elbow in the two unloading paths are considerably different, i.e. the slopes are not parallel. The disparity is caused by the geometric effects associated with the large displacements-the elbow is stiffer in the opening direction and more flexible in the closing direction than in the original, undeformed configuration.

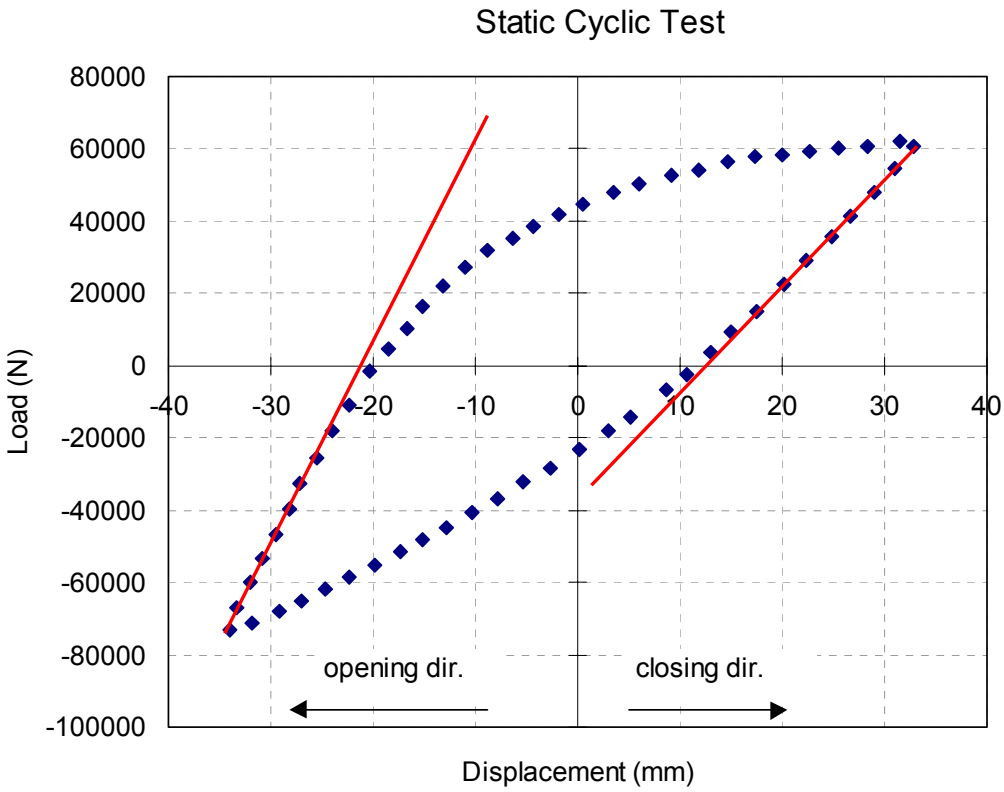

Fig. 1 Load-Displacement Relationship for Elbows
(digitized from Fig.6, Ref.[11])

Fujiwaka et al. concluded that, between the static cyclic tests and the dynamic

tests, there is no significant difference of the fatigue strength, the crack penetration locations, or the shape of the hysteretic loops.[11] In their FEA simulations of the static cyclic tests, "the bilinear material model and the kinematic hardening theory" [11] were used. Since they focused on strain responses, load-displacement FEA results were not reported.

Another important source of information in the area of cyclic collapse is the Piping and Fitting Dynamic Reliability (PFDR) Program [12]. This program was initiated in 1985 by EPRI, with cooperation from the U.S. Nuclear Regulatory Commission (NRC) and General Electric (GE), to develop extensive experimental evidence of the dynamic load effect for code rule improvement [12]. It consisted of "a matrix of 41 component tests, 4 system tests and 170 material specimen tests"[12]. The component test No. 37 was a 6" Schedule 10, long radius stainless steel elbow subjected to in-plane seismic loading without internal pressure. An inertia arm extension with eccentric weight of the specimen was adjusted to achieve a fundamental frequency of 1.4 Hz and the input seismic load was tuned to 1.3 Hz with 110.3 seconds duration. Low, mid and high level tests were run (peak accelerations ≅ 0.45g, 1.7g and 3.5g respectively) [13]. The low and mid level runs did not produce any significant gross deformation. However, the elbow began to incrementally close after 45 seconds during the high level test [13]. This test demonstrated that collapse is a potential failure mode for elbows under dynamic loading.

3. MATERIAL MODEL

Constitutive models are fundamental to finite element simulation. The material

constitutive models for cyclic loading are much more complex than for monotonic loading. To begin this phase of the work, it was then necessary to clarify the relationship between stress-strain (σ-ε) curves for Stainless Steel 304L (SS304L), which is the material type of our specimen, and the standard material options provided by ANSYS and ABAQUS.

Boyer states that "The cyclic stress-strain curve may be determined in several ways, but it is usually obtained by connecting the tips of stable hysteresis loops from constant-strain-amplitude fatigue tests of companion samples at different strain amplitudes."[14] However, as described earlier, the test used in this part of the study consisted of only a ¾ of a cycle. The σ-ε curves constructed in the manner described by Boyer would only be an approximation to the actual σ-ε behavior, which includes the transition from the fully annealed condition to the initiation of cyclic hardening. Therefore, this approach is not utilized in the current study.

The cyclic hardening behavior of SS304 digitized from Hassan and Kyriakides[15], though not specifically for our specimen, is illustrated in Fig. 2 below. In the first quarter cycle, the σ-ε curve shows a rather sharp knee while, after unloading and reloading, the knees become more round. Assuming σ_0 is the initial yield stress, it is observed that the yield surface decreases in size during the 1st half cycle and increases its size a little during the 2nd half cycle. It seems that, for SS304, the kinametic hardening rule is more realistic than isotropic for the first cycle. In our FEA simulation later, we investigate the use of both.

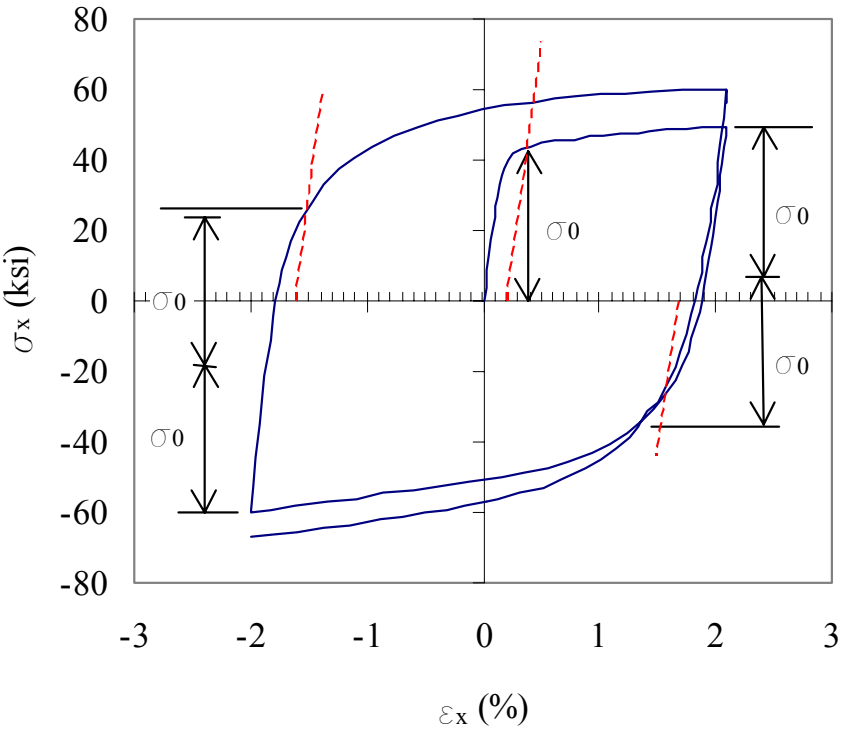

Fig. 2 Cyclic hardening behavior of SS304

(digitized from Ref. [15], Fig.1)

In the reconciliation studies in Parts III to V, it was concluded that, compared with measured experimental data, both ANSYS SHELL181 and ABAQUS ELBOW31 provide quite accurate predictions of the nonlinear behavior of elbows under monotonic loading. ANSYS SHELL43 also works well for moderately thick pipes. For thin-walled pipes, however, convergence difficulties were encountered using SHELL43; and the ANSYS help manual [16] recommends using SHELL181 instead for nonlinear structures. This statement is consistent with our observation as presented in Part III. For these reasons, we used ANSYS SHELL181 and ABAQUS ELBOW31 in the FEA simulations in Parts IV to V. In this preliminary study, we used the standard plasticity options provided by ANSYS and ABAQUS. To accurately understand these options, we apply an ex-

perimental SS304L σ-ε curve with different standard material hardening options to a single beam element subjected to monotonic uniaxial load. Then the element σ-ε responses are output to reveal the material behavior implemented by the two commercial FEA packages directly.

For ANSYS, both multilinear isotropic hardening and multilinear kinematic hardening options are furnished. SHELL43 is supported by both the options, but multilinear kinematic hardening plasticity is not available to SHELL181. Therefore, we only test SHELL43 in our study of the hardening rule options. As illustrated in Fig. 3, the output σ-ε curves using both the multilinear isotropic option and the multilinear kinematic option are seen to agree with the respective model assumptions, as expected.

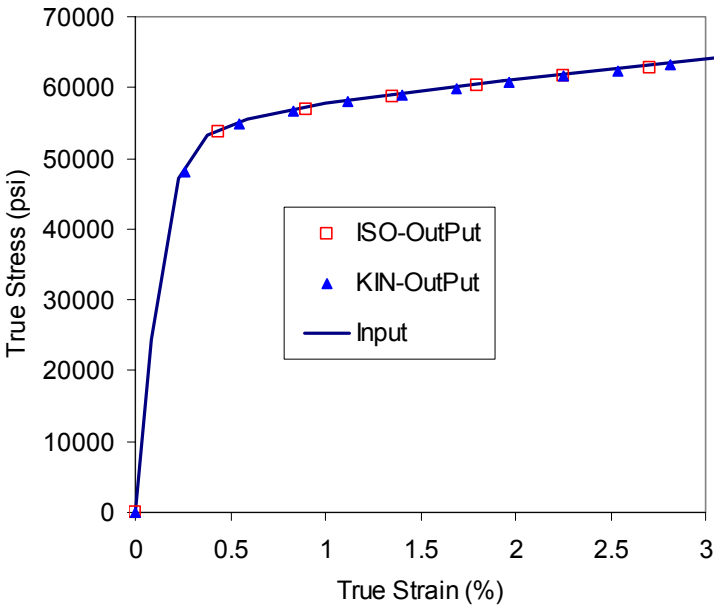

Fig. 3 ANSYS Material Models Verification

For ABAQUS, material models for metals subjected to cyclic loading are specifically provided. The users can define "linear kinematic hardedning model" and "non-

linear isotropic/kinematic hardening model". The latter is actually a combined hardening rule consisting of a nonlinear isotropic hardening component and a nonlinear kinematic hardening component. Obviously, pure kinematic hardening plasticity is obtained by setting the isotropic term to be zero. ABAQUS provides an option to define the kinematic hardening component by specifying half-cycle tests data from a unidirectional tension or compression experiment. As with ANSYS, these ABAQUS standard material options are tested using the experimental uni-axial σ-ε curve of SS304L mentioned before. The results are interesting, as shown in Fig. 4 below.

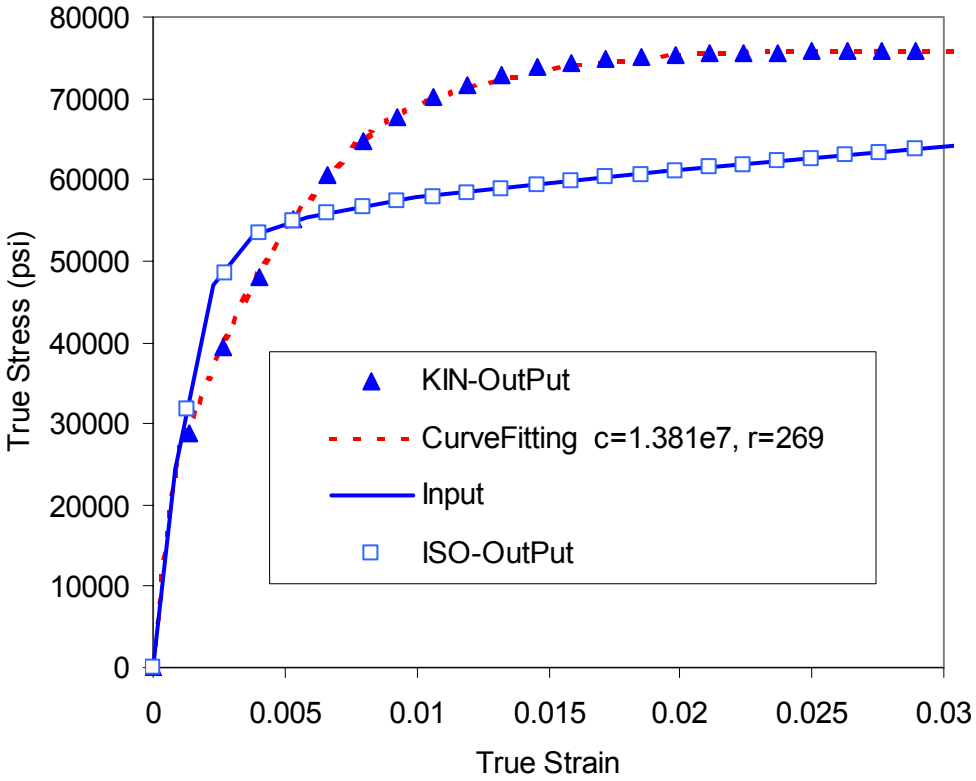

Fig. 4 ABAQUS Material Models Verification

The solid line, labeled "Input", is the input σ-ε curve. The discrete rectangular marks, labeled "ISO-OutPut", shows the output material behavior using the Isotropic

Hardening option implemented by ABAQUS, which agrees with the input model excellently, as expected. However, the output material behavior using the Kinematic Hardening option deviates significantly from the input half cycle test data. According to the ABAQUS online help manual [17], ABAQUS uses the experimental σ-ε data to obtain a curve in the following form:

$$\sigma_i - \sigma_0 = \frac{C}{\gamma}(1 - e^{-\gamma \varepsilon_i^{pl}}) \qquad (1)$$

where C and γ are parameters obtained from the first half cycle of a uniaxial test curve; σ_i and σ_0 are as illustrated in Fig. 5.

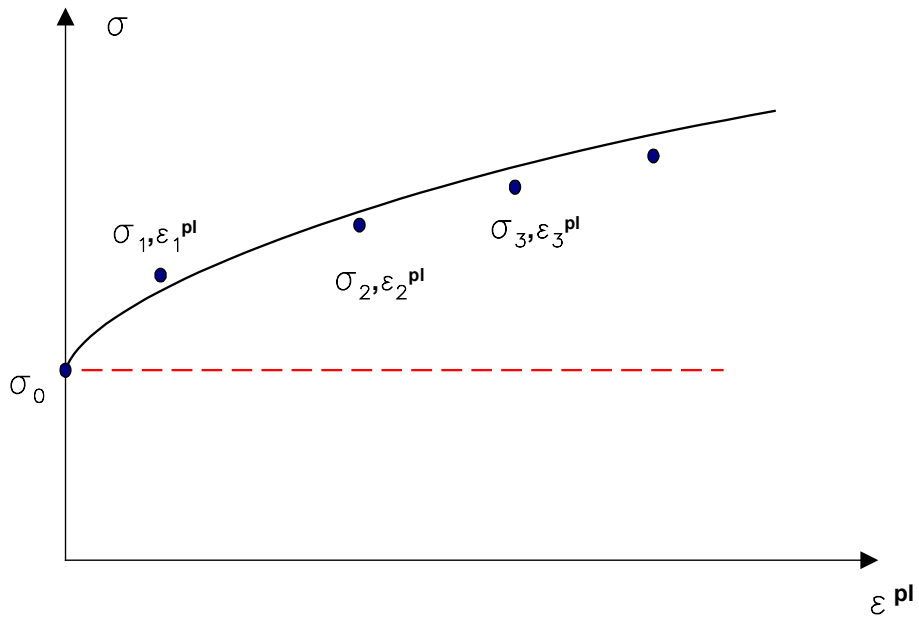

Fig. 5 An Example of a Half Cycle of Stress-Strain Data [17]

To confirm this implication, we used the curve fitting algorithm in Microsoft Excel (SOLVER) to minimize the sum of squared differences between the FEA stresses and those given by Eq. (1). The best fit value for C and γ are 1.381e7 and 269 respectively. Using Eq.(1) with these values of C and γ, we plot the corresponding σ-ε curve

as illustrated in Fig. 4, labeled as "CurveFitting". It closely agrees with the output curve of using Kinematic Hardening option. This result indicates that the curve fitting technique is the actual implementation of this ABAQUS option. As illustrated in Fig. 4, the actual σ-ε curve for SS304L is not even close to the shape of Eq.(1). Obviously, the ABAQUS Kinematic Hardening option is not a good choice for our SS304L monotonic σ-ε data.

On the basis of the work described above, the following conclusion can be drawn: at present, a reasonable and accessible choice for us is to use ANSYS SHELL43 for the current preliminary study for cyclic B_2' index. In the work described later, we conducted two elbow tests subjected to cyclic load (¾ cycle). Finite element analysis was performed to simulate the tests. Since the experimental cyclic σ-ε curve for our specimen is unavailable, we used the monotonic test σ-ε curve. Because the specimen in this current work is from the same product batch as the specimens described in Parts IV and V (the monotonic σ-ε curves were shown in Fig. 6 of Part IV and Fig. 6 of Part V), we are able to use the same monotonic σ-ε data. This approximation approach should be acceptable for a ¾ cycle test.

4. EXPERIMENT [18]

In this work, two long radius 2" Schedule 10, 90° stainless steel 304L elbows, called Pipe-1 and Pipe-2 respectively, were tested under the cyclic loading. The major difference between these two specimens is, for Pipe-1, the welds on the outer surface at the joints of the elbow and the straight tangent segments were intentionally grounded

smooth before test, while those for Pipe-2 were kept unaltered. The other difference is the loading device.

For Pipe-1, since the hydraulic pump in our laboratory was out of order, the test setup described in Parts III to V was unavailable and an alternate one was utilized, as shown in Fig. 6 below.

The specimen was pin connected at both ends. The upper pin was bolted to the wide flange beam of the supporting frame and the lower pin was attached to the load cell which was connected to the screw actuator, as illustrated in Fig. 7. Two LVDTs were used to record the two end displacements - one was mounted to the column of the supporting frame and attached to the upper wide flange beam and the other was attached to the lower pin.

The elbow was subjected to in-plane opening load until the relative end displacement was equal to 0.55", then loaded to the maximum in-plane closing relative displacement. The 0.55" limit was determined by FEA prediction before the test –it was the displacement at which the Code-defined collapse load was just reached under the monotonic in-plane opening bending.

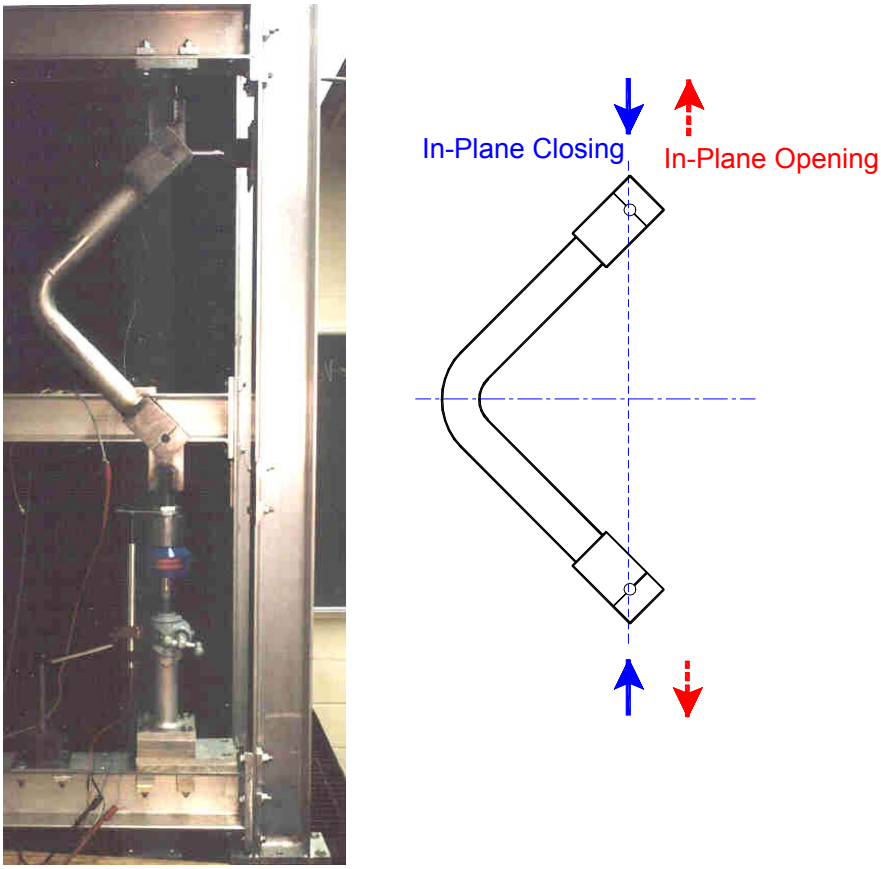

Fig. 6 Test Setup

Fig. 7 Pin Connection, Load Cell and Screw Actuator

During the test, the load was applied manually through the screw actuator. At each load step, we stopped the test and recorded the signals of the load cell and the LVDTs manually. Then we continued to the next step. It was observed that, following a load application, the load relaxed rather quickly, which could drop as much as 5%, while the load and displacement were being recorded. Since we were not always quick enough to catch the first reading, it is reasonable to think that the actual loads could be a little bit higher (up to 5%) than the current recorded data.

The test was performed smoothly as expected for the first load phase – in-plane opening mode bending and then unloading. However, while applying the 2nd load phase – in-plane closing mode bending, at around 800 pounds, the screw actuator bent slightly and the test had to be stopped. The test was then restarted and continued until the component was well into the nonlinear region. The obtained experimental load-displacement curve is illustrated in Fig. 11.

For Pipe-2, the hydraulic pump in our laboratory had been fixed and the test setup was the same as Fig.1 in Part IV, in which loads and displacements were recorded automatically by computer.

To help with the numerical analysis, similarly to Parts III to V, the geometric dimensions of the specimen were measured before test, as presented in Fig. 8.

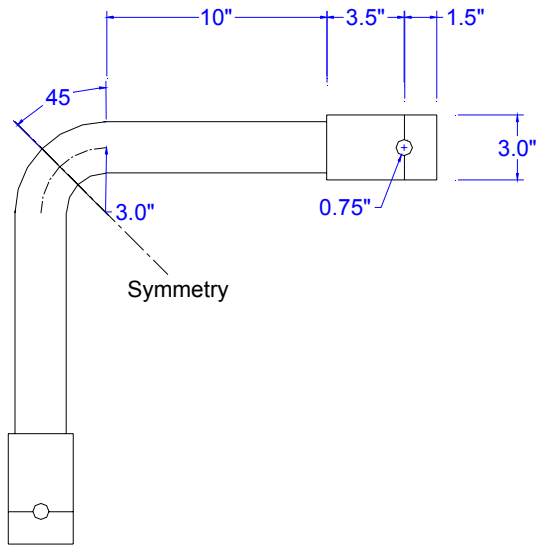

Fig. 8 Geometric Dimensions of the Specimens

The outside diameters and wall thicknesses at extrados, intrados and flanks along five planes named P-1 to P-5 along the pipe bend direction, as shown in Fig. 9, were also measured. The obtained measurements are provided in Table 1 and Table 3, and the average values are given in Table 2 and Table 4 for Pipe-1 and Pipe-2 respectively.

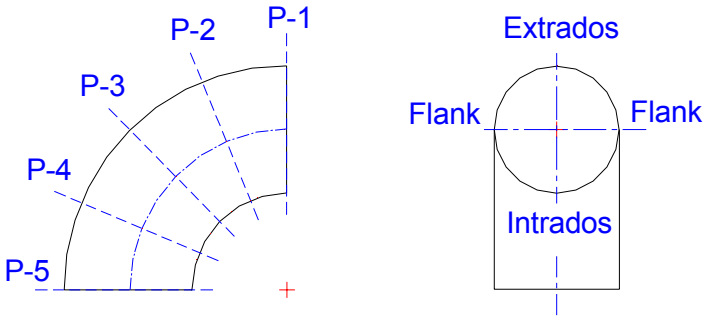

Fig. 9 Measured Cross-Sections

Table 1 Measured outside diameters and wall thicknesses for Pipe-1 (in)

	P-1	P-2	P-3	P-4	P-5
$D_{o\ Flank-Flank}$	2.377	2.393	2.393	2.390	2.359
t - Flank	0.134	0.131	0.132	0.132	0.139
t– Flank	0.141	0.141	0.144	0.143	0.141
$D_{o\ Intra-Extra}$	2.360	2.361	2.335	2.355	2.385
t - Intrados	0.151	0.132	0.138	0.138	0.155
t - Extrados	0.131	0.127	0.124	0.126	0.132

Table 2 Average Geometric Characteristics of Elbows Tested for Pipe-1

Segments of Test Specimens		average t	D_o			D_o / t
			average		average	
			Extrados -Intrados	Flank - Flank		
Elbow	(in)	0.137	2.359	2.382	2.371	17.3
	(cm)	0.349	5.992	6.051	6.022	
Straight Pipe	(in)	0.108	/	/	2.373	22.0
	(cm)	0.274	/	/	6.027	

Table 3 Measured outside diameters and wall thicknesses for Pipe-2 (in)

	P-1	P-2	P-3	P-4	P-5
$D_{o\ Flank-Flank}$	2.381	2.369	2.365	2.379	2.377
t - Flank	0.144	0.139	0.139	0.139	0.143
t– Flank	0.142	0.142	0.138	0.138	0.139
$D_{o\ Intra-Extra}$	2.395	2.380	2.371	2.373	2.379
t - Intrados	0.165	0.156	0.140	0.156	0.162
t - Extrados	0.127	0.128	0.128	0.128	0.127

Table 4 Average Geometric Characteristics of Elbows Tested for Pipe-2

Segments of Test Specimens		average t	D_o			D_o / t
			average		average	
			Extrados -Intrados	Flank - Flank		
Elbow	(in)	0.141	2.380	2.374	2.377	16.9
	(cm)	0.358	6.045	6.030	6.038	
Straight Pipe	(in)	0.110	/	/	2.376	21.6
	(cm)	0.279	/	/	6.035	

Similarly to Part IV, the size of weld bead for Pipe-2 was measured. The extrusion of the weld on the outer surface was obtained by subtracting the outside diameters of the welding regions from the outside diameters of the adjacent pipe. On the internal surface, it's observed that the welds were also extruded. We assumed that the profile of the welds on the inside were the same as on the outside of the specimens. Since welds were non-uniform, only the average welding dimensions could be obtained, as illustrated in Fig. 10.

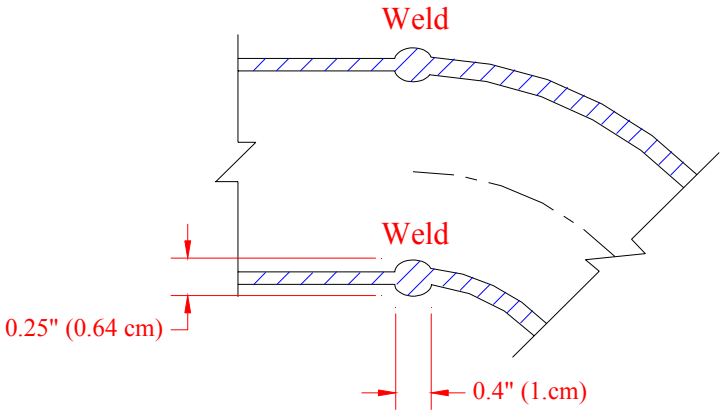

Fig. 10 Average Welding Dimensions for Pipe-2

The measured experimental load-displacement curves are illustrated in Fig. 11 below. The load bearing capacity of Pipe-2 is evidently up to 20% higher than that of Pipe-1 for both loading directions (in-plane opening and in-plane closing modes). This is consistent with the investigations in Part VI, i.e., the existence of welds can significantly increase load capacity of elbows.

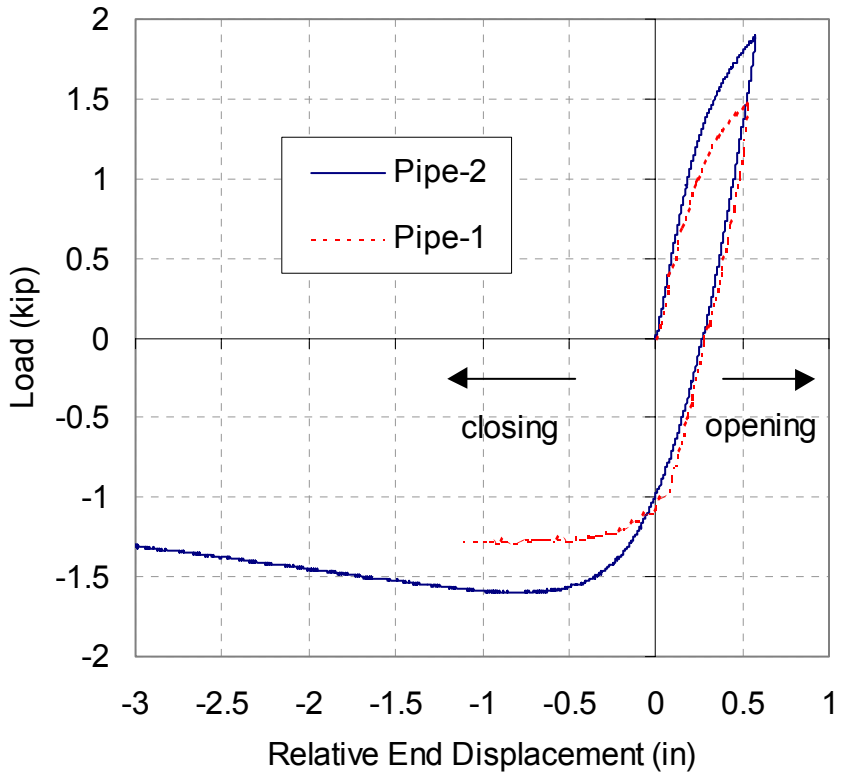

Fig. 11 Experimental Curves, Pipe-1 vs. Pipe-2

5. FINITE ELEMENT ANALYSIS

As described earlier in section 3, ANSYS v5.5 element SHELL43 was used in this study. Taking the initial variation of thickness and outside diameters into account, shell models were constructed with either the multilinear Isotropic Hardening option

selected or the multilinear Kinematic Hardening option selected.

Pipe-1

For Pipe-1, the computed results compared with measured experimental data are illustrated in Fig. 12. The discrete circles show the test data. The solid line, labeled "FEA-cyclic-ISO" shows the FEA results from Isotropic Hardening option; and the dashed line, labeled "FEA-cyclic-KIN" presents the FEA results from Kinematic Hardening option. In the first half cycle, i.e. applying in-plane opening load then unloading to zero, the FEA results of both models follow the test very well. Then after applying in-plane closing load, the test data lie between the FEA results from isotropic hardening and kinematic hardening. This result suggests that the actual behavior would be represented better by a combination of isotropic and kinematic hardening, rather than pure isotropic or kinematic hardening.

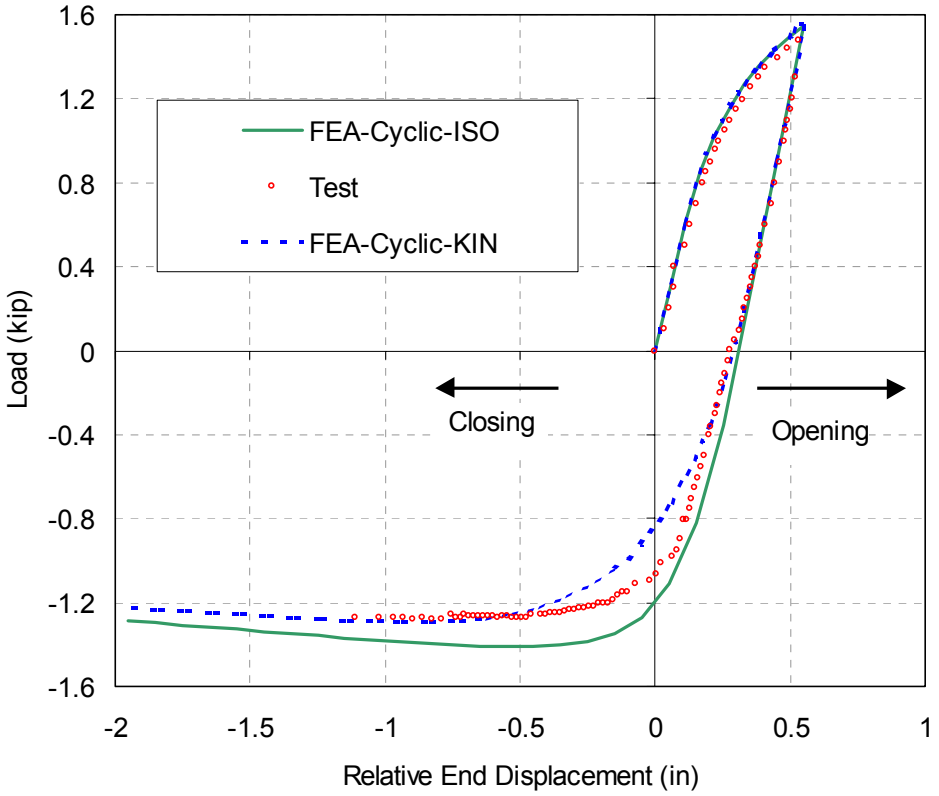

Fig. 12 FEA vs. Test Data for Pipe-1

For the same specimen, the FEA results for monotonic in-plane closing and opening bending against the cyclic responses are shown in Fig. 13 (a) along with the cyclic test data and simulations. The dashed line with small rectangle marks, labeled "FEA-monotonic-Closing", presents the monotonic in-plane closing bending behaviors. It looks very much like the cyclic in-plane closing test data. If shifting the test data right to the origin, illustrated by cross marks, labeled "Test (Shifted)", it is very interesting to observe that they closely agreed with the monotonic FEA results, as shown in Fig. 13 (b). It seems that the first half cycle of loading history has no effects on it.

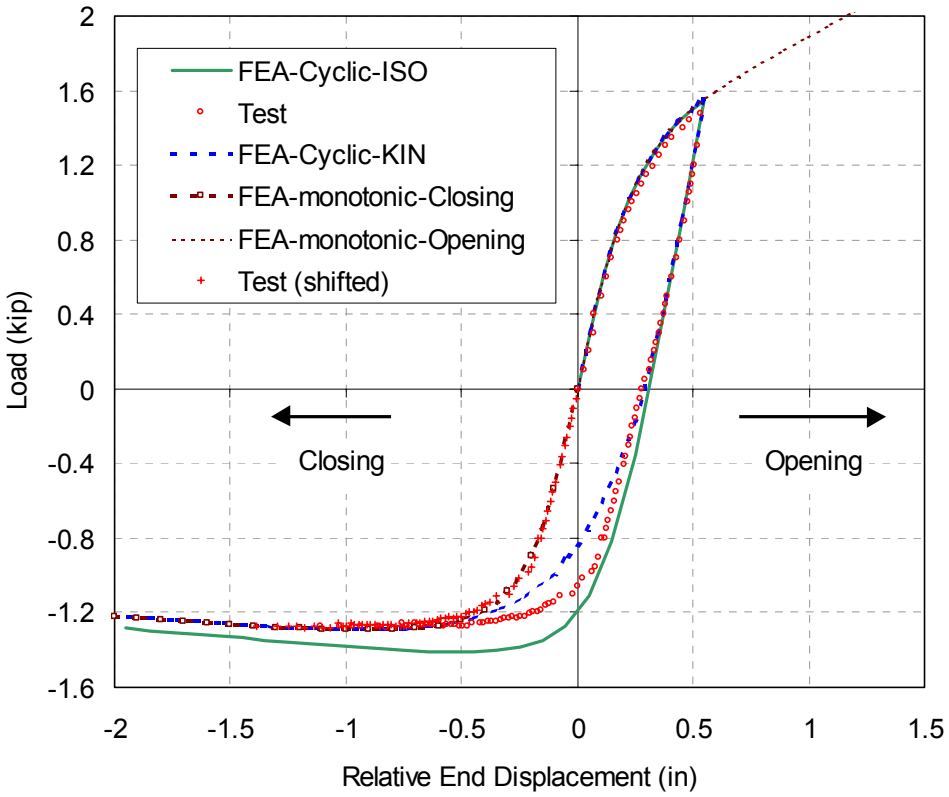
FEA-Cyclic-ISO
Test
FEA-Cyclic-KIN
FEA-monotonic-Closing
FEA-monotonic-Opening
Test (shifted)
Closing
Opening
Load (kip)
Relative End Displacement (in)
2
1.6
1.2
0.8
0.4
0
-0.4
-0.8
-1.2
-1.6
-2
-1.5
-1
-0.5
0
0.5
1
1.5

(a)

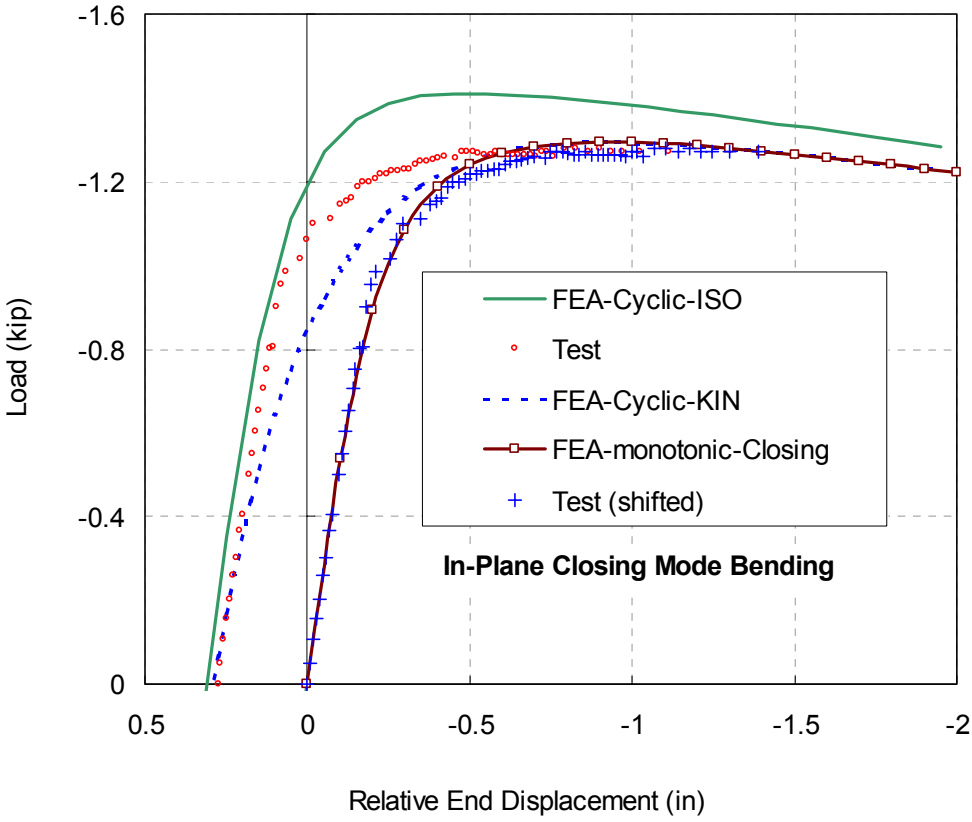

(b)

Fig. 13 FEA vs. Test Data (2) for Pipe-1

Pipe-2

For Pipe-2, the FEA models considering welds were constructed based on the previous investigations in Part IV. It is assumed that the welds were uniform along the circumference and were 0.25" (0.64 cm) high and 0.38" (0.97 cm) wide. This width is 95% of the measured width of 0.4" (1. cm). This reduction was included because the actual welds were not rectangular in cross-section. The reduction factor was selected by observation and using engineering judgement. It was also assumed that the welds were located half in the elbow and half in the straight tangent segments. In the corresponding

FEA models, a half ring of shell elements with uniform width and thickness was used to simulate the weld beads.

The FEA results against the test data are illustrated in Fig. 14 below. The fine solid line, labeled "FEA-ISO-Weld", shows the FEA results using Isotropic Hardening option. The dashed line shows those using Kinematic Hardening rule. Welds were taken into account as described above in both of the FEA models. In this case, the FEA simulation using Kinematic Hardening option shows very good agreement with the measured experimental data, while that using Isotropic Hardening option overpredicted the load bearing capacity.

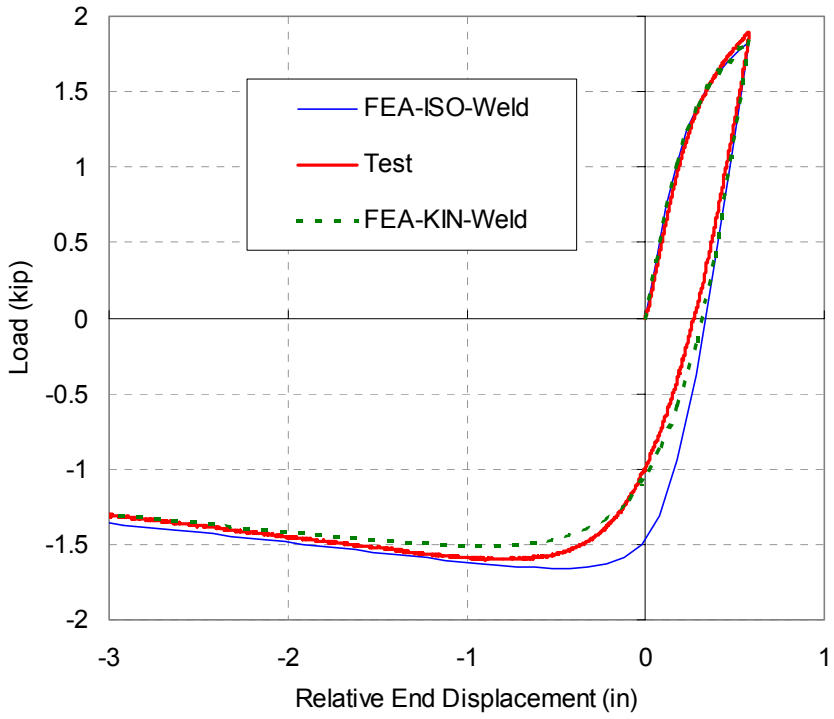

Fig. 14 FEA vs. Test Data for Pipe-2

To demonstrate the welding effects, FEA results with and without welds consid-

ered are shown in Fig. 15. It is evident that ignoring the welds leads to a significant underestimate the loads.

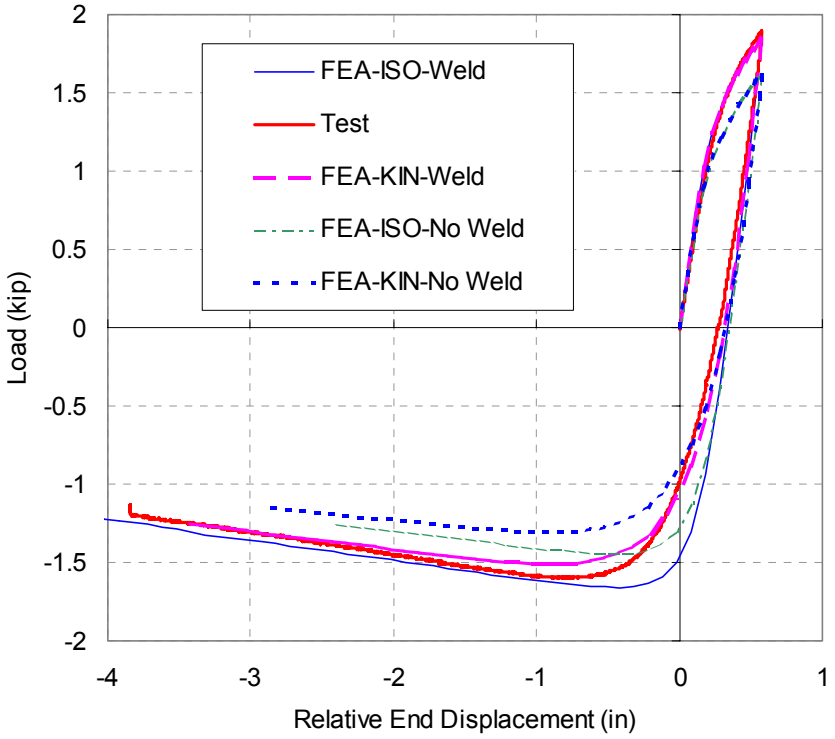

Fig. 15 FEA vs. Test Data (2) for Pipe-2

Similarly to Pipe-1, for the same specimen of Pipe-2, the FEA results for monotonic in-plane closing and opening bending against the cyclic responses are shown in Fig. 16. The dash line with rectangle marks, labeled "FEA-monotonic-Closing", presents the monotonic in-plane closing bending behaviors. However, it is stiffer than the cyclic in-plane closing phase test data and the first half cycle of loading history has considerable effects on it.

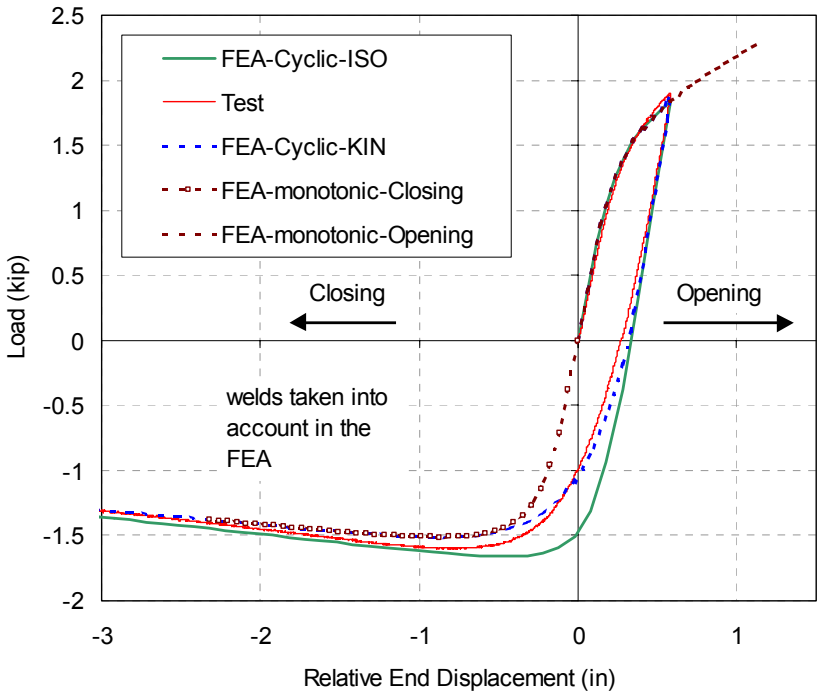

Fig. 16 FEA vs. Test Data (3) for Pipe-2

It is probably wise not to draw firm conclusions from two tests. Also, the test procedure itself for Pipe-1 leads us to question the results, as described in Section 4. However, we believe that it is still possible to draw some conclusions from the data about cyclic collapse and how it can be used in the calculation of a B_2' stress index, which will be briefly discussed in the following section.

6. CYCLIC B_2' STRESS INDEX

The definition of B_2 stress index proposed in Eq. 7 of Part II is shown again here:

$$B_{2,normalized} = \frac{M_{CL,straight\ \ pipe}}{M_{CL,component}} \qquad (2)$$

To apply the same definition shown above for piping components under cyclic loading, we need to obtain the collapse moments of the elbow and the corresponding straight pipe. Here a 2" Schedule 40 elbow is studied, in which nominal dimensions (Table A-1, Appendix A) and Code defined SS304L material properties (Fig. A-1, Appendix A) were used.

Applying the code definition of monotonic collapse loads as illustrated in Fig. 1 of Part I, i.e., at twice the extrapolated elastic displacement to cyclic loading, we obtained the collapse moments for isotropic and kinematic hardening options, as shown schematically in Fig. 17 and Fig. 18 for both the elbow and the corresponding straight pipe from the FEA moment-rotation curves. The collapse moments for the elbow and corresponding straight pipe are tabulated in Table 5 and Table 6 respectively.

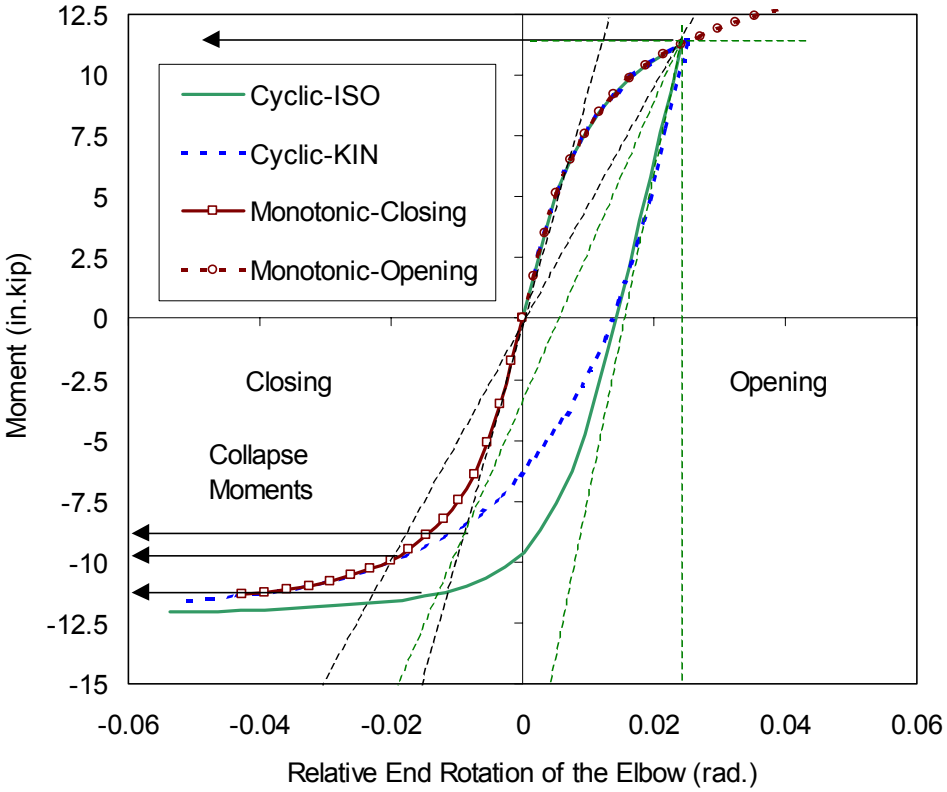

Fig. 17 Collapse Loads for 2" Schedule 40 Elbow

Table 5 Collapse Moments for 2" Schedule 40 Elbow

Elbow		$M_{CL,elbow}$ (in·kip)		
cyclic		1st load phase (In-Plane Opening)	2nd load phase (In-Plane Closing)	Controlling Moment
	ISO	11.3	11.7	11.3
	KIN	11.3	9.2	9.2
monotonic	In-plane opening		11.3	
	In-plane closing		9.6	

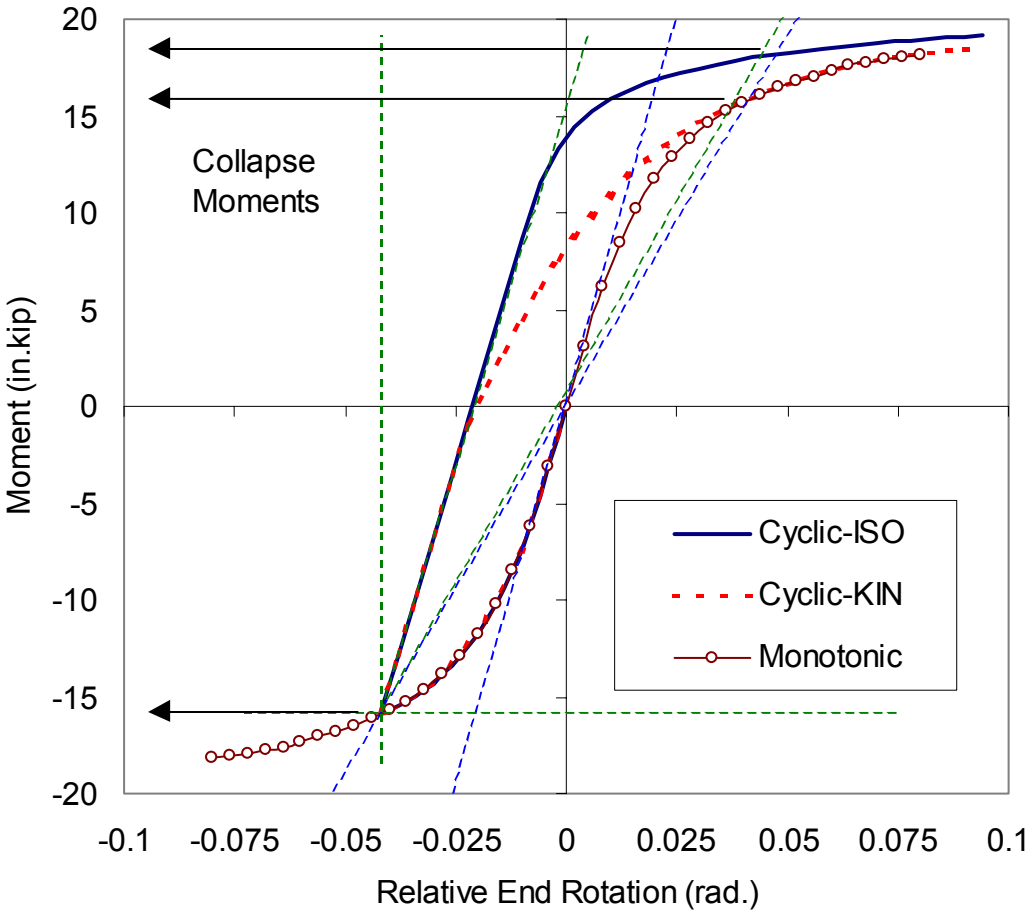

Fig. 18 Collapse Moments for 2" Schedule 40 Straight Pipe

Table 6 Collapse Moments for 2" Schedule 40 Straight Pipe

Straight Pipe		$M_{CL,straight\ pipe}$ (in.kip)	
cyclic		1st load phase	2nd load phase
	ISO	15.9	18.0
	KIN	15.9	15.3
monotonic		15.9	

Using Equation (2), the values of B_2' and B_2 for the tested elbow are obtained as

the following:

$$B'_{2,\text{cycic-ISO}} = \frac{18.0}{11.3} = 1.59$$

$$B'_{2,\text{cyclic-KIN}} = \frac{15.9}{9.2} = 1.73$$

$$B_{2,\text{monotonic -In plane opening}} = \frac{15.9}{11.3} = 1.41$$

$$B_{2,\text{monotonic -In plane closing}} = \frac{15.9}{9.6} = 1.66$$

The code value of the B_2 stress index (See Eq. 3 & 4 in Part II) for the elbow tested is 2.50. The calculated B_2' values using the new definition and the FEA procedure described above is 69% of the current code value for kinematic hardening assumptions, while, for monotonic loading, it is in-plane closing mode controlled and the calculated value of B_2 is 66% of the code value.

7 CONCLUSIONS

The work described in this part of the dissertation is a preliminary study of collapse following cyclic deformation and then the application of the defined collapse load to the calculation of the B_2' stress index. The reconciliation study, based on the two three-quarter cycle experiments, indicates that, using existing commercial FEA technology, it is possible to simulate reasonably well the cyclic behavior of piping elbows at room temperature with no internal pressure.

Much more research needs to be done to arrive at a final definition of collapse

following some history of cyclic behavior. In addition to the variables considered in monotonic collapse, such as internal pressure, elevated temperature, etc., the possible variations of the cyclic history itself will need to be studied. Following these studies, the definition of the B_2 stress index used for monotonic loading can be investigated to see if it remains useful for the cyclic case. All of this additional work is beyond the scope of the present study.

8 NOMENCLATURE

B_1' = primary stress index for pressure under cyclic loading

B_2 = primary stress index for bending

B_2' = primary stress index for bending under cyclic loading

C = constitutive model parameter in Eq. (2)

D_o = outside diameter of pipe

F_{CL} = collapse load

I = moment of inertia

M_E = amplitude of the resultant moment due to the inertial loading from the earthquake, other reversing type dynamic events and weight.

P_D = pressure occurring coincident with a reversing dynamic load

S_m = allowable design stress intensity value

t = nominal wall thickness

M_{CL} = collapse moment

γ = constitutive model parameter in Eq. (2)

9 REFERENCES

1. Beaney, E.M., 1991a, "Failure of Elbows Under Seismic Loading," Nuclear Electric, Technology Division, Report No. TD/SID/REP/0134, April

2. Slagis, G.C., “Earthquake Performance of Welded Steel Pipe”, WRC Proceedings IIW, 1997

3. Hassan, T., private communication, 1995

4. Gurdal, R., Maxham, D., Matzen, V.C., and Hassan, T., “Pipe Elbows – Reduction in Indices for Primary Bending,” DOE - NERI proposal, 1998

5. Bari, S. and Hassan, T., “Anatomy of Coupled Constitutive Models for Ratcheting Simulation”, International J. of Plasticity, Vol 16, pp381-409

6. Bari, S. and Hassan, T., “An Advancement in Cyclic Plasticity Modeling for Multi-axial Ratcheting Simulation”, International J. of Plasticity, Sept. 2000

7. Greenstreet, W. L., “Experimental Study of Plastic Responses of Pipe Elbows,”, ORNL/NUREG-24, 1978.

8. Diem, H., and Müller, K.U., “Deformation and Failure Behavior of Elbows”, SMiRT-8, F1 7/9, pp 269-274, 1985

9. Kussmaul, K., Diem, H., Roos, E., and Uhlmann, D., “Geometry Influence on the Location of Incipient Cracking of Pipe Bends under In-plane Bending”, 1989, 3rd International Conference on Biaxial/Multiaxial Fatigue, Stuttgart

10. Diem, H., Roos, E., Wachter, O., and Tolksdorf, E., “Failure Behavior of Thick walled Austenitic Pipe Bends Subjected to cyclic Bending Load and constant Internal Pressure,” (in german, with approximate English translation), 18th MPA-Seminal, Stuttgart, Oct.8-9, 1992, pp1.1-1.34

11. Fujiwaka, T., Endou, R., Furukawa, S., Ono, S., and Oketani, K., “Study on strength of piping components under elastic-plastic behavior due to seismic loading”, PVP-Vol. 387, Seismic Engineering-1999, ASME 1999, pp19-26

12. Tagart, S.W., Tang, Y.K, Guzy, D.J. and Ranganath, S., “Piping dynamic reliability and code rule change recommendations”, Nuclear Eng. And Design 123 (1990), pp373-385

13. Slagis, G.C., “Experimental Data on Seismic Response of Piping, Part 3”, PVP-Vol. 345, Seismic Eng. , 1997, pp163-171

14. Boyer, H.E., *Atlas of Stress-Strain Curves*, ASM International, 1987, ISBN: 0-87170-240-1

15. Hassan, T. and Kyriakides, S., "Ratcheting in Cyclic Plasticity, Part I: Uniaxial Behavior", International Journal of Plasticity, Vol. 8, pp. 91-116, 1992, Fig. 1

16. ANSYS online Manual, v.5.5

17. ABAQUS online Manual, v6.1, 3-9

18. Wilkins, K., Tan, Y. and Matzen, V.C., "Cyclic In-plane Tests on 2-inch, Schedule 10 Elbows," Data developed at the Center for Nuclear Power Plant Structures, Equipment and Piping, North Carolina State University, 2001

PART VII

CONCLUSIONS AND RECOMMENDATIONS

Based on the knowledge and experience gained in this research, a summary of the conclusions and recommendations for the future work is as follows.

(1) In Part II of this dissertation, a procedure was suggested for calculating the B_2 index as the ratio of collapse moments. It was demonstrated that, using this procedure, the B_2 for a straight pipe will always be 1.00 and the margin for any component will be the same as for a straight pipe with the same material and geometric properties.

To make a more definitive statement regarding the values of B_2 stress index for elbow, a complete investigation of B_2 values for different elbow configurations subjected to in-plane bending, out-of-plane bending and torsion seems necessary in the future work. Variables to be considered might be internal pressure, elevated temperature, material type, loading rate, flange location and bend angle.

(2) Parts III, IV and V focused on verifying the FEA procedures, in which moderately-thick wall elbows and thin-wall elbows, with or without welds grounded smooth, under in-plane closing, in-plane opening and out-of-plane bending, were investigated. All the FEA results of the load-displacement curves show close agreement with experimental data. It is concluded that the nonlinear FEA using ANSYS SHELL181 and ABAQUS ELBOW31 can provide quite accurate predictions for the global behavior of elbows under monotonic loading. In the FEA simulations, the choice of constitutive

model is a high priority issue. For small diameter elbow, e.g. 2” elbows, the existence of a raised weld bead can significantly increase the load bearing capacity.

(3) The work described in Part VI is a very preliminary phase study for B_2' stress index for cyclic loading. FEA using ANSYS SHELL43 was applied to simulate two ¾ cycle quasi static cyclic tests. Under cyclic loading, the actual collapse modes, the definition of collapse, the definition of B_2' index and the correlation between experiments and FEA are remaining questions.

APPENDICES

APPENDIX A

An Example Illustrating How to Obtain the Values of B_2 in Part II, Table 2

Example

The following is an example showing how to obtain the B_2 stress index for a typical commercial 2" Schedule 40, 90° Long-Radius Stainless Steel 304L (SS304L) Elbow, subjected to in-plane closing mode pure bending.

Procedure

1. Select an appropriate constitutive model.

Code defined material properties for SS304L are used in this example:

$$S_y = 25\,\text{ksi} \tag{1}$$

$$S_u = 70\,\text{ksi} \tag{2}$$

Using theses values of S_y and S_u, and an experimental stress-strain curve of SS304L, as shown in Fig. A-1 (labeled "ASTM-Straight Pipe Test"), the scaling procedure described in Part III was utilized to construct a constitutive model. The resulting curve is labeled "Code (scaled from test)". The constructed curve possesses the same values of S_y and S_u as defined in the Code and retains the general characteristics of the curve obtained from the ASTM experiment for SS304L. This constitutive model was applied in both of the following FEA for the elbow and the corresponding straight pipe.

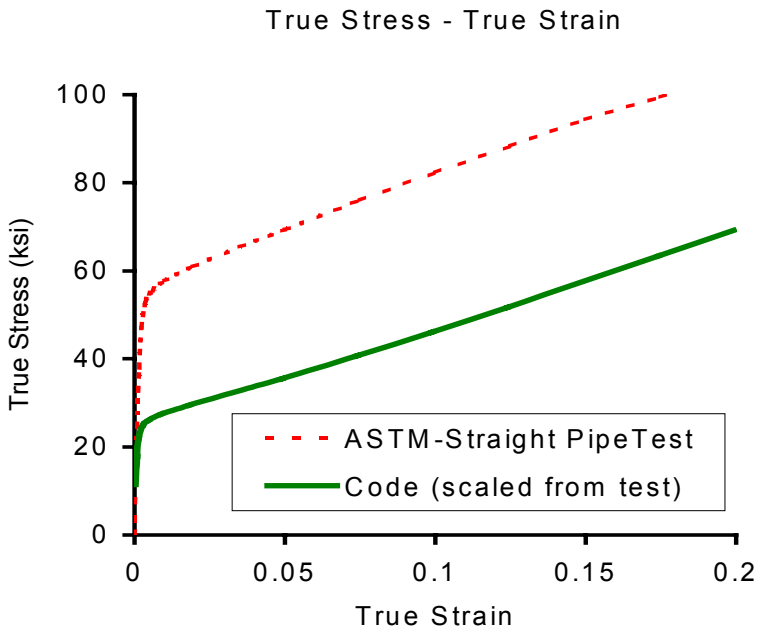

Fig. A-1 Constitutive Model

2. FEA Model for the Elbow.

FEA was used to obtain the moment-rotation curve of the elbow. Nominal dimensions shown in Table A-1 were used.

Table A-1 Nominal Dimensions of Typical Commercial 90° Long-Radius Elbow

Nominal pipe size	Outside diameter (in)	Wall thickness (in)	Pipe Bend Radius (in)
2"Sch 40	2.375	0.154	3

To eliminate end effects, a straight pipe segment of the same nominal outside diameter and wall thickness as the elbow and five times the nominal outside diameter in length was included at the end of the model, as illustrated in Fig. A-2. The analysis was displacement controlled and the rotation(s) was applied at the end(s). Large deformation and the stress stiffness effects were taken into account. Both ANSYS SHELL181 and

ABAQUS ELBOW31 are able to give quite accurate predictions, as demonstrated in Parts III to V. In this study, ABAQUS ELBOW31 was utilized. The relative end rotations of the elbow and the reaction moments are output, as illustrated in Fig. A-2.

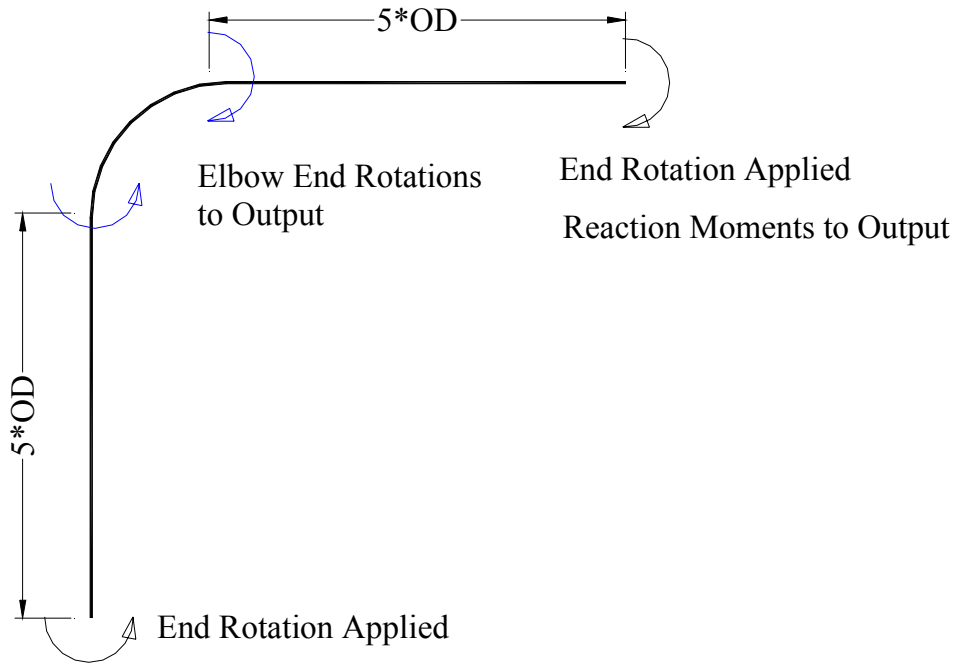

Fig. A-2 Model for the elbow

3. Obtain representative Moment-Rotations curve from FEA and obtain the collapse moment of the elbow based on the code definition of collapse load.

The FEA using ABAQUS ELBOW31 give the following moment-rotation curve of the elbow as shown in Fig. A-3 below.

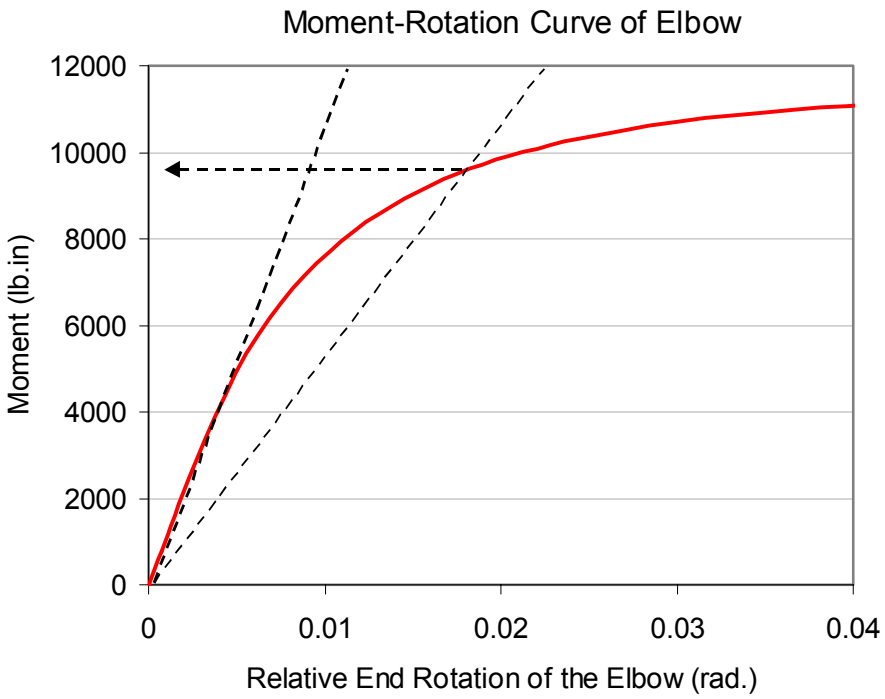

Fig. A-3 Moment-Rotation Curve of the Elbow

Based on the code definition of collapse load, provided in the Code, Appendix II, the collapse moment of the elbow is:

$$M_{CL,Elbow} = 9{,}604 \text{ lb.in} \qquad (3)$$

4. FEA Model for the corresponding straight pipe.

A corresponding straight pipe model, subjected to pure bending, was built as shown in Fig. A-4. It has the same nominal outside diameter and wall thickness (Table A-1) and material properties as the elbow investigated above.

End Rotation Applied End Rotation Applied

Reaction Moments to Output

Fig. A-4 Model for the Straight Pipe

5. Obtain representative Moment-Rotations curve from FEA for the straight pipe and obtain the collapsed moment of the straight pipe.

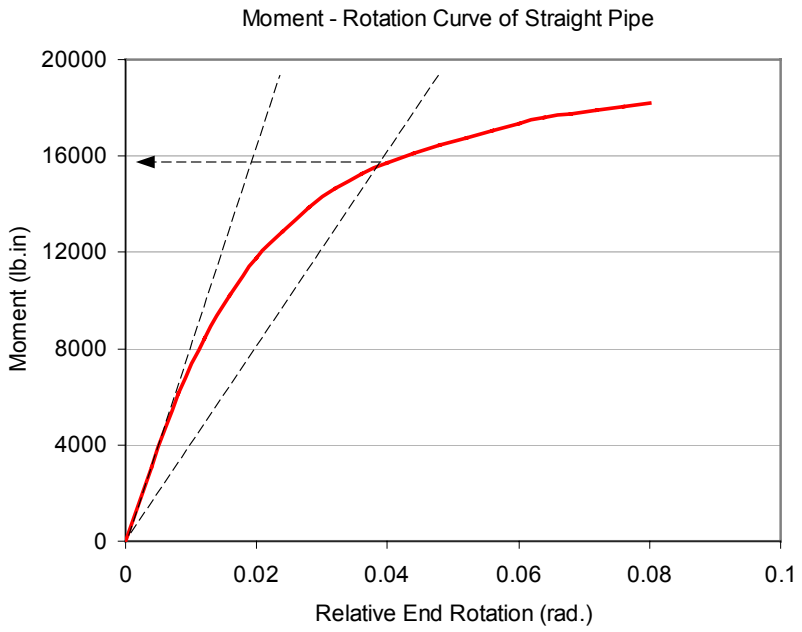

Fig. A-5 Moment-Rotation Curve of the Straight Pipe

$$M_{CL,Straight\ Pipe} = 15{,}850 \text{ lb.in} \tag{4}$$

6. Calculate the value of B_2 based on the new definition of the B_2 stress index.

According to Part II, Equation (6),

$$B_{2,normalized} = \frac{M_{CL,straight\ pipe}}{M_{CL,component}} = \frac{15{,}850}{9{,}604} = 1.65 \tag{5}$$

APPENDIX B

ABAQUS 6.1 Input File Using Element ELBOW31 for 8"Schedule 5 Straight Pipe for the Calculation of B_2 Value

```
* HEADING
 SPECIMEN: 8INSCH5 STRAIGHT PIPE
 GEOMETRY: NOMINAL
        R_O=4.3125 IN, D_O=8.625 IN, T=0.109 IN
        L=10*D_O
 LOADING:  PURE BENDING, ROTATION CONTROL
 MATERIAL: STAINLESS STEEL 304L, CODE VALUE
 ELEMENT:  ELBOW31
 MESH:     10 ELEMENTS
 SECTION INTEGRATION: 5,24,6
** ROTATIONAL CONTROLED
*NSET, NSET=NEND
100,200
*NODE, NSET=FIXEDEND
100,0,0,0
*NODE, NSET=LOADEND
200,86.25,0,0
*NGEN,NSET=STRTPIPE
100,200,10
*NSET, NSET=ALLNODE
STRTPIPE
*ELEMENT,TYPE=ELBOW31
1,100,110
*ELGEN,ELSET=SP
1,9,10,1
*ELEMENT,TYPE=ELBOW31,ELSET=LOADEND
10,190,200
*ELSET,ELSET=ALLELM
SP,LOADEND
*MATERIAL,NAME=SP
*ELASTIC
28310000,0.3
*PLASTIC
  11451.024 ,            0
  17753.299 ,   .00021260685
  22072.019 ,   0.0006497802
  25004.239 ,   0.0019467317
  26128.392 ,   0.0039240588
  27421.749 ,   0.0079821238
  29466.159 ,    0.017239377
  32569.363 ,    0.032767493
  35477.294 ,    0.047665257
  40690.659 ,    0.072490058
  46098.365 ,    0.097324325
  51672.517 ,     0.12216681
  57593.957 ,      0.1470054
*BEAM SECTION, SECTION=ELBOW,ELSET=ALLELM, MATERIAL=SP
```

```
4.3125,0.109
10,-1,0
5,24,6
*BOUNDARY
FIXEDEND,1,6
FIXEDEND,NOWARP
LOADEND, NODEFORM
*RESTART,WRITE,FREQUENCY=1
*STEP,INC=30,NLGEOM
APPLY END ROTATION
*STATIC,RIKS
.01, 1,.00001,.04,,
*BOUNDARY
LOADEND,5,,0.3
*OUTPUT, HISTORY, OP=NEW, FREQUENCY=1
*NODE OUTPUT,NSET=LOADEND
U,RF
*END STEP
```

(Note: The above program was developed and run at North Carolina Super Computing Center.)

APPENDIX C

ABAQUS 6.1 Input File Using Element ELBOW31

for 8"Schedule 5 Elbow under In-Plane Closing Mode Bending

for the Calculation of B_2 Value

```
* HEADING
 Reconciliation for the NCSU 2inSch40 In-Plane Closing Bending.
 Element: ELBOW31
 Mesh:16 for Straight Pipe Leg1
      16 for Elbow
      16 for Straight Pipe Leg2.
 Section Integration: 5,24,6
 Elbow portion: D_o=8.625 in  t=0.109 in
 SP portion:    D_o=8.625 in  t=0.109 in
 SP length:     L=43.125 in
** Force Controled is used in this analysis
*NSET, NSET=NEND
100,580
*NODE, NSET=LOADEND
580,55.125,55.125,0
*NODE, NSET=PIPEEND2
570,53.125,55.125,0
*NODE, NSET=PIPEEND1
110,0, 3.625, 0
*NODE,NSET=EBOWEND1
260,0,43.125,0
*NODE, NSET=EBOWEND2
420,12,55.125,0
*NODE, NSET=FIXEDEND
100,0,0,0
*NGEN,NSET=STRTPIPE
110,260,10
420,570,10
*NGEN,LINE=C,NSET=ELBOW
260,420,10,0,12,43.125,0
*NSET, NSET=ALLNODE
STRTPIPE,ELBOW,FIXEDEND,LOADEND
*NSET, NSET=ELBOWENDS
LOADEND,EBOWEND1,EBOWEND2
*ELEMENT,ELSET=RIGIDEND,TYPE=ELBOW31
1,100,110
48,570,580
*ELEMENT,TYPE=ELBOW31
2,110,120
17,260,270
33,420,430
*ELGEN,ELSET=LEG1
2,15,10,1
*ELGEN,ELSET=LEG2
```

```
33,15,10,1
*ELGEN,ELSET=LBOW
17,16,10,1
*ELSET,ELSET=ALLELEM
LEG1,LEG2,LBOW,1,48
*ELSET,ELSET=PIPEELEM
LEG1,LEG2,
*MATERIAL,NAME=ELBOW
*ELASTIC
28310000,0.3
*PLASTIC
   11451.024 ,              0
   17753.299 ,   .00021260685
   22072.019 ,   0.0006497802
   25004.239 ,   0.0019467317
   26128.392 ,   0.0039240588
   27421.749 ,   0.0079821238
   29466.159 ,    0.017239377
   32569.363 ,    0.032767493
   35477.294 ,    0.047665257
   40690.659 ,    0.072490058
   46098.365 ,    0.097324325
   51672.517 ,     0.12216681
   57593.957 ,      0.1470054
    63341.43 ,     0.17186504
   69199.635 ,     0.19672781
*MATERIAL,NAME=SP
*ELASTIC
28310000,0.3
*PLASTIC
   11451.024 ,              0
   17753.299 ,   .00021260685
   22072.019 ,   0.0006497802
   25004.239 ,   0.0019467317
   26128.392 ,   0.0039240588
   27421.749 ,   0.0079821238
   29466.159 ,    0.017239377
   32569.363 ,    0.032767493
   35477.294 ,    0.047665257
   40690.659 ,    0.072490058
   46098.365 ,    0.097324325
   51672.517 ,     0.12216681
   57593.957 ,      0.1470054
    63341.43 ,     0.17186504
   69199.635 ,     0.19672781
*MATERIAL,NAME=RIGID
*ELASTIC
28300000000,0.3
*BEAM SECTION, SECTION=ELBOW,ELSET=LEG1, MATERIAL=SP
4.3125,0.109
10,-1,0
5,24,6
*BEAM SECTION, SECTION=ELBOW,ELSET=LEG2,MATERIAL=SP
4.3125,0.109
-1,10,0
5,24,6
*BEAM SECTION, SECTION=ELBOW,ELSET=RIGIDEND,MATERIAL=RIGID
```

```
4.3125,0.109
-1,10,0
5,24,6
*BEAM SECTION, SECTION=ELBOW,ELSET=LBOW,MATERIAL=ELBOW
4.3125,0.109,12
0,55.125,0
5,24,6
*BOUNDARY
FIXEDEND,1,5
FIXEDEND,NODEFORM
LOADEND, NODEFORM
*RESTART,WRITE,FREQUENCY=1
*STEP,INC=50,NLGEOM
APPLY IN-PLANE CLOSING LOAD
*STATIC,RIKS
0.8, 40,.1,1.2,,
*BOUNDARY
FIXEDEND,6,,0.2
LOADEND,6,,-0.2
*Output, history, op=NEW, frequency=1
*Node Output, nset=ELBOWENDS
U,RF
*EL PRINT,FREQUENCY=1
PE
*NODE PRINT,NSET=ALLNODE
U
RF
*END STEP
```

(Note: The above program was developed and run at North Carolina Super Computing Center.)